TREX1 C-TERMINUS REGULATES OLIGOSACCHARYLTRANSFERASE TO PREVENT THE ACCUMULATION OF AN ENDOGENOUS BIOACTIVE DISACCHARIDE ASSOCIATED WITH AUTOIMMUNE DISORDERS

APPROVED BY SUPERVISORY COMMITTEE

_____
Nan Yan, Ph.D.

_____
Mark A. Lehrman, Ph.D.

_____
Jennifer J. Kohler, Ph.D.

_____
Benjamin P. Tu, Ph.D.

DEDICATION

To my beloved wife Sarahí,
for your unconditional support and for
always believing in me and my dreams.

“Titles and wealth are inherited from parents,
but a prudent wife is from the LORD”
(Proverbs 19:14).

ACKNOWLEDGEMENTS

I would like to thank my mentors Dr. Nan Yan and Dr. Mark A. Lehrman for their guidance, patience, and commitment to training me to become the scientist that I am today. They have taught me, among other things, how to do rigorous scientific research, to efficiently communicate my scientific findings, and how to establish collaborations with scientific colleges. Thank you for believing in me and supporting my bold scientific ideas and desire to combine glycobiology with immunology. In addition, I would also like to thank Dr. Nancy E. Street for her guidance and mentorship in many aspects of my academic and non academic life, and for imparting me with a strong desire to become a role model for the future generation of scientists. I am also grateful for my excellent thesis committee members, Dr. Jennifer J. Kohler and Dr. Benjamin Tu for their availability, help and advice throughout my graduate school journey. Your genuine keenness for addressing issues and concerns related to my project drove many of the discoveries that made this thesis possible.

Also, I would like to thank my UTSW graduate school friends, Dr. Wayne Doyle, Dr. Jason Miller, Dr. Sofya Perelman, Pamela de la Cruz, Claudio Morales-Perez, Angel Jimenez, and Ricardo Irrizary-Caro for their constant moral and emotional support and all the past and present members of the Yan lab, the Lehrman lab and the Kohler lab, especially Vladislav Pokatayev and Dr. Nicole Dobbs whom I count as my closest friends and have helped me in every aspect of this process since day one. I would like to give special thanks to my group of Puerto Rican friends for allowing me to continue experiencing and celebrating

my cultural traditions here in Dallas and to my friends back in Houston, Alexander Costa, Gladys Costa, and Melvin Mata, who has always kept me in their prayers.

Lastly, I would like to thank my family for their unwavering support and positive encouragement especially my parents and most importantly, I would like to thank my best friend and beloved wife, Sarahí, who always finds the right words to encourage me to continue moving forward. You are the author and the reason for all of my successes.

TREX1 C-TERMINUS REGULATES OLIGOSACCHARYLTRANSFERASE TO PREVENT THE ACCUMULATION OF AN ENDOGENOUS BIOACTIVE DISACCHARIDE ASSOCIATED WITH AUTOIMMUNE DISORDERS

by

Charles Steven Fermaintt

DISSERTATION / THESIS

Presented to the Faculty of the Graduate School of Biomedical Sciences

The University of Texas Southwestern Medical Center at Dallas

In Partial Fulfillment of the Requirements

For the Degree of

DOCTOR OF PHILOSOPHY
The University of Texas Southwestern Medical Center at Dallas

Dallas, Texas

May 2018

TREX1 C-TERMINUS REGULATES OLIGOSACCHARYLTRANFERASE TO PREVENT THE ACCUMULATION OF AN ENDOGENOUS BIOACTIVE DISACCHARIDE ASSOCIATED WITH AUTOIMMUNE DISORDERS

Publication No. _____

Charles Steven Fermaintt, Ph.D.

The University of Texas Southwestern Medical Center at Dallas, Graduation Year

Supervising Professor: Nan Yan, Ph.D.

The innate immune system is the first line of defense against infectious pathogens and serves a vital role in activating the adaptive immune system. Detection of viral and bacterial intracellular DNA by cytosolic DNA sensors (CDS) is crucial for the activation of the innate immune system and for eliciting a proper immune response. However, self-DNA species that originate from retro-elements, genomic DNA replication, and damaged mitochondria can

inappropriately activate the innate immune system through recognition by CDS. The cell employs strategically placed DNases to remove these self-DNA ligands that would otherwise cause chronic activation of the innate immune system leading to autoimmunity.

DNase III, also known as TREX1, is one of the negative regulators of CDS-mediated innate immune response. TREX1 is a 314 amino acid endoplasmic reticulum (ER) tail-anchored 3' exonuclease where the N-terminal region contains the DNase domain and the C-terminal end controls TREX1 localization to the surface of the ER. Disease mutations that abrogate the N-terminal DNase function of TREX1 lead to chronic activation of CDS-mediated innate immune response to self-DNA ligands leading to autoimmunity. In contrast, disease mutations in the C-terminal region are mostly frame-shift (fs) mutations that alter TREX1 localization to the ER, without affecting the DNase function. This difference invoked the hypothesis that TREX1 C-terminus engages in the interaction with ER-residing proteins and such interaction could contribute to the C-terminus associated diseases.

Through the investigation of this possibility, I identified that TREX1 interacts with the oligosaccharyltransferase (OST) subunits Ribophorin 1 (RPN1) and DDOST. This interaction was dependent solely on TREX1 C-terminus. Furthermore, TREX1 C-terminus modulates OST's preference to hydrolyze lipid-linked oligosaccharides (LLOs) into bioactive free oligosaccharides (fOS) in a switch-like manner. Introduction of TREX1 disease fs mutations stably switched OST to promote rapid release of bioactive free oligosaccharides that activates immune signaling (**Chapter 2**). Structural analysis of the bioactive fOS revealed that they differ from typical N-glycans structures with high accumulation of mannosyl tetra, tri and disaccharides species. Among these, the structure

responsible for the bioactivity is a mannose (Man) β1-4 N-acetylglucosamine (GlcNAc) disaccharide. The bioactive disaccharide is produced from OST's hydrolyzed LLOs in the cytoplasm and activates a TBK1 dependent immune signal that leads to the upregulation of interferon-stimulated genes (ISGs) and chemokine genes (**Chapter 3**).

The TREX1 C-terminal region is composed of 72 amino acids from residues 242 to 314. I examined what portion of TREX1 C-terminus was required for interaction with RPN1 and DDOST. The TREX1 and OST's interaction interface was mapped to residues 235 to 290 where a regulatory phosphorylation site was identified at serine 261. The phosphorylation event takes place during mitosis. Phosphomimetic mutant ofTREX1 S261 disrupted the interaction between TREX1 and OST, implying that the phosphorylation event regulates the interaction between TREX1 and OST as well as potentially OST hydrolysis of LLOs into free oligosaccharides (**Chapter 4**).

Altogether, these results provide mechanistic insights into how TREX1 C-terminus fs mutations cause accumulation of a bioactive disaccharide which triggers immune activation and suggests potential therapeutic options for TREX1-fs mutant-associated diseases.

TABLE OF CONTENTS

PRIOR PUBLICATIONS

1. Pham N.D., **Fermaintt C.S.**, Rodriguez A.C., McCombs J.E., Nischan N and Kohler J.J. Cellular metabolism of unnatural sialic acid precursors. Glycoconjugate Journal May 10, 2015

2. Hasan M.*, **Fermaintt C.S.***, Gao N., Sakai T., Miyazaki T., Jiang S., Li Q., Atkinson J.P., Morse III H.C., Lehrman M.A. and Yan N. A novel function of TREX1 associated with the C-terminus connects oligosaccharyltransferase dysregulation to immune disorders. Immunity September 15, 2015 ***Co-first author**

3. Kucej M.*, **Fermaintt C.S.***, Yang K., Irizarry-Caro R. and Yan N. Mitotic phosphorylation of TREX1 C-terminus disrupts TREX1 regulation of the oligosaccharyltransferase complex. Cell Reports March 14, 2017 ***Co-first author**

4. Sakai T., Miyazaki T., Shin D., Kim Y., Qi C., Fariss R., Munasinghe J., Wang H., Kovalchuk A.L., Kothari P.H., **Fermaintt C.S.**, Atkinson J.P., Perrino F.W., Yan N., Morse III H.C. DNase-active TREX1 frame-shift mutants induce serologic autoimmunity in mice. Journal of Autoimmunity March 18, 2017

5. **Fermaintt C.S.**, Sano K., Seino J., Dobbs N., Suzuki T., Lehrman M.A., Matsuo I. and Yan N. A bioactive monovalent mammalian disaccharide activates a TBK1-dependent immune signaling and is associated with chronic autoimmune disease. Manuscript ready for submission 2018

6. **Fermaintt C.S.**, Khan S., Tu X. Raj P., Wakeland E. and Yan N. TREX1 expression and function dictate the association with Aicardi–Goutières syndrome or systemic lupus erythematosus. In preparation 2018

LIST OF FIGURES

CHAPTER ONE FIGURES

CHAPTER TWO FIGURES

CHAPTER THREE FIGURES

CHAPTER FOUR FIGURES

CHAPTER FIVE FIGURES

LIST OF TABLES

CHAPTER ONE TABLES

CHAPTER THREE TABLES

LIST OF ABBREVIATIONS

ACM: Aclacynomyc A
ADAR: Double-stranded RNA-specific adenosine deaminase
ANDS: 7-amino-1,3-naphthalenedisulfonic acid
AMP: Adenosine monophosphate
AS: Asynchronized
ATP: Adenosine triphosphate
AGS: Aicardi–Goutières syndrome
BSA: Bovine sereum albumin
BMDM: Bone marrow derived macrophages
CADASIL: Cerebral autosomal dominant arteriopathy subcortical infarcts leukoencephalopathy
CDS: Cytosolic DNA sensor
CDK: Cyclin-dependent kinase
CFG: Consortium of Functional Glycomics
cGAMP: Cyclic GMP-AMP
cGAS: Cyclic GMP-AMP synthase
Clq or CQ: Chloroquine
CLR: C-type lectin receptors
CSF: Cerebrospinal fluid
CSN: Castanospermine
Con A: Concanavalin A
CXCL: C-X-C motif chemokine
DAD1: Defender against cell death 1
DAPI: 4,6-diamidino-2-phenylindole
DC2: Oligosaccharyltransferase complex subunit OSTC
DDOST: Oligosaccharyltransferase 48 kDa subunit
Dectin: Dendritic cell-associated C-type lectin 1
DMEM: Dulbecco's modified Eagle's medium
DMJM: Deoxymannojirimycin
DNA: Deoxyribonucleic acid
DNase: Deoxyribonuclease
dsDNA: Double-stranded DNA
DTT: Dithiothreitol
EBV: Epstein–Barr virus
ENGase: Cytosolic endo-beta-N-acetylglucosaminidase
Endo H: Endoglycosidase H
ER: Endoplasmic reticulum
ERAD: ER-associated degradation
FACE: Fluorescence-assisted carbohydrate electrophoresis
FBS: Fetal bovine serum
FCL: Familial chilblain lupus

FEN1: Flap endonuclease 1
fOS: Free Oligosaccharides
fs: Frame-shift
GAPDH: Glyceraldehyde 3-phosphate dehydrogenase
GDP: Guanosine diphosphate
GFP: Green fluorescents protein
GMP: Guanosine monophosphate
GTP: Guanosine triphosphate
Gal: Galactose
Glc: Glucose
GlcNAc: N-acetylglucosamine
HEPES: 4-(2-hydroxyethyl)-1-piperazineethanesulfonic acid
HSV: Herpes Simplex Virus
htDNA: Herring testes DNA
IFIT: Interferon Induced Protein With Tetratricopeptide Repeats
IFN: Interferon
IFNAR: IFN receptor
IKK: IκB kinase
IP: Immunoprecipitation
IPA: Ingenuity Pathway Analysis
IRF: Interferon regulatory factor
ISG: Interferon-stimulated gene
JAK: Janus kinase
KCP2: Keratinocyte-associated protein 2
Kif: Kifunensine
LAM: Lipoarabinomannan
Le^X: Lewis X
LLO: Lipid linked oligosaccharide
LPS: Lipopolysaccharide
M6P: Mannose 6 phosphate
Man: Mannose
Man2C1: Cytosolic alpha-mannosidase 2C1
ManBA: Lysosomal beta A mannosidase
MagT1: Magnesium transporter protein 1
MAVS: Mitochondrial antiviral-signaling protein
MCL: Macrophage C-type lectin
MDL: Myeloid-DAP12-associating lectin
MDA5: Melanoma differentiation-associated protein 5
MEFs: Mouse embryonic fribroblasts
MGL: Macrophage galactose lectin
MINCLE: Macrophage-inducible C-type lectin
MyD88: Myeloid differentiation primary response 88
NGLY1: N-glycanase 1
NF-κβ: Nuclear factor kappa light chain enhancer of activated B cells

Noc: Nocodazole
NP-40: Nonidet 40
OST: Oligosaccharyltransferase
OST4: Oligosaccharyltransferase subunit 4
PAMP: Pathogen-associated pattern molecules
PBS: Phosphate buffered saline solution
PGN: Peptidoglycan
PNGase F: N-glycosidase F
PLK: Polo-like kinase
PP: Protein phosphatase
PRR: Pattern recognition receptors
PTM: Post-translational modification
qRT-PCR: Quantitative real time polymerase chain reaction
RIG-I: Retinoic acid-inducible gene I
RIPA: Radioimmunoprecipitation assay buffer
RNA: Ribonucleic acid
RNase: Ribonuclease
RPN: Ribophorin
RPMI: Roswell Park Memorial Institute medium
RUX: Ruxolitinib
RVCL: Retinal vasculopathy with cerebral leukodystrophy
SAMHD1: SAM And HD Domain Containing Deoxynucleoside Triphosphate Triphosphohydrolase 1
SEM: Mean and standard deviation
SFTPD: Surfactant protein D
siRNA: Small interfering RNA
SLE: Systemic lupus erythematosus
SS: Sjögren's syndrome
SSc: Systemic sclerosis
ssDNA: Single-stranded DNA
STING: Stimulator of interferon genes
STT3: Oligosaccharyltransferase subunit STT3
Swain: Swainsonine
SYK: Spleen tyrosine kinase
TBK1: Tank binding kinase 1
TDB: Synthetic Cord factor
Thy: Thymidine
TM: Transmembrane
TLR: Toll like receptors
TREX1: Three prime repair exonuclease 1
TRIF: TIR-domain-containing adapter-inducing interferon-β
Tusc3: Tumor suppressor candidate 3
UDP: Uridine diphosphat
WT: Wild type

CHAPTER ONE: AN INTRODUCTION TO TREX1, THE SWEET DNASE

Innate immunity and pattern recognition receptors

Mammalian cells are equipped with an arsenal of innate immune receptors that constitutes the host first line of defense against invading pathogens [1]. These innate immune receptors, also known as pattern recognition receptors (PRRs), efficiently recognize microbial components termed pathogen-associated molecular patterns (PAMPs), and examples of these range from microbial DNA to bacteria and fungi cell wall components to large polysaccharides like β-glucans [2]. The recognition of PAMPs by PRRs triggers the activation of a specific innate immune response which could range from the production of anti-viral type Iinterferons (IFNs) and IFN stimulated genes (ISGs), inflammatory cytokines and or chemokines. However, PRRs can be activated erroneously by host macromolecules or by gain-of-function mutations in the settings of autoimmune disease [3, 4]. As a mechanism to avoid incorrect activation of the innate immune system by host macromolecules, the cell places PRRs in locations where they would not normally interact with host self-ligands or utilizes the activity of negative regulators of innate immune signaling [5, 6].

TREX1: A negative regulator of DNA-mediated immune signaling

TREX1/DNAse III is one of the negative regulators of DNA-mediated innate immune signaling. TREX1 is one of four DNases found in humans which includes DNase I, DNase II, DNase III or three prime repair exonuclease 1 (TREX1) and DNase IV or flap endonuclease 1 (FEN1). The primary function of TREX1 is to remove self-DNA

ligands from locations where DNA should not be present [7-9]. Unlike prokaryotes, eukaryotic DNA is organized into the nucleus and mitochondria, leaving the cytoplasm as a self-DNA free environment. TREX1 is responsible for removing self-DNA substrates that originate from the nucleus (e.g. retro-elements) or damaged mitochondria and make their way into the cytoplasm (**Figure 1.1**) [10]. If not removed, these self-DNA ligands could erroneously trigger the activation of a class of PRRs designed to recognize microbial DNA known as cytosolic DNA sensors (CDS) in particular the cGAS-STING pathway (**Figure 1.1**) [11, 12].

The TREX1 N-terminus vs. C-terminus paradox

TREX1 is the most abundant exonuclease in mammalian cells. Unlike the other three DNases, TREX1 is anchored to the cytosolic surface of the ER (**Figure 1.2 A**) [13, 14]. The TREX1 gene contains a single exon located on chromosome 3p21.31 that encodes a 314 amino acid 3'→5' exonuclease [15-17]. In the cell, TREX1 exists as a stable homodimer and is composed of an exonuclease domain in the first 242 amino acid N-terminus and a 72 amino acid C-terminus important for anchoring TREX1 to the surface of the ER (**Figure 1.2 A**) [14, 18, 19]. TREX1 exonuclease domain preferentially degrades ssDNA or dsDNA substrates with mispaired 3' overhangs with high efficiency and dsDNA substrates with a 5' overhangs or blunt ends with reduced efficiency [16, 20]. The evolutionarily conserved TREX1 active sites are positioned at the opposite outer edges of each dimer and contain key acidic residues (e.g. D18 and D200) required for coordinating two Mg^{2+} ions that enable catalysis (**Figure 1.2 B-C**).

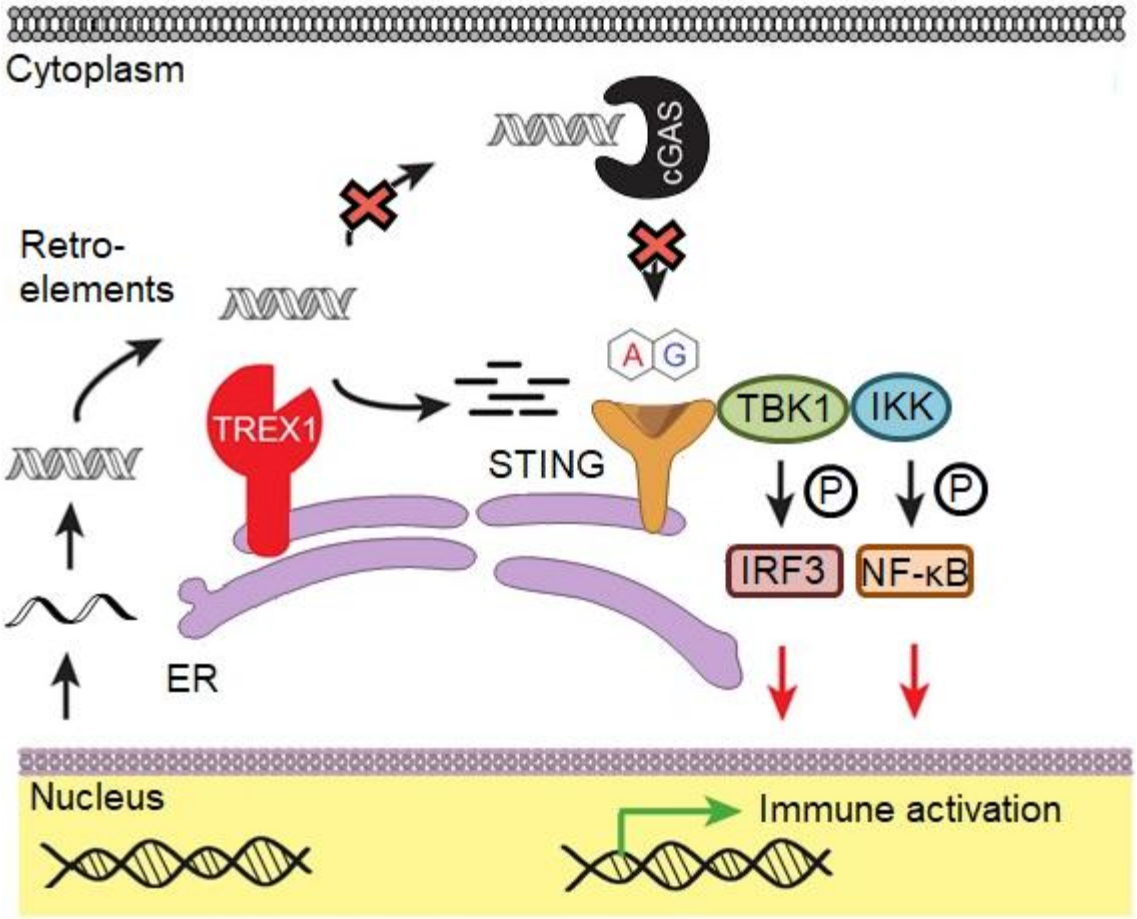

Figure 1.1: Summary of TREX1 as a negative regulator of the cGAS-STING pathway.

TREX1 removes ssDNA retro-element species that gain access to the cytoplasm. These species have the potential to incorrectly activate the cGAS-STING pathway.

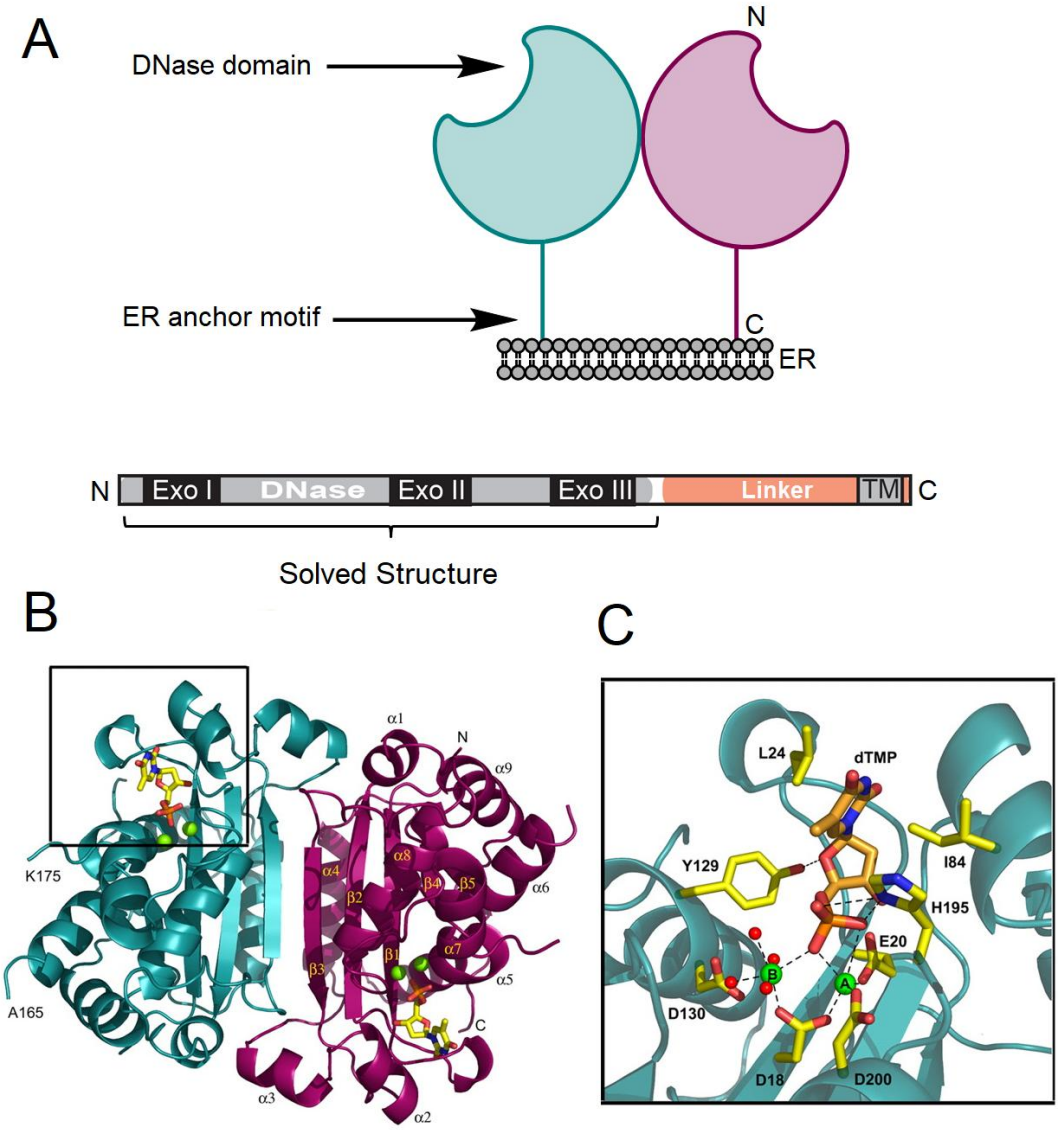

Figure 1.2: Topology of TREX1.

(A) Topological illustration of the TREX1 homodimer. TREX1 can be divided into two domains; The DNase domain located at the N-terminal region and the ER anchoring motif located at the C-terminal region of TREX1. The crystal structure of human TREX1 contains the first 242 amino acids (DNase domain).
(B) The crystal structure of the human TREX1 DNase domain as a homodimer bound to DNA. The PDB file is 2O4G and is published in [22]. Adapted from [22]
(C) The human TREX1 catalytic core and key residues (e.g. D18 and D200) involved in catalysis. The green A and B spheres represent the two Mg^{2+} ions. The PDB file is 2O4G and is published in [22]. Adapted from [22]

The H195 residue is important for the deprotonation of a water molecule to generate an active nucleophile that carries out the phosphodiester bond cleavage of the DNA substrates (**Figure 1.2 C**) [21]. The C-terminus, on the other hand, is not evolutionary conserved and mostly consists of a structurally unresolved linker region and a tail-anchored insertion motif [22].

Mutations on TREX1 have been associated with a broad spectrum of autoimmune disorders ranging from Aicardi–Goutières syndrome (AGS), to systemic lupus erythematosus (SLE), familial chilblain lupus (FCL), Sjögren's syndrome (SS), systemic sclerosis (SSc), cerebral autosomal dominant arteriopathy subcortical infarcts leukoencephalopathy (CADASIL) and retinal vasculopathy with cerebral leukodystrophy (RVCL) (**Figure 1.3 and Table 1.1**) [23-26]. Most of the mutations found in the N-terminus DNase domain of TREX1 are recessive missense mutation associated with AGS (**Figure 1.3 and Table 1.1**) [27]. The most studied mutations are those that directly affect residues involved in coordinating the Mg^{+2} ions required for catalysis, such as D18N, D200N, and D200H. These mutations completely abrogate TREX1 catalytic function (**Table1.1**) [20, 28, 29]. Mutations that destabilize the homodimer have also been associated with AGS like in the case of the R114H mutation (**Table 1.1**). The R114 residue is present in the dimer interface and plays an important role in maintaining the stability and structure of the TREX1 homodimer. Interestingly, the R114H mutation present in one protomer affects the catalytic activity of the opposite protomer [30]. Because of this poisoning feature, R114H has a high disease frequency (**Table 1.1**). In contrast, most of the disease mutations associated with the C-terminus are dominant

RVCL and SLE causing fs mutations (e.g. V235fs and D272fs) that lead to TREX1 mislocalization from the ER without affecting the exonuclease function (**Figure 1.3 and Table1.1**) [31, 32]. This difference results in the manifestation of two very different clinical disorders.

TREX1 associated diseases pathogenesis and clinical features

Aicardi–Goutières syndrome (AGS) is an early-onset inherited encephalopathy autoimmune disorder that affects newborns and is characterized by basal ganglia calcification, white matter abnormalities, chronic cerebrospinal fluid (CSF) lymphocytosis, severe mental and physical handicap, recurrent chilblain lesions and high levels of IFN and ISGs in the CSF and the blood of the affected infants [33]. A total of 7 genes that encode the proteins TREX1, RNase H2 A, B and C, SAMHD1, ADAR, and MDA5 all of which have been involved with nucleic acid metabolism, have been associated with AGS. In the case of TREX1, the accepted mechanism of disease is that in the presence of mutations that impair the DNase function, self-DNA ligand accumulates and activate CDS, in particular, the cGAS-STING pathway which stands out as the most important contributor to AGS pathogenesis [34, 35]. The cGAS-STING pathway is a member of the CDS family involved in the recognition of pathogenic DNA that has breached the plasma membrane from the invading pathogen [36-38]. Upon recognition, cGAS catalyzes the synthesis of the second messenger, 2'-3' cGAMP from GTP and ATP. The dinucleotide activates STING, a multipass transmembrane protein on the ER, and initiates its translocation to the ERGIC where it recruits the kinases TBK1 and IKK

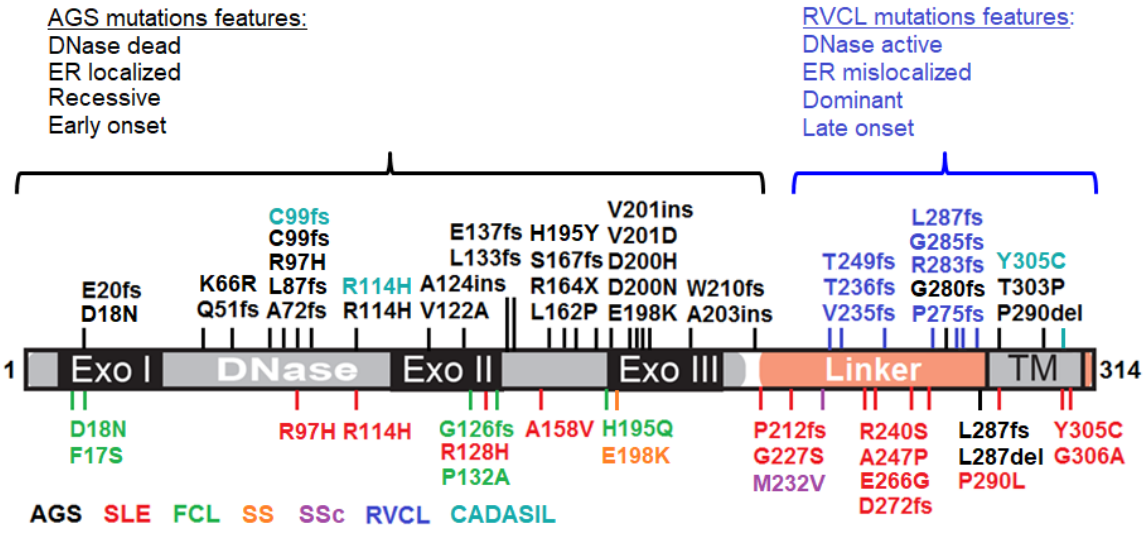

Figure 1.3: Summary of TREX1 mutations and associated diseases.

Most of the mutations that impair the exonuclease function are associated with AGS and are found in the DNAse domain while mutations outside the DNAse domain mostly retain the exonuclease activity and are fs associated with RVCL or misesnse mutations associated with SLE. See **Table 1.1**for more details.

TREX1 Variant	Nucleotide change	DNAse activity	Disease	Inheritance	Ref
F17S	50T>C	Normal	FCL	Comp het, G126fs	[30, 39]
D18N	52G>A	Decreased	FCL	Het	[28, 29.42, 45, 50]
			AGS	Hom	
E20fs	58_59insG	NT	AGS	Hom	[27]
Q51fs	152_153del	NT	AGS	Comp het, T303P	[24]
K66R	197A>G	NT	AGS	Hom	[55]
A72fs	212_2l3dupTG	NT	AGS	Hom	[35]
L87fs		NT	AGS	Comp het, R97H	[52]
R97H	290G>A	Decreased	AGS	Comp het, L87fs	[52, 53]
			SLE	Het	
C99fs		NT	CADASIL	Het	[54]
R114H	341G>A	Decreased	AGS	Hom	[24, 27, 30, 31, 46, 48]
			AGS	Comp het, D201ins	
			SLE	Het	
			CADASIL	Het	
			AGS	Comp het,S166fs	
			AGS	Comp het, P212fs	
V122A	365T>C	Normal	AGS	Hom	[40, 41]
A124ins	366_368dupGGC	Decreased	AGS	Hom	[30, 40]
G126fs	375dupT	Decreased	FCL	Comp het, F17S	[27, 39]
R128H	383G>A	Normal	SLE	Het	[28, 48]
P132A	394C>G	Decreased	FCL	Het	[49]
L133fs	397delC	NT	AGS	Hom	[40]
E137fs	393_408dup	NT	AGS	Hom	[40]
A158V	473C>T	NT	SLE	Het	[31]
L162P	485T>C	NT	AGS	Hom	[55]
R164X	490C→T	Decreased	AGS	Hom	[27]
S167fs	500delG	NT	AGS	Hom	[40]
H195Y	583C>T	NT	AGS	Het	[50]
H195Q	585C>G	NT	FCL	Hom	[43]
E198K	592G>A	Normal	AGS	Hom	[24, 25, 41]
			SS	Het	
D200N	598G>A	Decreased	AGS	Het	[28, 39, 50]
D200H	598G>C	Decreased	AGS	Het	[24]
V201D	602T>A	Decreased	AGS	Hom	[27]
V201ins	600_60linsGAT	Decreased	AGS	Comp het, R114H	[27, 30]
A203ins	609_662dup	NT	AGS	Hom	[40]
W210fs	625_628dupCAGT	NT	AGS	Hom	[40]

P212fs	634delC	Decreased*	SLE	Het	[31, *]
			AGS	Comp Het, R114H	
A223T	667G>A	NT	AGS	Comp Het, G280fs	[50]
G227S	679G>A	Normal*	SLE	Comp Het, A247P	[31, *]
M232V	694A>G	NT	SSc	Het	[25]
V235fs	703_704insG	Normal	RVCL	Het	[32, 65]
T236fs	706_707insA	Normal	RVCL	Het	[32]
R240S	720G>C	Normal*	SLE	Het	[31, *]
A247P	739G>C	Normal*	SLE	Comp Het, G227S	[31, *]
T249fs	742_745dupGTCA	Normal	RVCL	Het	[32]
E266G	797G>A	NT	SLE	Het	[46]
D272fs	812_8l3insAA	Normal	SLE	Het	[31, 65]
P275fs	822delT	NT	RVCL	Het	[44]
G280fs	839delG	NT	AGS	Comp Het, A223T	[50]
R284fs	850_851insA	NT	RVCL	Het	[32]
G285fs	850dup	NT	RVCL	Het	[51]
L287fs	857_858insG	NT	RVCL	Het	[32, 50]
			AGS	Comp Het, G280fs	
L287del	859-876del	NT	AGS	Hom	[24]
P290L	869C>T	Normal	SLE	Het	[31, 41]
P290del	868_885del	NT	AGS	Hom	[40]
T303P	907A>C	Normal	AGS	Hom	[24, 40, 41]
				Comp het, Q51fs	
Y305C	914A>G	Normal	SLE	Het	[31, 41, 46, 48]
			CADASIL		
G306A	917G>C	Normal*	SLE	Het	[31]

Table 1.1: List of reported TREX1 mutations and their associated diseases.

NT = not tested
Green = DNAse active variants.
Red = DNAse inactive variants.
* Evidence presented here.

[56, 57]. In turn, these kinases activate the transcription factors IRF3 and NF-κB to initiate the transcription of pro-inflammatory cytokines, chemokines, IFNs and ISGs that are essential for antimicrobial immunity (**Figure 1.1**) [58, 59]. The *Trex1 -/-* mouse has served as a model to study AGS in animals since it exhibits most of the lethal inflammatory phenotypes associated with the disease like elevated levels of IFN and ISGs, reduced survivability and retardation as well as higher basal concentrations of cGAMP [34, 60]. Removal of cGAS or STING in the *Trex1 -/-* mice rescues survivability, pathological and immune phenotypes associated with AGS [34, 61]. However, an unexpected finding came from a recently established *TREX1-D18N* knock-in mouse model that develops similar autoimmune disease phenotypes as the *Trex1 -/-* mice but with less severity [62]. The D18N mutation directly affects the catalytic function of TREX1 yet, the animal model did not fully present the severe pathology observed in the *Trex1 -/-* mice suggesting that lack of TREX1 ER localization domain also contribute to the pathology of the *Trex1 -/-* mice.

Unlike AGS, retinal vasculopathy with cerebral leukodystrophy (RVCL) is a late-onset genetic disease that causes progressive loss of blood vessels in the retina and the brain. The disease usually manifests in the middle age years (35 to 45) and is characterized by severe migraines, strokes, visual impairment, white matter lesions and calcification [63]. RVCL has a high mortality rate, leading to death after 5 to 10 years following diagnosis [64]. Another difference between AGS and RVCL is that only mutations in TREX1 C-terminus have been linked to RVCL [32]. All of the RVCL associated mutations are dominant fs that truncate TREX1 C-terminus without affecting

the DNase function (**Table 1.1**) [44, 51, 65, 66]. Since the RVCL fs mutations do not affect the DNase function, the pathogenesis of the disease remains unknown. Aside from localizing TREX1 to the surface of the ER, the function of TREX1 C-terminus is poorly understood.

The oligosaccharyltransferase (OST) complex

The mammalian OST is an ER multi-subunit membrane protein complex responsible for catalyzing all N-linked protein glycosylation events in the cell. The OST plays an important role in protein folding, quality control, and the intracellular trafficking through the secretory pathway. The OST transfers fully assembled glycans ($Glc_3Man_9GlcNAc_2$) from a lipid-linked oligosaccharide (LLO) donor to asparagines (N) residues of newly nascent glycoproteins within a N-X-S/T sequon where X could be any amino acid except P, in a co- or post-translational manner [67, 68]. Out of the 7-8 subunits that make up the OST complex, the STT3 subunit harbors the glycan transfer catalytic activity [69]. Two STT3 isoforms (STT3A and STT3B catalytic subunits) have been identified in mammals, each with a unique function. While STT3A mostly transfers the fully assembled glycan co-translationally, STT3B attaches the fully assembled glycan on unfolded glycoproteins post-translationally primarily on sequons found on the C-terminal end [70]. In addition to STT3A or STT3B, the OST complex is composed of 5 shared subunits, RPN1, RPN2, DDOST (OST48), DAD1 and OST4. The accessory subunits DC2 and KCP2 specifically assemble with the STT3A complex while MagT1 and Tusc3 are exclusively associated with the STT3B complex (**Figure 1.4**) [71, 72].

Another reaction catalyzed by the OST is the hydrolysis of LLOs to generate unbound neutral free oligosaccharides (fOS) (**Figure 1.5**) [73, 74]. Once generated, fOS are processed by ER residing glucosidases and transported to the cytoplasm through an ATP and Ca^{2+} dependent transporter where they join the pool of fOS generated by NGLY1 deglycosylation activity [75, 76]. In the cytosol, products of LLO hydrolysis by OST and NGLY1 are sequentially processed by the cytosolic endo-β-N-acetylglucosaminidase (ENGase) and Man2C1 to generate a $Man_5GlcNAc$ structure [77]. The $Man_5GlcNAc$ product is moved to the lysosomes through a lysosomal ATP-driven transporter [78]. In the lysosomes, lysosomal mannosidases remove the α mannose units to generate a Manβ1-4GlcNAc disaccharide that ultimately gets cleaved by the β-mannosidase ManBA to generate the mannose and GlcNAc monosaccharides [79]. Previous work has demonstrated that fOSs release by OST contribute to approximately 35% of the transferred glycans [80]. This raises the question what is the biological function of fOS. At first glance, the hydrolysis of LLOs by OST might appear as a waste of energy and resources. However, rapid release of fOS has been previously associated with events that create a stressful burden in the cell, like ER stress and Herpes Simplex Virus (HSV1) infection [73]. Both of these events have been associated with immune activation [81, 82]. Thus, a link could exist between the accumulation of fOS and immune activation. Since TREX1 C-terminus interacts with the OST, it is possible that TREX1 modulate the preference for OST's LLO hydrolysis.

Glycans as immune ligands

In addition to DNA, bacterial and fungi glycans are well-established PAMPs that can be sensed by the host immune system [83, 84]. The family of PRRs that has been designated the microbial glycan sensors are C-type lectin receptors (CLR). CLR family is composed of hundreds of receptors that have evolved to recognize a large spectrum of monosaccharides moieties and linkages [85]. Most of the CLR receptors recognize large polysaccharides like β–glucan ($[Glc(\beta1\text{-}3)Glc]_n$), chitin ($[GlcNAc(\beta1\text{-}4)GlcNAc]_n$), yeast mannan ($[Man(\alpha1\text{-}6)Man]_n$) and many more [86-88]. In some cases, carbohydrates can activate immune pathways that do not involve direct carbohydrate-receptor recognition, like in the case of chitosan and GlcNAc from peptidoglycan (PGN). In these two cases, the cGAS-STING pathway is activated through an indirect mechanism that involves the release of mitochondrial DNA into the cytoplasm [89, 90]. Although, much progress has been made to characterize the effect of microbial or exogenous glycans little is known about whether mammalian self-glycans also activate innate or adaptive immune responses in the settings of autoimmune diseases, especially in the context of fOS. One unexplored idea is that, like in the case of self-DNA, self-glycans could also be strong modulators of the innate immune system and be responsible for the development of autoimmune diseases like RVCL.

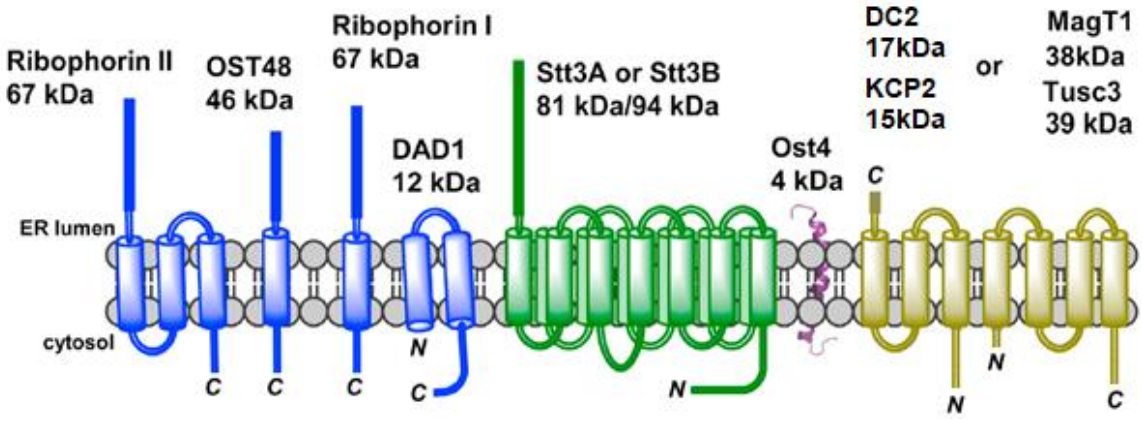

Figure 1.4: Diagram of OST's subunits.

DC2 and KCP2 are specific to STT3A and MagT1 and Tusc2 are specific to STT3B. RPN1, RPN2, DDOST, DAD1, and OST4 are shared subunits. Adapted from [70].

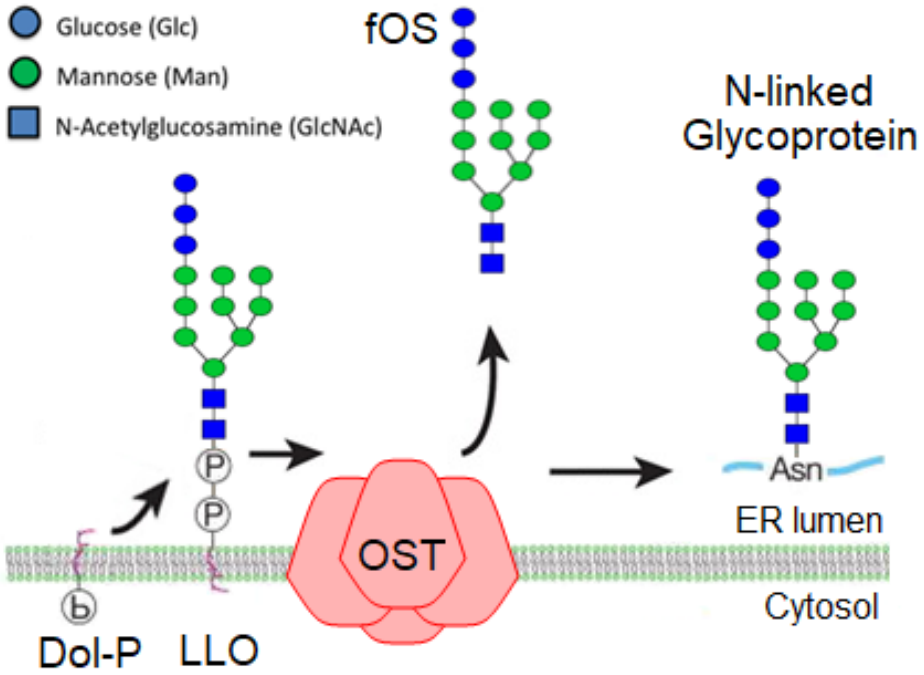

Figure 1.5: Summary of OST's catalyzed reactions.

OST catalyzes the addition of a fully assembled $Glc_3Man_9GlcNAc_2$ to N residues of newly synthesized glycoprotein or the hydrolysis of LLOs to generate fOS.

CHAPTER TWO: A NOVEL FUNCTION OF TREX1 ASSOCIATED WITH THE C-TERMINUS CONNECTS OLIGOSACCHARYLTRANSFERASE (OST) DYSREGULATION TO A HUMAN IMMUNE DISORDER

This chapter is a modification of the published article - A novel function of TREX1 associated with the C-terminus connects oligosaccharyltransferase dysregulation to immune disorders. Immunity September 15, 2015

Introduction

Mammalian cells have evolved negative regulators of innate immunity to protect against autoimmune activation. These negative regulators either remove immunogenic self-ligands that have accumulated in the wrong place (e.g. self-DNA in the cytosol) [91] or act upstream to prevent the production of self-ligands or their precursors (e.g. erroneous lipids or glycans with abnormal branching) [4, 92]. TREX1 (DNase III), a 3'→5' exonuclease is one of these negative regulators [93, 94]. As a single exon gene, TREX1 mutations are associated with a surprisingly broad spectrum of autoimmune and inflammatory phenotypes, including AGS, FCL, SLE, and RVCL [26]. The TREX1 protein has an exonuclease domain at the N-terminus and an ER tail-anchor insertion motif at the C-terminus [14, 31]. Recessive missense mutations in the TREX1 DNase domain (e.g. D18N and D200N [20, 28]) are predominantly associated with AGS, an early onset autoimmune disease with severe clinical presentations. In contrast, dominant fs mutations that truncate the C-terminus remain DNase-active (e.g. V235fs and D272fs [19, 31, 32]) and largely associated with RVCL (and in some cases SLE) with later onset and less severe disease (**Figure 1.3 and Table 1.1**) [26, 32]. In AGS the diminished TREX1 DNase activity leads to accumulation of self-DNA from replication debris, or

endogenous retroelements, likely contributing to sterile inflammation [10, 18]. However, such etiology does not explain disease caused by C-terminal frame-shift mutations. Here, I describe a new function of the TREX1 C-terminus for maintaining catalytic precision of the oligosaccharyltransferase (OST) complex. OST dysregulation caused by TREX1 C-terminal truncations lead to hydrolytic release of fOS from LLOs, as well as immune activation. The identification of distinct functions of the TREX1 N-terminal and C-terminal regions, with connection between OST and immune disorders in the latter case, provides a biochemical framework for understanding the two classes of TREX1 diseases and more specifically the effects of RVCL frame-shift (fs) truncations.

Experimental procedure

Cells, viruses, and mice

MEFs, BMDM and 293T cells have been described [93]. These cells were maintained in Dulbecco's modified Eagle's medium (DMEM) with 10% (v/v) heat-inactivated fetal bovine serum (FBS), 2 mM L-glutamine, 10 mM HEPES and 1 mM sodium pyruvate (complete DMEM) with the addition of 100 U/ml penicillin, 100 mg/ml streptomycin and cultured at 37°C with 5% CO2. EBV-transformed patients lymphoblasts from healthy control, R114H, D18N and TREX1 RVCL patients were maintained in RPMI with the same 10% FBS and supplements. Bone marrow-derived macrophages (BMDM) were generated from the indicated genotyped mice as described [94]. For *Trex1-/-* MEFs reconstituted with various TREX1 rescuing constructs, WT or mutant or truncated TREX1 were cloned into retroviral MRX-ibsr vector [95] (a kind gift from S. Akira)

using EcoRI and NotI sites. Retroviruses were packaged in 293T cells and used for infection of *Trex1-/-* MEFs followed by selection with blasticidin (Sigma).

Reagents and antibodies

TRI Reagent (Invitrogen) was used for RNA isolation. Lipofectamine 2000 (Invitrogen) was used for nucleic acid transfections. Antibodies used in this study include: anti-TREX1 (raised against the N terminus, generated in-house, rabbit, 1:2000), anti-STING (rabbit; 1:1,000 dilution; D2P2F;Cell Signaling), anti-TBK1 (rabbit; 1:1,000 dilution; D1B4; Cell Signaling), anti-cGAS (MB21D1) (rabbit; 1:200 dilution; HPA031700; Sigma), anti-Tubulin (mouse; 1:2,000 dilution; B-5-1-2; Sigma), anti-V5 (mouse; 1:5,000 dilution; R-960-25; Life Technologies), anti-Myc (rabbit; 1:2,000 dilution; sc-40 ac; Santa Cruz), secondary antibodies (1:4,000 dilution; BioRad) were used for immunoblot analysis according to standard protocols.

qRT-PCR analysis, qPCR array and fluorescence microscopy

RNA isolation and qRT-PCR analysis were performed as described previously [94]. The oligonucleotides used are *mGapdh* (TTCACCACCATGGAGAAGGC, GGCATCGACT GTGGTCATGA), *mCxcl10* (GGGATCCCTCTCGCAAGGACGGTCC, ACGCTTTCA TTAAATTCTTGATGGT), *hIFNb* (GAATGGGAGGCTTGAATACTGCCT , TAGCAA AGATGTTCTGGAGCATCTC), *hCXCL10* (GCATTAGTAATCAACCTGTTAATCC, TCCTTGCTAACTGCTTTCAGTAAAT) and *hGAPDH* (GCAAATTCCATGGCACCG

T, TCGCCCCACTTGATTTTGG). qRT-PCR array analyses of immune gene profiles were performed using custom ordered PCR array plates containing primer sets pre-aliquoted (Bio-Rad). For microscopy, cells grown on coverslips were fixed in 4% (wt/vol) paraformaldehyde and were permeabilized and stained by standard protocols. Samples mounted in Vectashield mounting medium containing DAPI (4,6-diamidino-2-phenylindole; Vector Laboratories) were imaged with a Zeiss Imager M2 fluorescence microscope equipped with AxioVision software. The following antibodies were used for immunostaining: anti-calnexin (Abcam, Ab4-100), anti-V5 (Invitrogen, R960-25), anti-Tubulin (Sigma, B-5-1-2), with Alexa Fluor 488 and 546 tagged secondary antibodies (Invitrogen, A21202, A21206, A10036, and A10040).

Fluorophore-assisted carbohydrate electrophoresis (FACE)

FACE analysis was used to assess total N-linked glycans, LLOs, and fOS. Cultured cells were disrupted in methanol, and the resulting suspensions were processed for FACE analyses as described [96]. A three-phase extraction process yielded an aqueous phase containing neutral fOS (purified further by deionization) and an interfacial layer which was extracted with chloroform: methanol: water (10:10:3) to separate soluble LLOs (which were subsequently depleted of neutral saccharides by ion-exchange chromatography) from insoluble N-linked glycoproteins. The glycan units of LLOs were released with weak acid, the N-glycans were released with N-glycosidase F (PNGase F) (C. meningosepticum, Prozyme) or Endoglycosidase H (S.picatus, New England Biolabs), and all glycan fractions were further purified with ion-exchange resins. All

glycans fractions were conjugated with 7-amino-1,3-naphthalenedisulfonic acid (ANDS) and resolved on an oligosaccharide profiling gel, with all loads normalized either to total protein or total cell number. Glucose oligomers (with four to seven glucosyl residues) and known LLO glycans were also loaded as standards. Fluorescently labeled oligosaccharides were detected with either a Biorad Fluor-S scanner and quantified with Quantity-One software, or a UVP Chemidoc-ItII scanner and quantified with VisionWorks software or ImageJ software.

In-vitro OST activity assay

SLO cells permeabilization was performed as described in [73]. Briefly, *Trex1-/-* and WT MEFs were grown to 80-90% confluency on 0.1% gelatin-coated plates to prevent loss of cells through the permeabilization process. Cells were subsequently washed with cold PBS twice and later incubated for 5 min with SLO (2 U/ml) on ice. Cells were then washed twice with cold PBS and incubated for 5 min in transport buffer (78 mM KCl, 4 mM $MgCl_2$ and 50 mM K-HEPES [pH 7.2]) at 37 ^{o}C followed by a 10 min incubation on ice in the same buffer to allow for the cytosolic content to diffuse out. Cells were next incubated for 60 min in the reaction buffer (400 uM UDP-Glc, 200 uM UDP-GlcNAc, 50 mM GDP-Man, 2 mM AMP, 10 ug/ml castanospermine (CSN) and 40 ug/ml deoxymannojirimycin (DMJM) in transport buffer) with either 50 uM of control peptide or acceptor peptide. After the incubation, cells were washed twice with cold PBS and disrupted by the addition of methanol for further FACE analysis.

Co-immunoprecipitation

Approximately $2x10^6$ of 293T cells were transfected with wild-type or mutant TREX1-V5 plasmids and c-Myc OST subunits (STT3A, DDOST, RPN1 or RPN2). Cells were subsequently collected, washed once with PBS, lysed in IP lysis buffer (20 mM Tris-HCl [pH 7.4], 150 mM NaCl, 0.5% NP-40 and 1x protease inhibitor mixture) and centrifuged at 20,000g for 20 min at 4 ^{o}C. The supernatants were mixed with primary antibody and Dynabeads Protein G (Life Technology) and incubated overnight at 4 ^{o}C. The following day, the beads were washed once with IP buffer, then, twice with high salt IP buffer (500 mM NaCl) and finally once with low salt IP buffer (50 mM). Immunocomplexes were eluted in 3x Sample buffer and boiled at 95 ^{o}C for 10 min. Samples were analyzed by immunoblotting.

Exonuclease activity assay

Exonuclease activity assay was performed as described in [97]. Briefly, approximately $1x10^6$ of 293T cells were transfected with wild-type or mutant TREX1-V5 plasmids. The post-nuclear supernatant isolated as described above was mixed with anti-V5 agarose beads (Bethyl) and incubated overnight at 4 ^{o}C. The next day the beads were washed twice with IP buffer and twice with low salt IP buffer. Washed beads were resuspended in 50 ul of DNase buffer (20 mM Tris-HCl [pH 7.5], 5 mM $MgCl_2$, 2 mM DTT, 100 ug/ml BSA and 0.5% NP-40). Either, 30-mer ssDNA oligo (TTTTTGGTTTGGTTTTGGCGGAGTTTTCGG) or 3' overhang 30-mer dsDNA (CGGTTTGGTTTTGGCGGAGTTTTCGGGTCGG, CCCGAAAACTCCGCCAAAAC

CAAACCGACCG) were allowed to intercalate SYBR Green II or SYBR Green I respectively (Life Technologies) for 30 min at 37 ^{o}C in DNase reaction buffer (20 mM Tris-HCl [pH 7.4], 5 mM $MgCl_2$, 2 mM DTT, 100 ug/ml BSA, 1/1200 SYBR Green and 10 ng/ul of DNA). A volume of 15 ul of TREX1 bound beads was mixed with 90 ul of DNase reaction buffer followed by real-time quantification of DNA/SYBR using a Synergy™HT microplate reader (Biotek) done in triplicates. Beads were later collected for detection of TREX1 expression by immunoblot analysis.

Statistical methods

Data are presented as the mean ± SEM. GraphPad Prism 6 was used for statistical analysis. Statistical tests performed were indicated in figure legend. *P< 0.05, **P< 0.01, ***P < 0.001, and ****P< 0.0001.

Results

TREX1 C-terminus plays a critical role in suppressing immune activation

Previous work demonstrated that *Trex1*-deficiency causes cell-intrinsic activation of ISGs in an IFN-independent manner [94], but whether TREX1 C-terminus had a role in immune activation remained to be elucidated (**Figure 2.1 A**). ISG array analysis on patient's lymphoblast carrying normal TREX1, the DNase dead R114H or the DNase active V235fs mutation revealed a unique signature associated with each mutant (**Figure 2.1 B**). The V235fs mutation truncates TREX1 C-terminus causing it to mislocalized throughout the cell without affecting its DNase function [32]. Analysis of six additional unrelated RVCL patients carrying the V235fs mutation and three healthy controls with

normal TREX1 confirmed the upregulation of the *CXCL10* ISG transcript (**Figure 2.1 C**). Since the V235fs is a dominant mutation, I confirmed the dual expressions of the full length and C-terminal truncated TREX1 in the RVCL patient cells. (**Figure 2.1 D**). I also found that human lymphoblasts are devoid of components of the cytosolic DNA sensing pathway such as cGAS and STING and that the lymphoblasts activate IFN expression in response to RNA, but not DNA, stimulation implying that the measured intrinsic immune response is not due to the activation of the cGAS-STING pathway (**Figure 2.1 E**). These data suggested that the TREX1 C-terminus have a key role in suppressing cell-intrinsic immune gene activation, independent of DNA sensing.

To examine the function of TREX1's C-terminus, *Trex1 -/-* mouse embryonic fibroblasts (MEFs) were reconstituted with full length human TREX1 (KO/TREX1) that localizes to the ER, a C-terminal truncation (KO/TREX1ΔTM) that localizes throughout the cell that mimics the RVCL causing V235fs mutation, TREX1's C-terminus fused to GFP that localizes to the ER but lacks the DNase domain (KO/GFP-TM), or GFP alone (KO/GFP) as a control (**Figure 2.2 A**). Full-length TREX1 strongly suppressed the overall expression of ISGs mRNA induced in *Trex1 -/-* cells. In contrast, V235fs only partially suppressed the ISGs expression (**Figure 2.2 B**). Conversely, the GFP-TM that localized to the ER reduced ISGs, suggesting that TREX1 C-terminus is functional by itself (without the DNase domain) for suppressing ISG induction and that both N-terminal DNase domain and C-terminal ER localization domain are required for fully suppressing ISG intrinsic activation in *Trex1 -/-* MEFs.

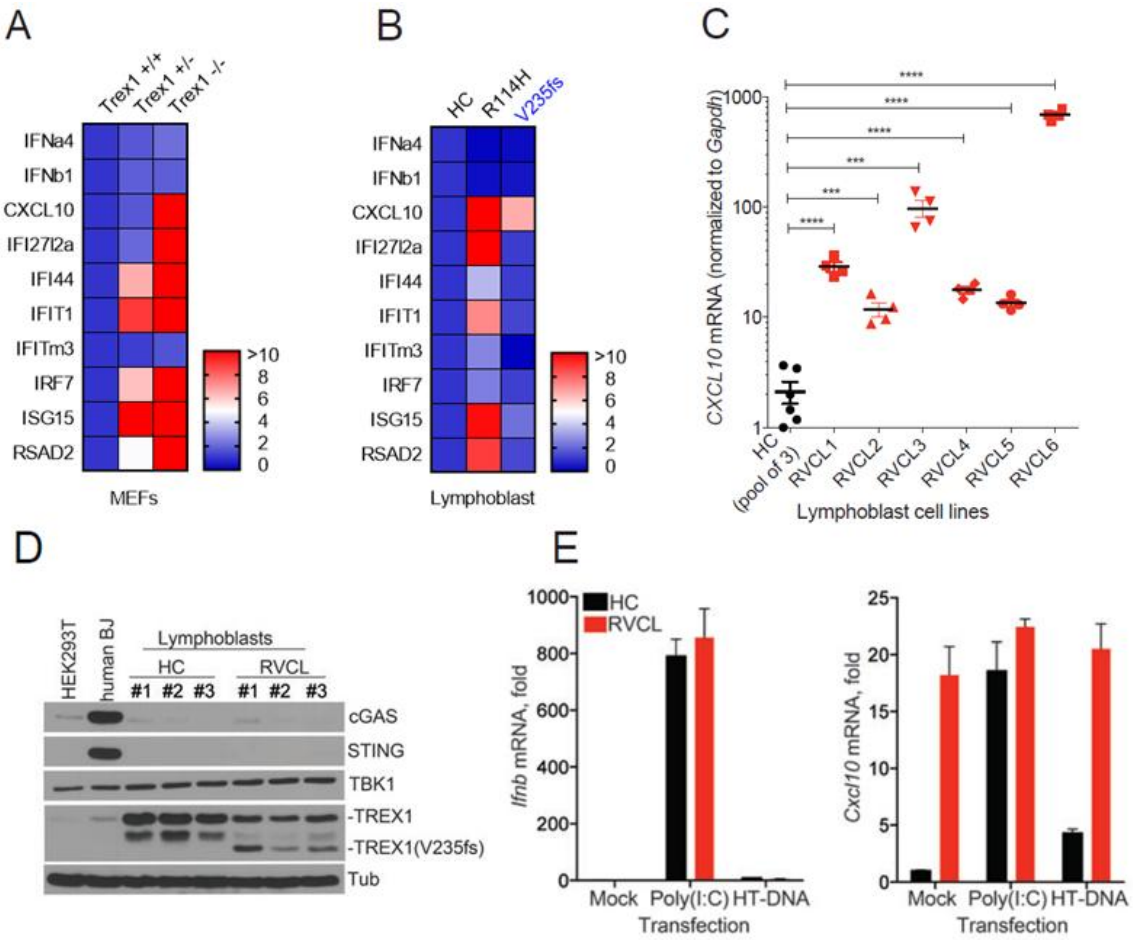

Figure 2.1: TREX1 C-terminus suppresses intrinsic immune activation.

(A) Heat map of qRT-PCR ISG profile of *Trex1 +/+, +/- and -/-* MEFs.
(B) Heat map of qRT-PCR ISG profile of HC, R114H (AGS) and V235fs (RVCL) human lymphoblasts.
(C) qRT-PCR analysis of CXCL10 in various HC and RVCL patients lymphoblast carrying the V235fs mutation.
(D) Immunoblot analysis of key proteins required for cytosolic DNA sensing and TREX1.
(E) qRT-PCR analysis of IFNb and CXCL10 in HC and RVCL patients lymphoblast after stimulation with Poly I:C (dsRNA) and HT-DNA (dsDNA).

I then proceeded to examine the exonuclease activity of all the variants to both dsDNA and ssDNA substrates *in vitro*. As previously shown the V235fs still retains the exonuclease activity (**Figure 2.2 C**) [32]. Collectively, the data with RVCL patient cells and *Trex1 -/-* MEFs rescue lines suggest that the TREX1 C-terminus is critical for suppressing cell-intrinsic immune activation, with a yet to be identified role in ER biology that may be the underlying cause of RVCL.

TREX1 interacts with the OST complex on the ER through the C-terminus

Previous work has implicated that the TREX1 C-terminus could interact with the OST complex in the ER [98]. The mammalian OST complex is composed of 7-8 subunits, with two alternative catalytic subunits (STT3A and STT3B) [99]. To investigate if any of the OST subunits could interact with TREX1, I co-expressed TREX1-V5 and various Myc-tagged OST subunits in 293T cells and assessed interactions by co-immunoprecipitation (co-IP). I observed a strong interaction between TREX1 and two subunits, DDOST and RPN1, but failed to detect interaction with two other subunits, RPN2 and STT3A (**Figure 2.3 A**). Immunoprecipitation of OST subunits was completely dependent upon the presence of TREX1 (**Figure 2.3 B**). Notably, the association of TREX1 with OST subunits RPN1 and DDOST is mediated by TREX1 C-terminus (**Figure 2.3 C-D**). These results demonstrate that TREX1 C-terminus is required for the interaction with OST on the ER.

OST activity is dysregulated in *Trex1-/-* MEFs

A major function of OST is to catalyze the transfers of the $Glc_3Man_9GlcNAc_2$ glycan to N residues within a tripeptide sequon of N-X-S/T in nascent proteins. However, under conditions such as ER stress, viral infection, or hereditary metabolic error, LLO hydrolysis by OST can be stimulated and the liberated fOS begin to accumulate in the ER lumen (**Figure 1.5**) [100, 101].The fOS are processed by the activity of local enzymes to produce smaller fragments that potentially span the entire lumenal space from ER to Golgi, cytoplasm, endosomes, and lysosomes [100]. To explore the biological role of the TREX1 C-terminus and its interaction with the OST, the products of OST catalysis (N-linked glycans and fOS) were examined by fluorophore-assisted carbohydrate electrophoresis (FACE), a quantitative technique for the assessment of steady-state levelsof several cellular saccharides [96]. Although no gross qualitative or quantitative changes in total cellular N-linked glycans was observed, *Trex1 -/-* MEFs contain a 6-fold increase of total fOS compared to wild-type cells and an approximate 40% reduction in the $Glc_3Man_9GlcNAc_2$-LLO pool (the precursors of fOS) (**Figure 2.4 A-C**). Steady-state LLO measurements are not expected to decrease to the same extent as the increase observed for fOS because LLOs are continuously re-synthesized while fOS accumulate. With an *in-vitro* OST assay, I showed directly that release of fOS by LLO hydrolysis was accelerated in *Trex1 -/-* MEFs, indicating OST dysfunction (**Figure 2.4 D**). Since ER localization of TREX1 is required for suppressing the elevated ISG signature in *Trex1 -/-* MEFs, I next examined whether TREX1 C-terminus could influence fOS release activity of the OST.

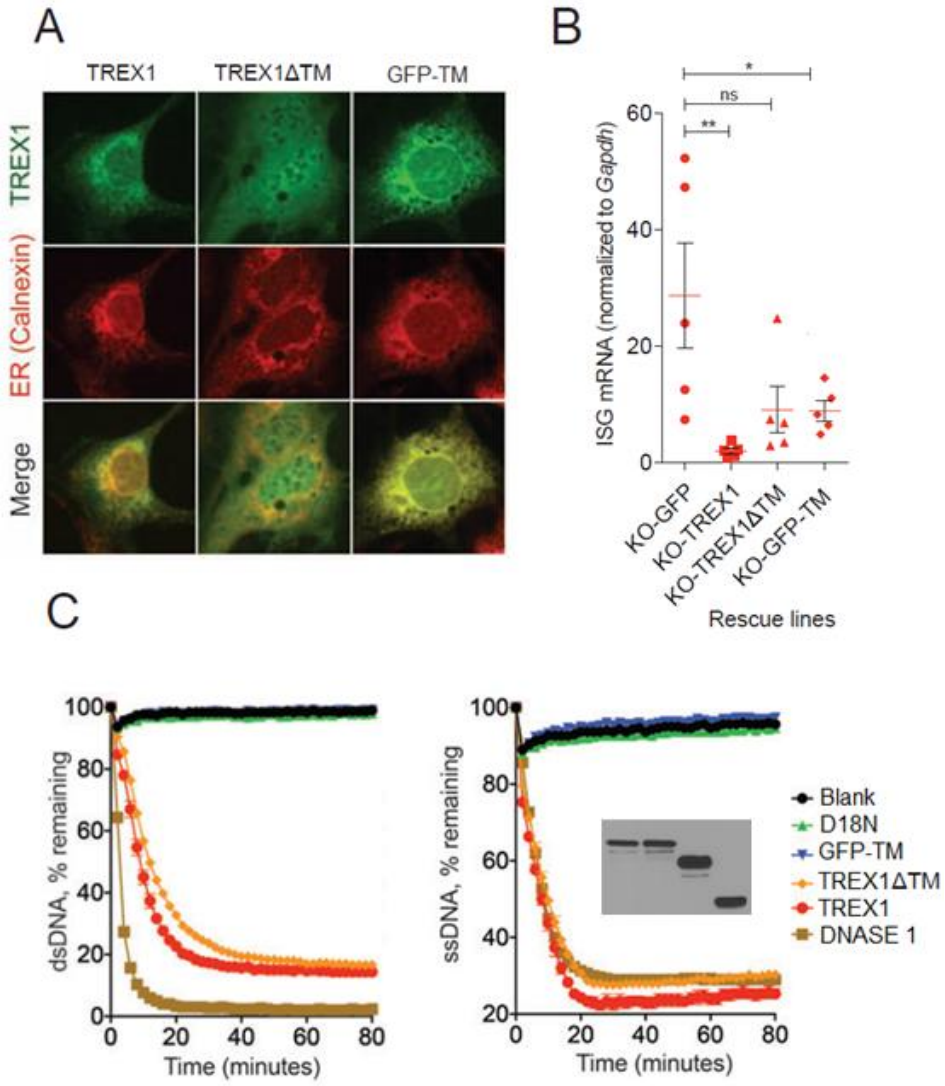

Figure 2.2: Truncation of TREX1 C-terminus causes mislocalization without affecting the DNase function

(A) Fluorescence microscopy analysis of the *Trex1* -/- MEFs rescue lines with the indicated construct. Staining included anti-V5 (Green), and anti-Calreticulin (Red, ER marker).
(B) ISG profile qRT-PCR analysis of the *Trex1* -/- MEFs rescue lines with the indicated construct. ISGs analyzed are *Cxcl10*, *Ifit1*, *Oasl2*, *Isg15* and *Irf7*.
human lymphoblasts.
(C) DNase activity analysis on the indicated isolated TREX1 variants by IP on 30-mer ssDNA and dsDNA substrate. Immunoblot represents isolation efficiency of TREX1-V5, D18N-V5, TREX1ΔTM-V5 and GFP-TM.

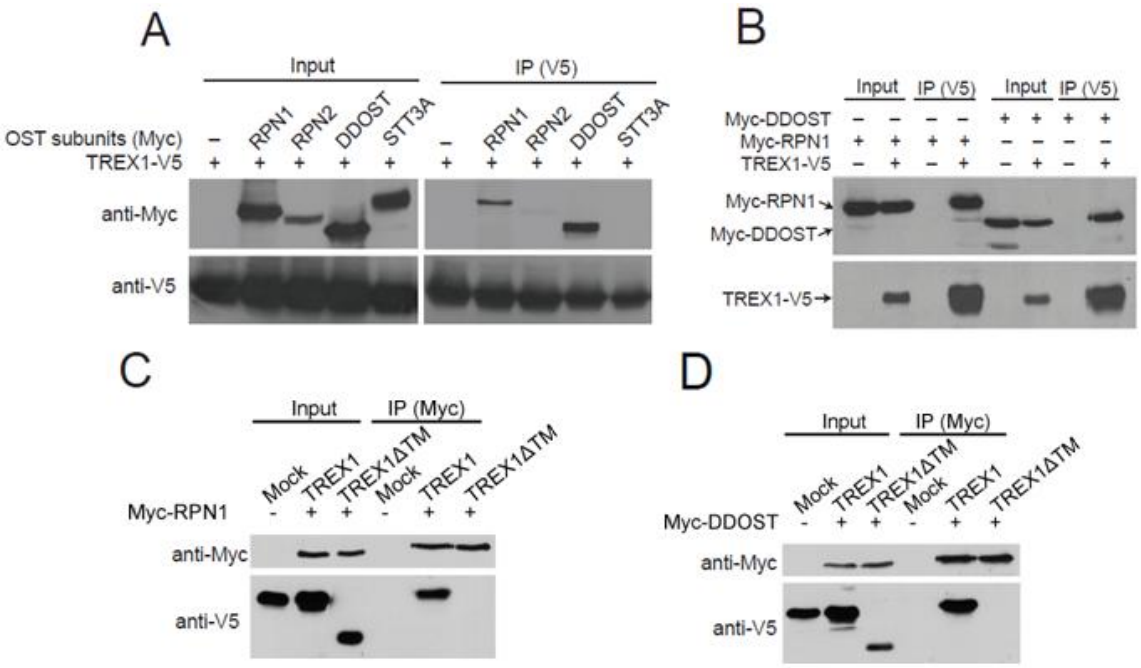

Figure 2.3: Truncation of TREX1 C-terminus causes mislocalization without affecting the DNase function

(A) Immunoblot of co-IP analysis of TREX1 interaction with Myc-OST subunits.
(B) Immunoblot of co-IP validation between TREX1:RPN1 and TREX1:DDOST interaction
(C) Immunoblot of co-IP analysis between TREX1 and TREX1ΔTM with RPN1. TREX1ΔTM-V5 does not interact with RPN1
(D) TREX1ΔTM-V5 does not interact with DDOST

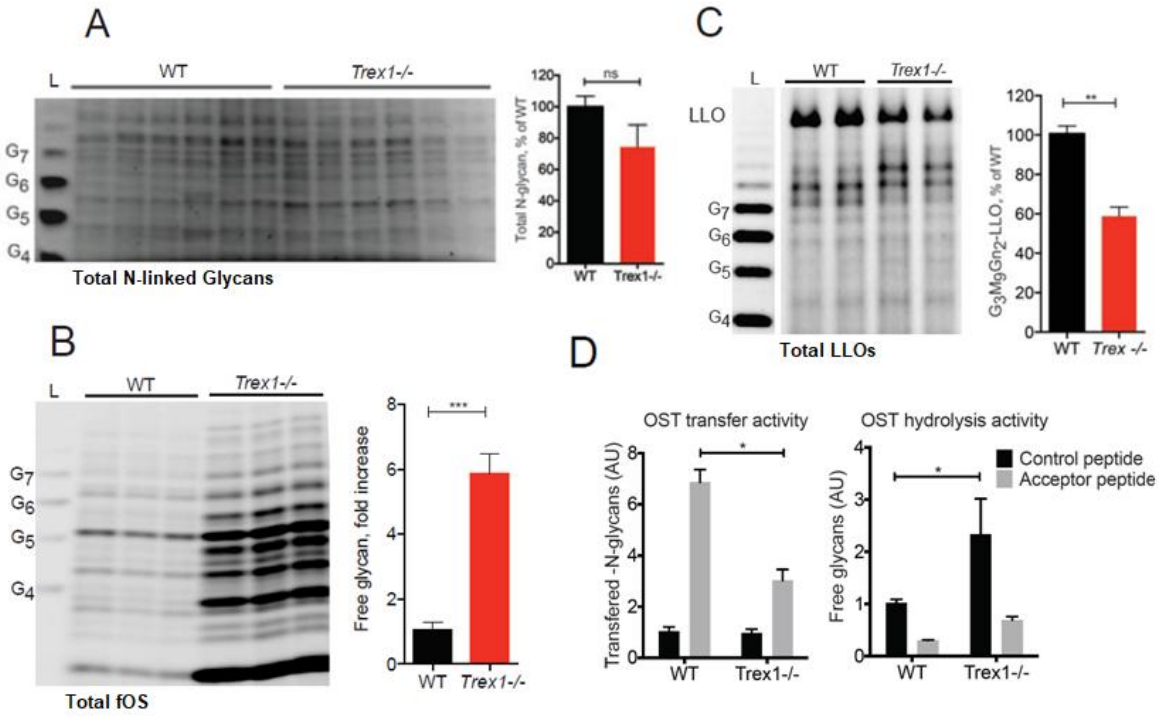

Figure 2.4: *Trex1* deficiency causes OST dysregulation

(A) FACE analysis of total N-glycans released from glycoproteins with PNGase F and quantification of the total signal from the gel
(B) FACE analysis of total fOS and quantification of the total signal from the gel
(C) FACE analysis of total LLOs and quantification of the total signal from the gel
(D) In vitro OST assay. SLO permeabilized MEFs were incubated with nucleotide sugars to produced LLOs. Acceptor peptides were incorporated to measure OST transfer activity or a control peptide to measure hydrolysis activity. The glycans from both sources were isolated and analyzed and quantified by FACE.

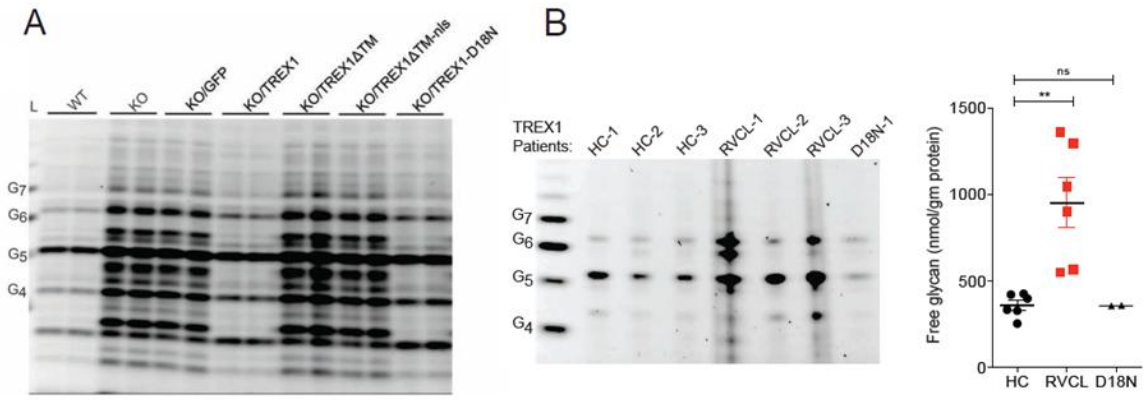

Figure 2.5: TREX1 C-terminus regulates OST preference to hydrolyze LLOs into fOS

(A) FACE analysis of total fOS from *Trex1 -/-* MEFs rescue line with the indicated constructs.
(B) FACE analysis of total fOS in HC and RVCL human patient lymphoblast and quantification.

While WT TREX1 strongly suppressed fOS accumulation in *Trex1-/-* cells, mislocalized but DNase-active TREX1ΔTM failed to reduce fOS (**Figure 2.5 A**). To further validate the role of the TREX1 C-terminus in OST dysregulation, patient lymphoblasts carrying the TREX1-V235fs mutation (associated with RVCL), the D18N mutation (DNase dead but ER-localized) and healthy controls were examined for fOS accumulation. All RVCL patient cells had elevated amounts of fOS compared to healthy controls and the D18N mutation (**Figure 2.5 B**). Thus, the TREX1 C-terminus has an unexpected DNase-independent function associated with ER glycan metabolism.

Products of OST dysregulation are immunogenic

I next asked whether the *Trex1-/-* fOS might contribute directly to the immune activation. To test this, fOS pools from WT and *Trex1-/-* MEFs were incubated with wild-type BMDMs and the expression of immune genes was measured by qRT-PCR array. The fOS pools from *Trex1-/-* MEFs, but not from WT cells, induced strong expression (5-20 fold increase) of many ISGs in wild-type BMDMs (**Figure 2.6 A**). Using BMDMs derived from specific knockout mice, I also determined that fOS induced immune activation is TBK1-dependent, but cGAS-STING-independent (**Figure 2.6 B**). I then became interested in understanding the structural composition of the *Trex1 -/-* derived fOS. Incubation of the *Trex1 -/-* fOS with ConA, a lectin that binds mannose and glucose, removed most of the structures suggests that the *Trex1-/-* MEF fOS are likely mannose containing glycans (**Figure 2.6 C**).

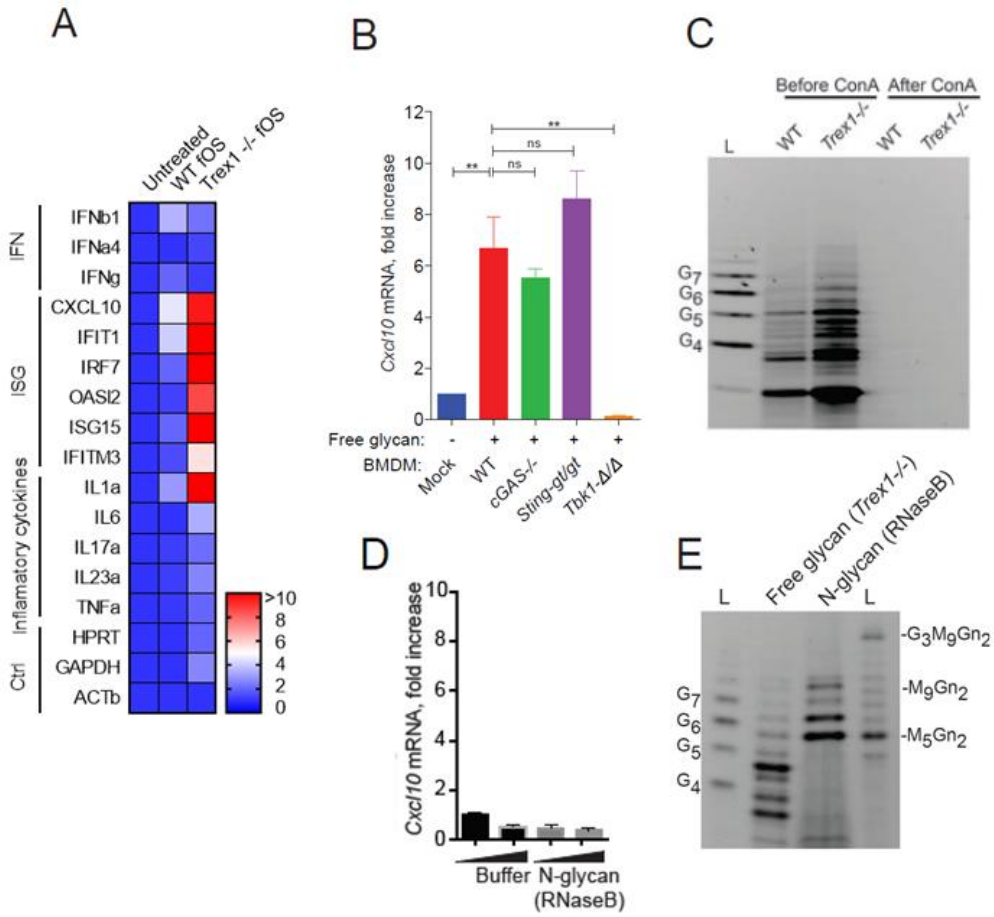

Figure 2.6: *Trex1* -/- fOS are immunogenic

(A) Heat map of qRT-PCR immune gene profile from BMDM stimulated with wild type or *Trex1* -/- fOS.
(B) qRT-PCR analysis of *Cxcl10* in various knockout BMDM as indicated after stimulation with *Trex1* -/- fOS.
(C) FACE analysis of total fOS from wild type or *Trex1* -/- before and after incubation with beads conjugated Con A.
(D) qRT-PCR analysis of *Cxcl10* generated by BMDM after stimulation with increasing concentrations (glycans isolated from 10 ug and 25 ug of RNase B) of N-glycans.
(E) FACE comparison of *Trex1* -/- fOS vs RNase B N-glycans.

This led to the hypothesis that perhaps high-mannose structures that include typical N-glycans could have immune activation properties. Surprisingly, typical $Man_{5-9}GlcNAc_2$ high-mannose N-glycan structures from RNase B after PNGase F treatment (consisting of at least 5 discrete species by FACE) did not stimulate ISGs when added to BMDM (**Figure 2.6 D**). This suggests that the bioactive *Trex1* -/- fOS is not a typical high-mannose containing structures. Indeed, I found that *Trex1* -/- free glycan pools contain smaller differing structures compared to the RNaseB N-glycans (**Figure 2.6 E**). Altogether, these findings suggest that fOS have the potential to induce the ISG signature commonly associated with TREX1 fs mutations and related diseases.

Discussion

The discordance between the genetics and clinical etiologies of AGS versus RVCL predicted a novel function of TREX1 associated with the C-terminus, and independent of DNase activity. By focusing on RVCL mutations (e.g. V235fs), I found that truncation of the TREX1 C-terminus dysregulates OST, which like TREX1 also localizes to the ER. This finding suggests that mutations disrupting different parts of TREX1 can cause clinically distinct phenotypes. I propose that TREX1 AGS (recessive) is caused by self-DNA sensing when both copies of the DNase domain are defective, consistent with a requirement for a catalytic function and severe clinical diseases in childhood. In contrast, TREX1 caused RVCL, is likely caused by OST dysregulation when one copy of TREX1 loses the C-terminus, disrupting its interaction with the OST complex and leading to a plethora of downstream effects. This is consistent with the

slower progression of RVCL disease, with typical onset in adulthood to older age [102]. Moreover, RVCL patient cells had strong induction of the ISG *CXCL10*. Since *CXCL10* inhibits angiogenesis and induces dissociation of newly formed blood vessels, elevated *CXCL10* could be a major contributor to systemic vasculopathy in RVCL patients [103, 104].

How might OST dysregulation lead to such immune phenotypes in RVCL? For C-terminal truncations of TREX1 typical of RVCL alleles, two robust biochemical effects on glycan metabolism were identified. First, dysregulated OST hydrolyzes LLOs at an abnormal rate. This reduces the steady-state concentrations of LLOs needed for N-linked glycosylation. Within the limits of sensitivity, I detected no global defects in total N-linked glycosylation in *Trex1* -/- cells. However, underglycosylation of a small subset of glycoproteins with unfavorable glycosylation acceptor sequons remains possible. Over an extended period, the absence of "glycan shielding" could lead to immune responses to bare epitopes that would lead to autoimmune response that targets self tissues. Second, accelerated LLO hydrolysis increased release of mannose-containing fOS. These "self" glycans could, for example, mimic surface glycans of certain pathogens that can be recognized by lectin receptors on macrophages and dendritic cells to activate immune responses. To support this notion, the fOS pools isolated from *Trex1* -/- MEFs do have immunogenic properties, although the exact immune pathway and glycan structure(s) being recognized require further investigation. These various hypotheses for OST dysfunction leading to immune disorders should not be mutually exclusive, and studying these aspects will be of immediate usefulness to further elucidate the exact nature of

glycan or glycosylation defects caused by TREX1 frame-shift mutations, and how they induce immune activation and the connection it holds with the development of TREX1 C-terminal frame-shift diseases.

Acknowledgments and contribution

I thank Min-Ae Lee-Kirsch (TU Dreston, Germany) for the TREX1 patient cells; Zhijian 'James' Chen for the *cGas* -/- mice, Russell Vance (UC Berkeley) for the *Sting* -/- mice, Ralf Brekken (UTSW) for the *Tbk1Δ/Δ* mice, Shizuo Akira (Osaka U) for the MRX-ibsr retroviral vector; James Koch for technical assistance; members of the Nan Yan lab, Mark Lehrman lab and Helbert C. Morse lab for discussions. This work was financially supported by the Rita C. and William P. Clements, Jr. Endowed Scholar Award from UT Southwestern, The John P. Perkins, Ph.D. Distinguished Professorship in Biomedical Science from UT Southwestern, the US National Institute of Health (AI098569, AR067135, GM038545) Alliance for Lupus Foundation, Welch Foundation, NSF graduate research fellowship (GRFP) and by the Intramural Research Program of the NIH, National Institute of Allergy and Infectious Diseases.

Maroof Hasan, Ph.D. contributed to figures 2.1 B, 2.2 A-B and 2.6 A-B, D.

Ningguo Gao, Ph.D. contributed to figures 2.4 B-C, 2.5 A-B and 2.6 C.

CHAPTER THREE: TREX1 PREVENTS THE ACCUMULATION OF AN ENDOGENOUS BIOACTIVE DISACCHARIDE ASSOCIATED WITH AUTOIMMUNITY

Introduction

The seminal work of immunologist Karl Landsteiner around 1900 identifying ABO blood groups led to the discovery that glycans can be powerful immunogens in humans. Later work demonstrated that innate immunity often recognizes glycans on pathogens to prevent infection. The mammalian innate immune system has evolved specific PRRs known as C-type lectins receptors (CLR) and Toll-like receptors (TLR) that recognize pathogenic bacteria and fungi glycans PAMPs [105, 106]. However, previous work has demonstrated that the PRRs immune surveillance network and other cell receptors can be erroneously activated by self-glycan ligands that accumulate in the presence of damaging mutations leading to chronic autoimmune and developmental diseases [4, 107, 108].

TREX1 mutations are associated with several autoimmune and autoinflammatory diseases [109]. TREX1 is an ER-anchored DNase with two independent functions, cytosolic DNA clearance function through the N-terminal DNase domain and glycan catabolism regulation function through the C-terminal ER domain [66, 110]. *Trex1 -/-* mice that lack both of TREX1 DNase and glycan functions, develop a severe early-onset systemic autoinflammatory disease with a short lifespan of 2-3 months. In contrast, inactivating either the DNase or glycan function alone in mice leads to a less severe disease. For example, the *TREX1-D18N* mutant mice that disrupt only the DNase activity

develop similar disease phenotypes as *Trex1 -/-* but significantly less severe and these mutant mice survive over 1 year of age [98]. On the other hand, the *TREX1-V235fs* mutant mice that remain DNase-active but losses the glycan regulatory function develop autoimmune-prone state by producing immunogenic fOS and autoantibodies against self-glycoprotein antigens [65, 110].

The glycan regulatory function of TREX1 is associated with its C-terminus. Frame-shift mutations that truncate TREX1 C-terminus are associated with dominant late-onset immune disorders such as SLE and RVCL [32, 65, 66]. Loss of TREX1 C-terminus dysregulates the mammalian OST's activity leading to accumulation of fOS in the cell [32]. These intracellular enriched fOSs can activate ISGs in macrophages [110]. However, the identities of the bioactive fOSs and the immune pathway that senses them remain elusive. Here, I identified a major bioactive mammalian fOS, Man(β1-4)GlcNAc a disaccharide associated with *TREX1* chronic diseases. I defined the structural requirement for bioactivity as well as biogenesis and immune sensing pathways for this fOS.

Experimental procedure

Cells, antibodies, and reagents

MEFs, RAW264.7, and BMDM were maintained in Dulbecco's modified Eagle's medium (DMEM) with 10% (v/v) heat-inactivated fetal bovine serum (FBS), with 2 mM L-glutamine, 10 mM HEPES and 1 mM sodium pyruvate (complete DMEM) with the addition of 100 U/ml penicillin, 100 mg/ml streptomycin and cultured at 37°C with 5%

CO_2 . BMDM were generated as described in [94]. The inhibitors used in this study include ACM (1 uM, Santa Cruz), Z-VAD-fmk (30 uM, BD), Q-VD-OPh (50 uM, BD), CSN (100 uM, Sigma-Aldrich), Kif (100 uM, Sigma-Aldrich), Swain (10 uM, Tocris), Clq (10 uM, Sigma-Aldrich), Compound II (1 uM, UTSW), BX759 (1 uM, Invivogen), Ruxolitinib (1 uM, Invivogen), Dexamethasone (100 nM, Invivogen), TPCA1 (1 uM, Sigma-Aldrich). The ligands used to stimulate macrophages are GalGlcNAc (Sigma-Aldrich), Mannose (Sigma-Aldrich), GlcNAc (Sigma-Aldrich), Manα1-CH3 (Sigma-Aldrich), Manβ1-CH3 (Santa Cruz), LPS (100 ng/ml, Invivogen), htDNA (1 ug, Sigma-Aldrich), Chitosan (10 ug/ml, Invivogen), Chitin (10 ug/ml, Sigma-Aldrich), Curdlan (10ug/ml, Invivogen), Zymosan (10 ug/ml, Invivogen), Le^X (10 ug/ml, Sigma-Aldrich), β-Mannan (10 ug/ml, Megazyme), α-Mannan (10ug/ml, Sigma-Aldrich), Furfurman (10 ug/ml, Invivogen), Lipoarabinomannan (LAM) (1 ug/ml, Invivogen), Cord factor (1 ug/ml, Invivogen).

Glycan isolation and Fluorophore-assisted carbohydrate electrophoresis (FACE)

FACE analysis was done as described in [110]. Briefly, MEFs were plated at 75 to 80% confluency and transfected (RNAiMAX, Thermo Fisher) with the ENGase siRNA (Sigma-Aldrich) or treated with inhibitors for 24 hrs and disrupted with methanol the next day. The methanol disrupted cells or the lyophilized media were subject to a three-phase (aqueous, interface and organic) extraction which yields an aqueous fraction containing neutral fOS (purified further by ion exchange chromatography) and an interface fractions which was extracted with chloroform: methanol: water (10:10:3) to

isolate total proteins that was used to normalize the loading of labeled fOS to gels, immunoblotting and for the isolation of N-linked glycans by PNGase F digestion (New England Biolabs). Isolated glycans (fOS and digested N-glycans) were conjugated with 7-amino-1,3-naphthalenedisulfonic acid (ANDS, AnaSpec) and subjected to reductive amination with $NaBH_3CN$ (Sigma-Aldrich) (1:1) for 24 hrs at 37^{o}C. Labeled fOS and digested N-glycans were resolved on an oligosaccharide profiling gel, with 10 pmol of glucose oligomers (ranging from four to seven glucosyl residues) and 100 pmol of $Man_9GlcNAc_2$ (Sigma-Aldrich), $Man_5GlcNAc_2$ (Sigma-Aldrich), $Man_2GlcNAc$ and ManGlcNAc as standards. Gels were visualized using a UVP Chemidoc-ItII scanner and quantified with VisionWorks software.

RNA isolation, RNA sequencing, and quantitative RT-PCR

Approximately $0.5x10^6$ of RAW264.7 cells or BMDM were seeded in a 12 well plate and stimulated the next day with the indicated ligands for 24 hrs by addition to the media or permeabilization as described in [110] and [111] respectively. Total RNA was subsequently isolated with TRI reagent (Sigma-Aldrich) as indicated by the manufacturer and cDNA was synthesized with iScript cDNA synthesis kit (Bio-Rad) and analyzed using a Bio-Rad CFX qRT-PCR. PCR array of immune gene groups was performed using PrimePCR Array plates using iTaq Universal SYBR Green Supermix (Bio-Rad). The oligonucleotides used in this study are *mGapdh* (TTCACCACCATGGAGAAGGC, GGCATCGACTGTGGTCATGA), *mCxcl10* (GGGATCCCTCTCGCAAGGACGGTCC, ACGCTTTCATTAAATTCTTGATGGT), *mIfit1* (GAACCCATTGGGGATGCACAAC

CT, CTTGTCCAGGTAGATCTGGGCTTCT), *mCxcl2* (CGGTCAAAAAGTTTGCCT TG, TCCAGGTCAGTTAGCCTTGC) and *mEngase* (ACCTCTGAGCCCTGAATGAA , TTCAATGTAGCCCTGGAACC). RNA-Seq was performed as previously described in [94]. Pathway analysis was done using the IPA software (Qiagen).

Gel-filtration chromatography and mannosidase digestion

A 0.5 x 20 cm column was packaged with 6 ml of a BioGel P4 resin (Bio-Rad) and conditioned with a 25 mM NH_4CH_3COO (Sigma-Aldrich) buffer. 10 nmol of the total fOS were loaded into the column and 24 fractions were collected and dried in vacuum. 10% of each fraction was collected for FACE analysis and the remaining 90% was divided in half and used for macrophage stimulation in biological duplicates. For the mannosidase digestion, 10 nmol of fOS or the synthetic ManGlcNAc disaccharide were treated with 40 U of α1-6 mannosidase (New England Biolabs) and 32 U of α1-2, 3 mannosidase (New England Biolabs) or with 40 U of β1-4 mannosidase (Glyko) for 24 hrs at 37^{o}C. Enzymes were removed by mixing with 3x ethanol and centrifugation. Supernatants were dried in vacuum. 10% of the digested product was collected for FACE analysis and the remaining 90% was divided in half and used for macrophage stimulation in biological duplicates.

Results

Identification of a bioactive mammalian disaccharide

Previously, it was shown that the fOS pools isolated from *Trex1* -/- cells was immunogenic when incubated with macrophages [110]. To determine the specific glycan

structure(s) that are responsible for immune activation, size exclusion fractionation of the *Trex1 -/-* fOS pool was performed and bioactivity was examined for each fraction on macrophages. In addition, each fraction was analyzed by FACE. The majority of the fOS eluted at fraction #8-11 with larger structures eluting in fraction 8, medium structures in fraction 9 and smaller structures in fractions 10 and 11 (**Figure 3.1 A**). To test bioactivity, each fraction, as well as the non-fractioned fOS pool, were incubated with RAW264.7 cells (a mouse macrophage cell line, digitonin-permeabilized) for 24 hrs and *Cxcl10* mRNA was measured by qRT-PCR as a readout for immune activation [110]. Fraction 10 stimulated the strongest immune response that was comparable to the non-fractionated fOS pool. Fraction 8 and 11 also appear to be immunogenic but less potency when compared to fraction 10 (**Figure 3.1 B**).

FACE analysis of the wild-type vs the *Trex1 -/-* MEFs fOS highlighted the differences in the amount and structures present in the *Trex1 -/-* fOS pool (**Figure 3.2 A**). To gain detailed structural information on these fOSs, the wild-type and *Trex1 -/-* fOS pool was analyzed by dual-gradient reversed-phase HPLC and mass spectrometry. This revealed that the most enriched fOS structures in *Trex1 -/-* MEFs are small oligomannose structures with one terminal GlcNAc ($Man_{1-4}GlcNAc$) at approximately 20 folds higher than wild-type (**Figure 3.2 B and Table 3.1**). Interestingly, these small glycan species match well with the predicted size of the fOSs observed in fraction 10. A comparison by FACE between fraction 10 and a chemically synthesized disaccharide (ManGlcNAc), trisaccharide ($Man_2GlcNAc$), and larger high-mannose glycans ($Man_5GlcNAc_2$ and $Man_9GlcNAc_2$, Sigma) standards, confirmed that the two major fOS species in fraction

10 are a disaccharide (ManGlcNAc) and a trisaccharide ($Man_2GlcNAc$) (**Figure 3.2 C**). To examine if any of these two fOS structures contribute to bioactivity, RAW264.7 cells were incubated with increasing concentrations of the synthetic $Man_2GlcNAc$ and ManGlcNAc and *Cxcl10* mRNA expression was measured. Only ManGlcNAc induced *Cxcl10* expression in a dose-dependent manner but not $Man_2GlcNAc$ (**Figure 3.2 D**). Together, these experiments suggest that the ManGlcNAc disaccharide is a bioactive glycan that is highly enriched in the *Trex1 -/-* fOS pool as well as in fraction 10.

Bioactivity is specific to only the Man(β1-4)GlcNAc stereoisomer

The Jack Bean (JB) Mannosidase (α mannosidase) digestion of the *Trex1 -/-* fOS pool implied that the nature of the ManGlcNAc disaccharide glycosidic bond is a β1-4 linkage (**Figure 3.2 B**). To confirm that the disaccharide present in the *Trex1 -/-* fOS is Man(β1-4)GlcNAc synthetic Man(α1-4)GlcNAc and Man(β1-4)GlcNAc standards were generated and compared by FACE to the fOS pool. FACE analysis confirmed that only Man(β1-4)GlcNAc, but not Man(α1-4)GlcNAc, co-migrate with the disaccharide band in the *Trex1 -/-* fOS pool (**Figure 3.3 A**). To further determine if the ManGlcNAc β1-4 linkage is critical for the bioactivity, cellular *Trex1 -/-* fOS pool and the synthetic Man(β1-4)GlcNAc disaccharide were treated with an α- or β-mannosidase that selectively cleaves α- or β-mannosylated linkages, respectively, and assayed the digested glycan structures by FACE and bioactivity by stimulating macrophages and measuring *Cxcl10* expression.

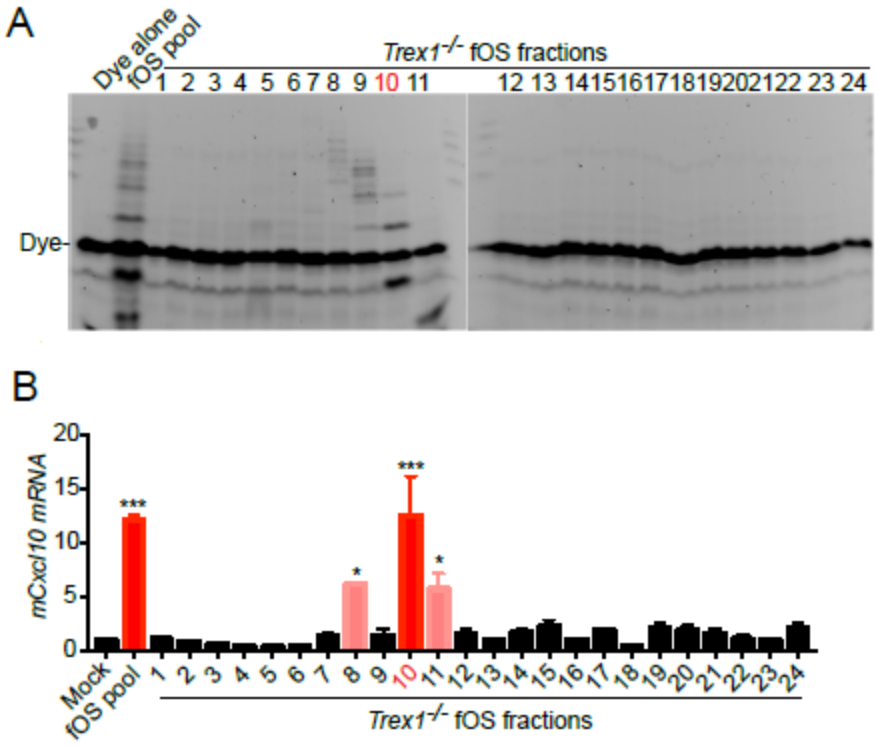

Figure 3.1: Size exclusion fractionation of the immunogenic *Trex1* -/- fOS.

(A) FACE analysis of all the collected fractions. Glycans eluted in fractions 7-11.
(B) qRT-PCR analysis of *Cxcl10* in RAW264.7 cells after stimulation with the various *Trex1* -/- fOS fractions.

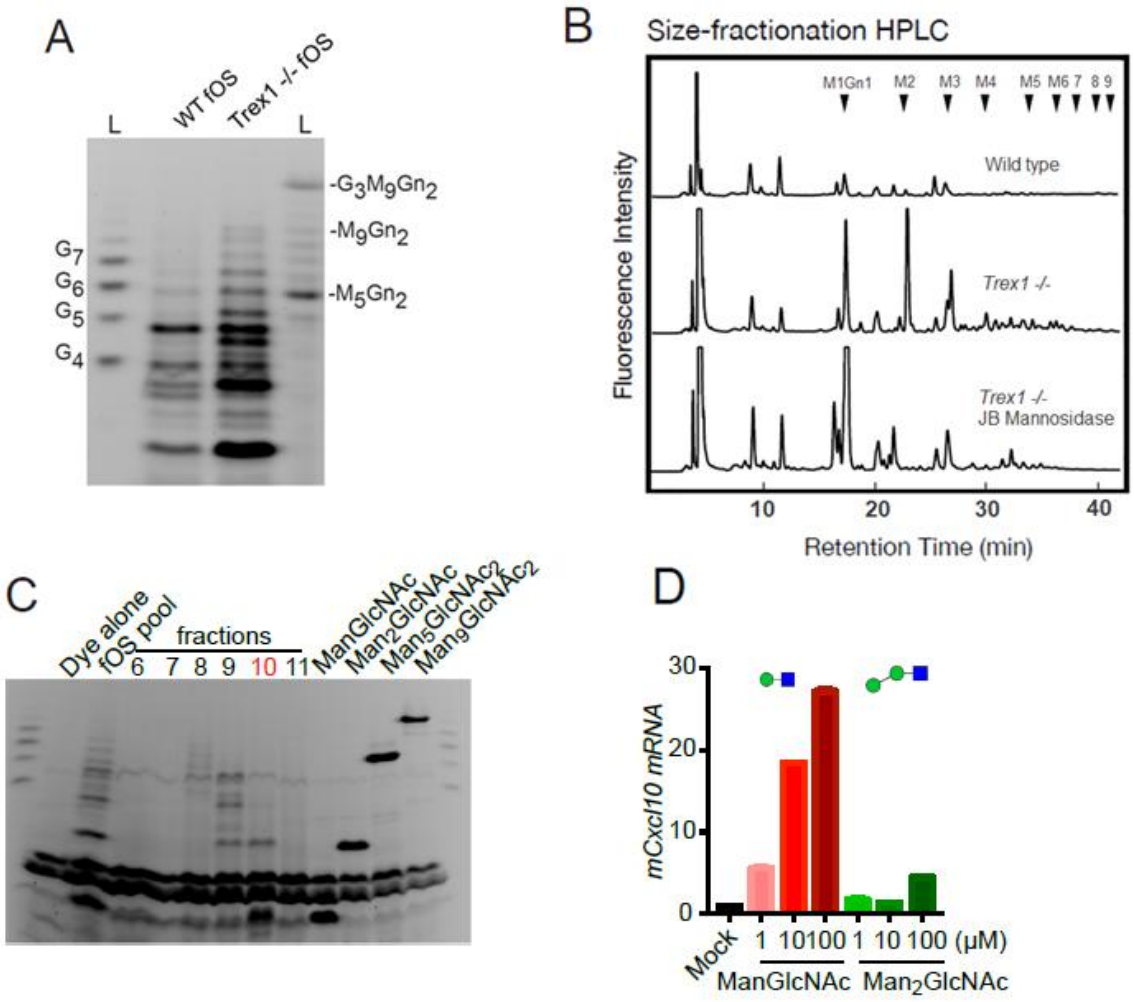

Figure 3.2: Trex1 -/- fOS is enriched with small oligomannose structure.

(A) FACE analysis of total fOS in wild type and *Trex1 -/-* MEFs. Note the enrichment of differing structures.
(B) Size fractionation HPLC analysis of the fOS pool from wild type and *Trex1 -/-* MEFs. *Trex1 -/-* MEFs accumulate small glycan structures that are sensitive to JB mannsoidase digestion except the ManGlcNAc disaccharide.
(C) FACE analysis of FACE a *Trex1 -/-* fOS fractions 6-11 and indicated standards. Fraction 10 contains a tri and disaccharide.
(D) qRT-PCR analysis of *Cxcl10* in RAW264.7 stimulated with increasing concentrations of the trisaccharide ($Man_2GlcNAc$) and the disaccharide (ManGlcNAc).

Glycan Abbreviations	Glycan isoforms	Glycan Structures	Amount(pmol/g cells) Wild type	*Trex1 -/-*
ManGlcNAc	M1A		448	2391
$Man_2GlcNAc$	M2A	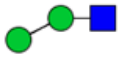	113	3299
$Man_3GlcNAc$	M3D		50	1001
$Man_4GlcNAc$	M4D	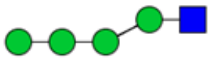	26	92
	M4E	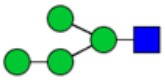	3	178

Table 3.1: Summary of enriched structures in the *Trex1* -/- fOS pool.

The main enriched structures in the Trex1 -/- fOS pool are glycans with 1 to 4 mannose and a single GlcNAc.

α-mannosidase treatment removed most of the high molecular weight fOSs from the *Trex1 -/-* fOS pool but had no effect on the disaccharide band in the cellular fOS pool or synthetic Man(β1-4)GlcNAc disaccharide (**Figure 3.3 B**). In contrast, β-mannosidase digested the synthetic ManGlcNAc disaccharide as well as the disaccharide band in the fOS pool (**Figure 3.3 B**). I also found that β-mannosidase treatment significantly reduced bioactivity of the fOS pool and of the synthetic ManGlcNAc disaccharide, whereas α-mannosidase treatment had no effect (**Figure 3.3 B**). The residual activity in β-mannosidase-treated fOS pool suggests that there are other immunogenic fOS species also present in the pool, consistent with our observation of bioactivity in multiple fractions from the fOS pool (**Figure 3.1 B**).

Disaccharides glycosidic bonds can exist in two anomeric conformations, α or β. I then asked if bioactivity was specific to only the Man(β1-4)GlcNAc or can the Man(α1-4)GlcNAc be bioactive as well. Remarkably, only Man(β1-4)GlcNAc, but not Man(α1-4)GlcNAc, stimulated *Cxcl10* and *Ifit1* (two ISGs) expression when incubated with RAW267.4 cells, suggesting that the bioactivity requires the β1-4 linkage (**Figure 3.4 A**). Next, I compared Man(β1-4)GlcNAc bioactivity to other disaccharide diastereomers that also contain the β1-4 linkage, such as Glc(β1-4)GlcNAc and Gal(β1-4)GlcNAc (**Figure 3.4 B**). Again, only Man(β1-4)GlcNAc disaccharide was immunogenic (**Figure 3.4 B**). I also examined the bioactivity of monosaccharides such as Man, GlcNAc, α-methyl mannose (Manα1-CH_3) and β-methyl mannose (Manβ1-CH_3) (**Figure 3.4 C**). None of the monosaccharides was able to stimulate *Cxcl10* expression to the extent of the Man(β1-4)GlcNAc disaccharide in macrophages.

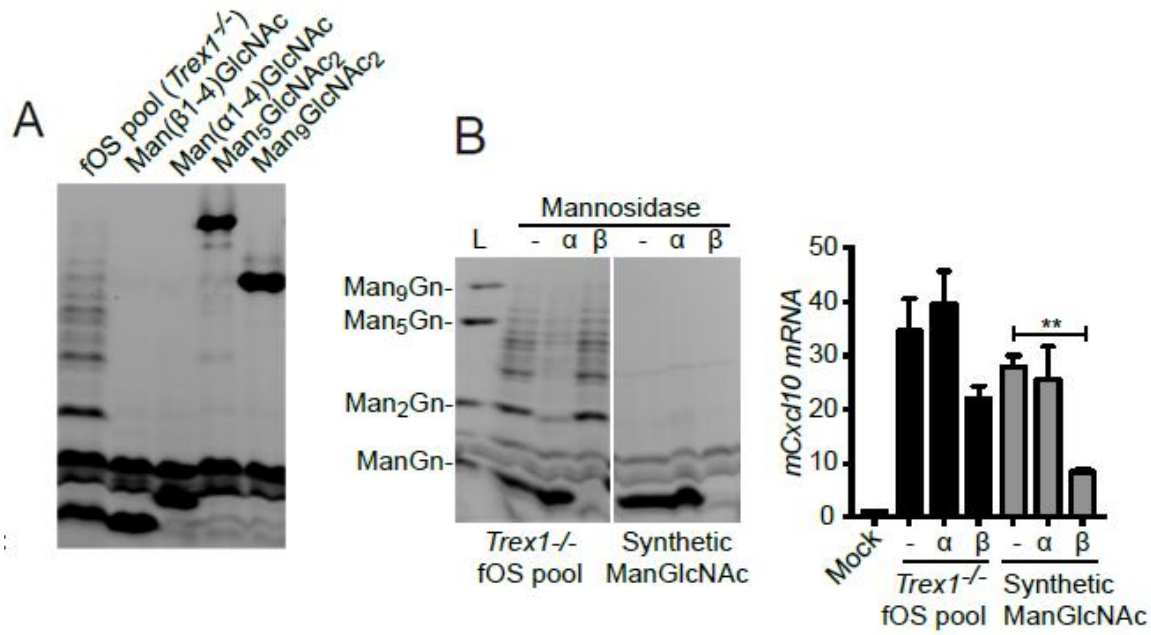

Figure 3.3: The Man(β1-4)GlcNAc disaccharide is bioactive

(A) FACE analysis of the *Trex1* -/- fOS and the Man(β1-4)GlcNAc and Man(α1-4)GlcNAc standards. The disaccharide in the Trex1 -/- fOS pool co-migrates with the Man(β1-4)GlcNAc standard.

(B) FACE analysis of the *Trex1* -/- fOS pool and the synthetic Man(β1-4)GlcNAc disaccharide treated with an α-mannosidase or a β-mannosidase. The treated products were used to stimulate RAW264.7 cells and *Cxcl10* was analyzed by qRT-PCR. β-mannosidase treatment of the Man(β1-4)GlcNAc disaccharide suppressed the immunogenicity associated with it.

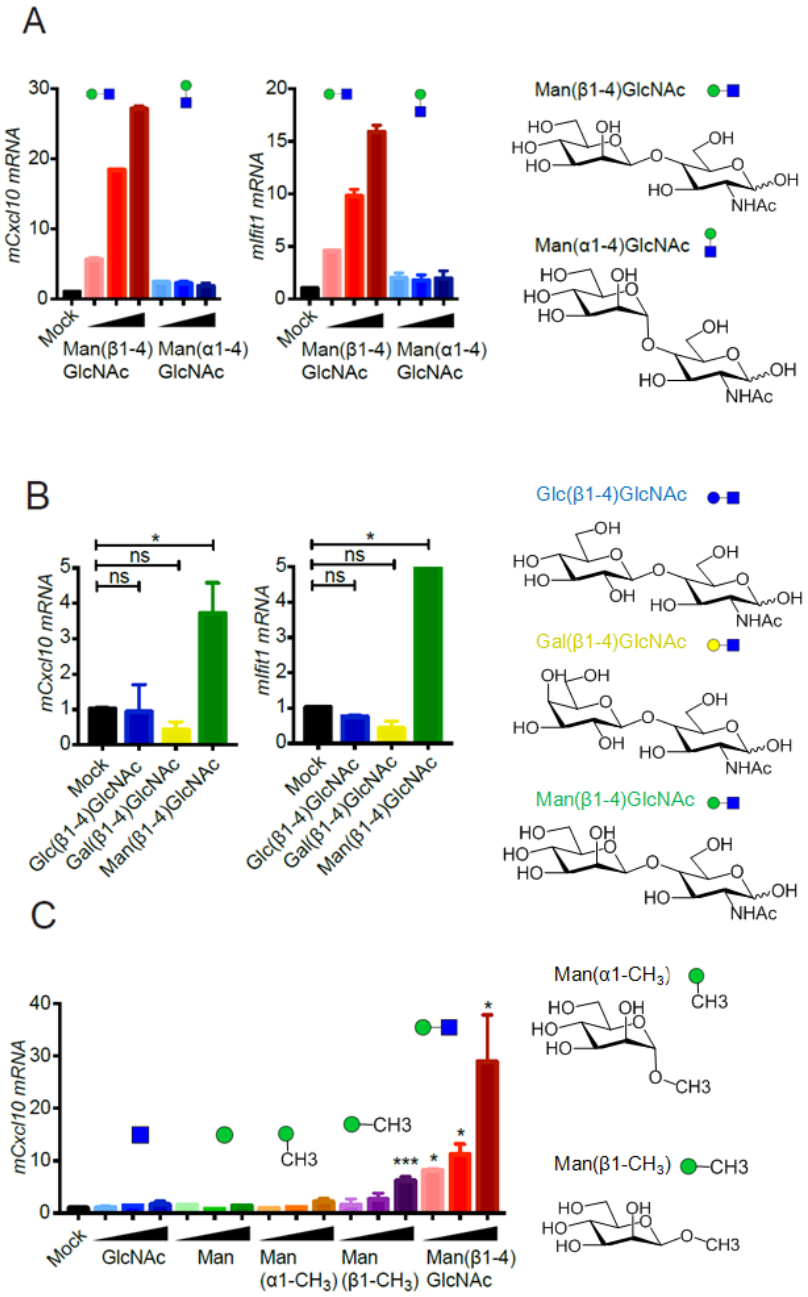

Figure 3.4: Bioactivity is specific to the Man(β1-4)GlcNAc disaccharide

(A) qRT-PCR analysis of *Cxcl10* and *Ifit1* in RAW264.7 stimulated with increasing concentrations of Man(β1-4)GlcNAc and Man(α1-4)GlcNAc.
(B) qRT-PCR analysis of *Cxcl10* and *Ifit1* in RAW264.7 stimulated with three different disaccharides as indicated.
(C) qRT-PCR analysis of *Cxcl10* in RAW264.7 stimulated with increasing concentrations of Man, GlcNAc, Man(α1-CH_3), Man(β1-CH_3) and (Man(β1-4)GlcNAc.

Manβ1-CH_3 had some activity but required 100x higher concentration than Man(β1-4)GlcNAc (**Figure 3.4 C**). Together, these results identify Man(β1-4)GlcNAc as a bioactive mammalian self-glycan and that both the Man and the GlcNAc, as well as the β1-4 linkage, are important for bioactivity.

Man(β1-4)GlcNAc disaccharide activates a TBK1- and NF-κB-dependent immune signaling.

To obtain a more comprehensive understanding of the immune response activated by the synthetic Man(β1-4)GlcNAc disaccharide or intracellular *Trex1 -/-* fOS pool RNA-seq was performed on stimulated RAW267.4 macrophages. I found that 2,044 genes were differentially expressed after the Man(β1-4)GlcNAc disaccharide stimulation, 1131 genes after fOS pool stimulation, and 760 genes that are shared between the two. Ingenuity pathways analysis (IPA) on the 760 shared genes revealed top pathways involved in T helper cell differentiation, antigen presentation, and T cell activation (**Figure 3.5 A**). Chemokines play an important role in connecting the bridge between innate immune activation and recruitment, activation and differentiation of the adaptive immune system [112, 113]. I seek to investigate the activation profile of several groups of immune genes including IFN, ISGs, inflammatory genes and chemokine genes by qRT-PCR. The Man(β1-4)GlcNAc disaccharide and fOS pool stimulated expression of IFN and ISGs as previously shown (**Figure 2.6 A**), although they are more potent at inducing expression of chemokine genes (**Figure 3.5 B**) [110]. To confirm the immune activity in primary cells, I treated wild-type BMDM with the Man(β1-4)GlcNAc disaccharide and

observed a dose-dependent increase in the expression of chemokine genes *Cxcl10* and *Cxcl2* (**Figure 3.5 C**).

Next, I sought to identify which immune pathway was sensing the Man(β1-4)GlcNAc disaccharide. A panel of knockout mice that are deficient in genes required for key immune signaling pathways was chosen. TBK1 is a protein kinase required by cytosolic nucleic acid sensing pathways (e.g. cGAS-STING-TBK1 pathway and RIG-I-MAVS-TBK1 pathway) as well as sensing of fOS and other types of glycoconjugates (e.g. Galectin-8-TBK1 [114]) (**Figure 2.6 B**). IFN receptor 1 (IFNAR1) is required for type I IFN response. IRF3 and IRF7 are key transcription factors for IFN and ISG expression. Myd88 and Trif are adaptor proteins required for TLR signaling. The response to the Man(β1-4)GlcNAc disaccharide on BMDMs derived from wild-type, *Tbk1-Δ/Δ*, *Ifnar1 -/-*, *Irf3/7 -/-*, *Myd88/Trif -/-* and *Mavs -/-* mice were compared and noticed that the wild-type, *Ifnar1 -/-*, *Myd88/Trif -/-* and *Mavs -/-* responded to the Man(β1-4)GlcNAc disaccharide stimulation to a similar level while *Tbk1-Δ/Δ* and *Irf3/7 -/-* completely ablated or partially suppressed immune activation, respectively (**Figure 3.6 A**). To corroborate and extend on these findings, wild-type BMDMs were pretreated with TBK1 inhibitors (BX795 and compound II), NF-κB inhibitors (TPCA-1 and dexamethasone), and JAK1/2 inhibitor ruxolitinib (also inhibits IFN receptor 1 signaling), then stimulated with the Man(β1-4)GlcNAc disaccharide. TBK1 and the NF-κB inhibitors suppressed the activation of *Cxcl10* and *Cxcl2* while ruxolitinib had no effect (**Figure 3.5 B**). Taken together, these studies suggest that the Man(β1-4)GlcNAc disaccharide activates a TBK1- and NF-κB-dependent but IFN- and TLR-independent immune response pathway.

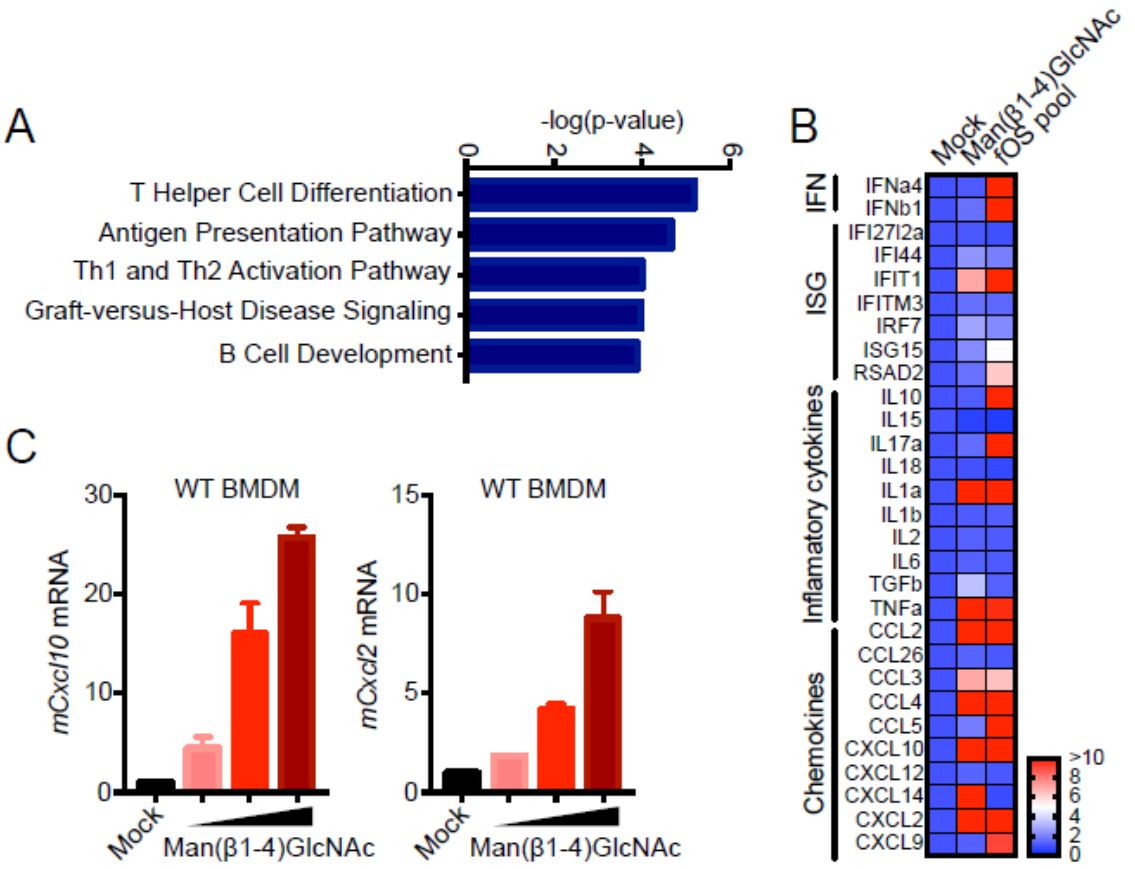

Figure 3.5: The Man(β1-4)GlcNAc disaccharide primarily activates ISGs and chemokines

(A) RNA seq IPA pathway analysis. Showing the top 5 modulated by stimulating qRT-PCR RAW264.7 with the Man(β1-4)GlcNAc disaccharide.
(B) Heat map of qRT-PCR immune gene profile of RAW264.7 cell stimulated with the Man(β1-4)GlcNAc disaccharide.
(C) qRT-PCR analysis of *Cxcl10* and *Cxcl2* in BMDM after stimulated with increasing concentrations of the (Man(β1-4)GlcNAc.

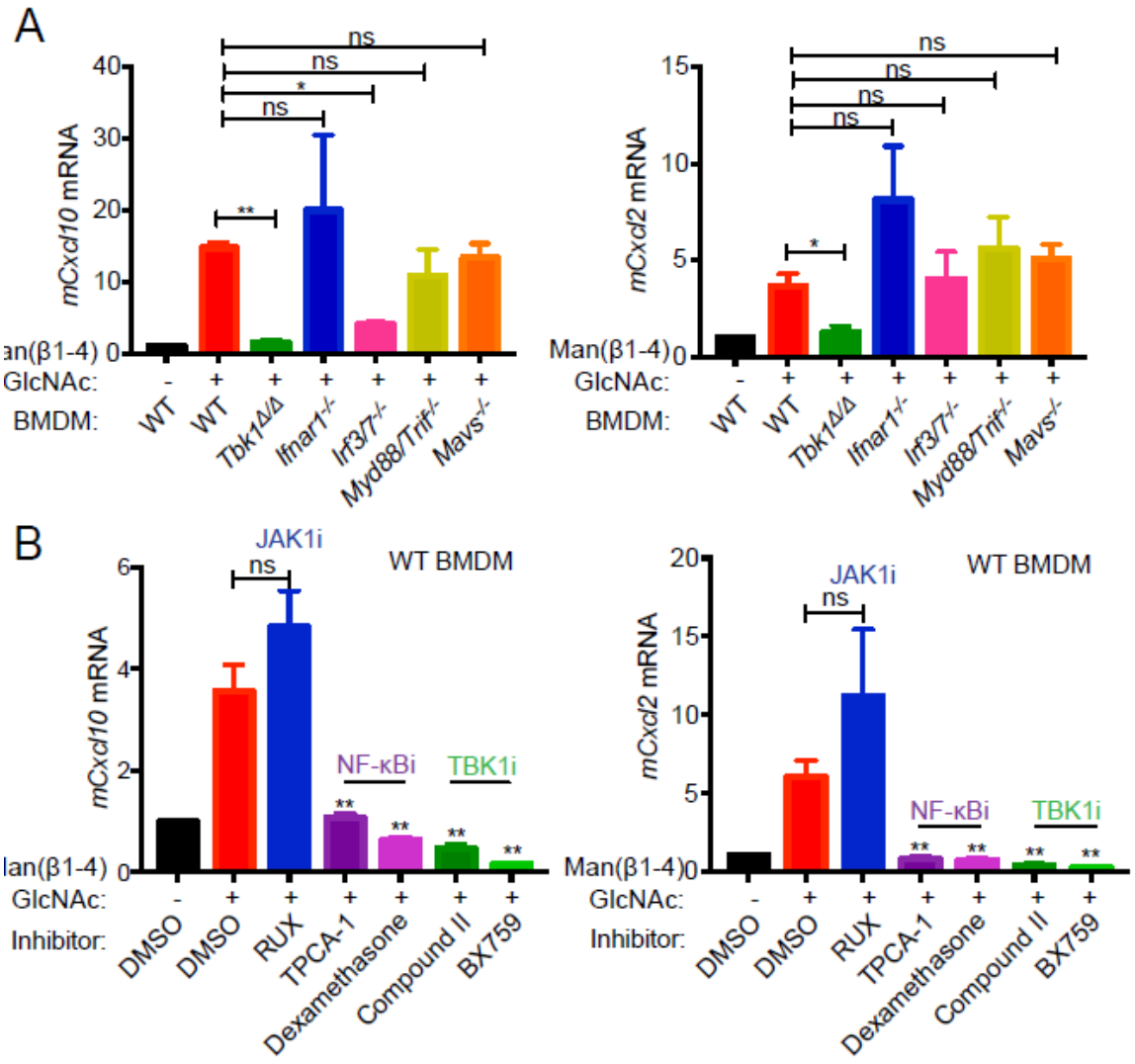

Figure 3.6: The Man(β1-4)GlcNAc disaccharide induced immune activation is dependent on TBK1 and NF-κB

(A) qRT-PCR analysis of *Cxcl10* and *Cxcl2* in various knockout BMDM as indicated that were stimulated with increasing concentrations of Man(β1-4)GlcNAc.
(B) qRT-PCR analysis of *Cxcl10* and *Cxcl2* in BMDM that were pre-treated with the indicated inhibitos and stimulated with the Man(β1-4)GlcNAc.

The Man(β1-4)GlcNAc disaccharide activates a chemokine profile that resembles DNA

Myeloid cells, which include macrophages, express an arsenal of carbohydrate binding proteins known as C-type lectins receptors (CLR) that function like PRRs and recognize a wide variety of glycan PAMPs. There are hundreds of lectins that can be potential candidate receptors for the Man(β1-4)GlcNAc disaccharide, making an individual knockdown approach impractical. Instead, I decided to examine whether the Manβ1-4GlcNAc disaccharide stimulates an immune profile that can be matched to other bioactive glycans. To do this, I incubated BMDMs with Dectin-1 ligands (Chitosan, Chitin, Curdlan and Zymosan), MGL ligand (Le^X), Dectin-2 ligands (β-Mannan, α-Mannan, Furfurman and Lipoarabinomannan (LAM)) and MCL/MINCLE ligand (Cord factor (TDB)) as well as htDNA (cGAS-STING-TBK ligands), LPS (TLR4 ligand), and the Man(β1-4)GlcNAc disaccharide. Since the Man(β1-4)GlcNAc disaccharide predominantly induces the expression of chemokine genes I focus on these. After hierarchical clustering (Morpheus) that groups immune gene profiles that are the most similar to each other, the Man(β1-4)GlcNAc disaccharide stimulated an immune gene profile similar to that of htDNA (**Figure 3.7 A**). htDNA is a ligand that activates the STING-TBK1 pathway in the cytosol. I next compared the immune profiles activated by the Man(β1-4)GlcNAc disaccharide in WT, *Tbk1-Δ/Δ* and *Sting -/-* BMDMs. *Tbk1-Δ/Δ* ablated all immune genes activated by Man(β1-4)GlcNAc, whereas *Sting -/-* only affected the activation of *Cxcl10* and *Cxcl9* (**Figure 3.7 B**). Together, these data suggest that the Man(β1-4)GlcNAc disaccharide activates a chemokine immune gene profile that resembles DNA and partially depends on the cytosolic innate immune protein STING.

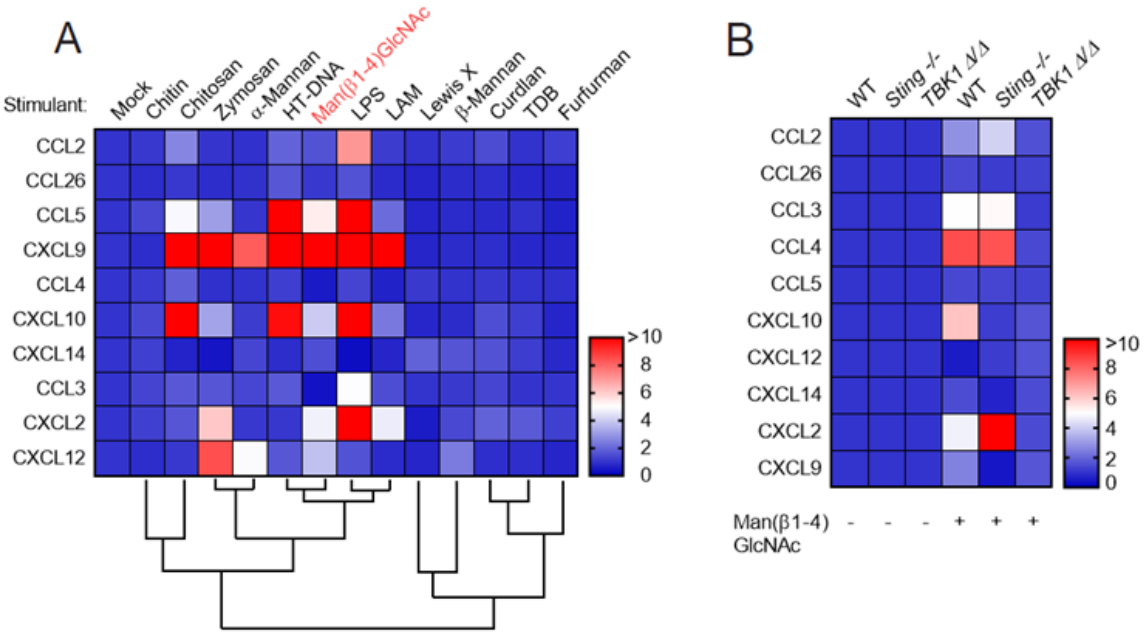

Figure 3.7: The Manβ1-4GlcNAc disaccharide induces a transcriptional signature different from other immunogenic polysaccharides

(A) Heat map of qRT-PCR chemokine profile of BMDM stimulated with the indicated ligand. The profile generated by the Man(β1-4)GlcNAc disaccharide is similar to the one generated by HT-DNA.

(B) Heat map of qRT-PCR chemokine profile of various knockout BMDM as indicated after stimulation with the Man(β1-4)GlcNAc disaccharide. Removal of STING only suppressed the induction of *Cxcl10* and *Cxcl9*. In contrast *TBK1 Δ/Δ* completely suppressed the immune activation generated by the Man(β1-4)GlcNAc disaccharide.

Biogenesis and cellular distribution of mammalian Man(β1-4)GlcNAc disaccharide

Oligomannose fOS are usually derived from the hydrolysis of LLOs by OST or from the deglycosylation of ER-associated degradation (ERAD) substrates by N-glycanase 1 (NGLY1) [74, 115]. Previous work has shown that the absence of TREX1 or its C-terminus (e.g. TREX1-fs mutants) dysregulate OST activity leading to accumulation of intracellular fOSs [110]. To determine the source that leads to the origin of the Man(β1-4)GlcNAc disaccharide, I used specific inhibitors that block either ERAD or OST's activity and measure the effect on fOS in *Trex1* -/- MEFs by FACE (**Figure 3.8 A**). Inhibiting OST activity with aclacinomycin A (ACM), [110, 116] led to a significant reduction of Man(β1-4)GlcNAc disaccharide as well as other high-mannose fOSs (**Figure 3.8 B**). In contrast, inhibiting NGLY1 with Z-VAD-fmk had no effect on the Man(β1-4)GlcNAc disaccharide or any other fOSs enriched in the *Trex1* -/- MEFs (**Figure 3.8 C**) [117]. I next examined ER translocation and glycan processing machinery in the lumen. Inhibiting ER glucosidases with castanospermine (CSN) blocks both the translocation of fOS to the cytoplasm as well as the progress through ERAD, while inhibition of ER mannosidases with kifunensine (Kif) only affects misfolded protein tagging for ERAD [75, 118-120]. Treatment of *Trex1* -/- MEFs with CSN significantly reduced Man(β1-4)GlcNAc disaccharide while treatment with Kif had no impact on the disaccharide levels (**Figure 3.8 D-E**). These data suggest that OST-hydrolyzed LLOs are the precursors of the bioactive Man(β1-4)GlcNAc disaccharide.

Next, I investigated how fOSs are generated from LLOs hydrolysis get further processed into the Man(β1-4)GlcNAc disaccharide. Once LLO derived fOS are generated

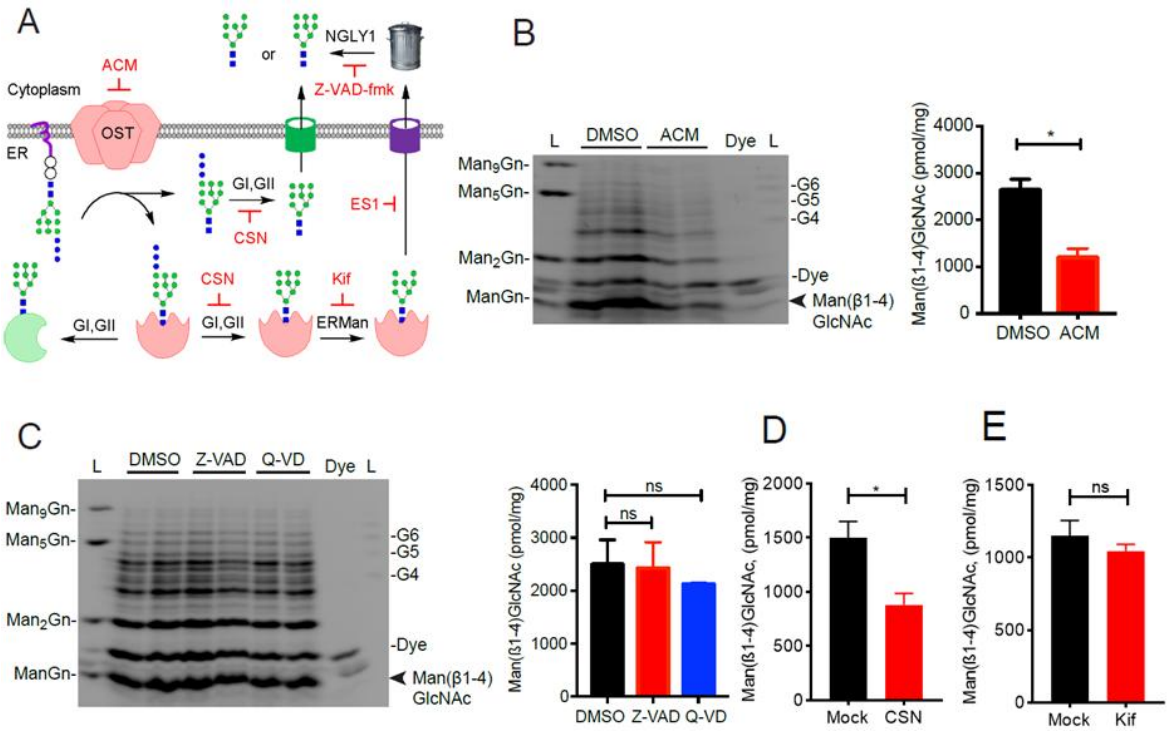

Figure 3.8: The Manβ1-4GlcNAc disaccharide originates from OST's hydrolysis of LLOs

(A) Summary of the fOS metabolic processing and the pharmacological inhibitors (red) that blocks these steps.
(B) FACE analysis of *Trex1* -/- MEFs fOS after treatment with ACM and the quantification of the Man(β1-4)GlcNAc disaccharide.
(C) FACE analysis of *Trex1* -/- MEFs fOS after treatment with Z-VAD or Q-VD and the quantification of the Man(β1-4)GlcNAc disaccharide.
(D) Quantification of the Man(β1-4)GlcNAc disaccharide in *Trex1* -/- MEFs treated with CSN. Values obtained from FACE analysis.
(E) Quantification of the Man(β1-4)GlcNAc disaccharide in *Trex1* -/- MEFs treated with Kif. Values obtained from FACE analysis

they are transported into the cytoplasm where they are processed by endo-β-N-acetylglucosaminidase (ENGase) in the cytosol [77]. I thus hypothesized two possibilities for LLO-derived fOS processing (**Figure 3.9 A**): First, fOSs generated in the ER lumen can stay in the luminal space, travel through the secretory pathway till they reach the lysosomes for degradation, or second fOSs can translocate from the ER lumen to the cytosol and get processed by the ENGase pathway, which includes first trimming the fOSs to $Man_5GlcNAc$, transfer into the lysosomes and then further processed by lysosomal α- and β-mannosidases into the Man(β1-4)GlcNAc disaccharide and monosaccharides [78, 79]. ENGase knockdown by siRNA in *Trex1 -/-* MEFs led to reduced Man(β1-4)GlcNAc disaccharide levels as well as a corresponding increase in high molecular weight fOSs that co-migrated with previously characterized species in *Engase -/-* MEFs (**Figure 3.9 B**) [76]. I also treated *Trex1 -/-* MEFs with swainsonine (Swain, a broad α-mannosidase inhibitor) and chloroquine (Clq or CQ, lysosome neutralizer, thus inactive the lysosomal mannosidase) and examined the effect on the Man(β1-4)GlcNAc disaccharide levels [121]. Swain completely eliminated the Man(β1-4)GlcNAc disaccharide from *Trex1 -/-* fOS and accumulated intermediate $Man_{3-5}GlcNAc$, while Clq increased the disaccharide presumably by inhibiting the only lysosomal β-mannosidase which is the slow step in the fOS catabolic pathway (**Figure 3.9 C-D**) [79]. Next, I examined the cellular distribution of the Man(β1-4)GlcNAc disaccharide within the cell. To determine if it resides in an enclosed organelle, I treated the *Trex1 -/-* MEFs with 10 μg/mL digitonin to only permeabilized the plasma membrane [111]. Nearly half of the disaccharide diffused from the cell, suggesting that a substantial fraction of the

Man(β1-4)GlcNAc disaccharide resides in the cytosol (**Figure 3.9 E**). I also compared the fOSs isolated from the media and from the cells, both originating from the same dish, and found that a substantial amount of the Man(β1-4)GlcNAc disaccharide was present in the *Trex1* -/- MEFs media when compared to that from WT cells (**Figure 3.9 F**). Together, these findings demonstrate that LLO-derived fOSs in *Trex1* -/- MEFs moves from the ER lumen to the cytosol followed by processing by ENGase and mannosidases to produce the Man(β1-4)GlcNAc disaccharide that resides in both the cytoplasmic and extracellular space.

Blocking the Man(β1-4)GlcNAc disaccharide production corrects the ISGs immune signature in *Trex1* -/- cells

Both ACM and swainsonine have been used in cancer therapeutic settings [122, 123]. ACM, in particular, is an FDA-approved drug for the treatment of acute myeloid leukemia. Since both of these compounds reduced the levels of the Man(β1-4)GlcNAc disaccharide levels in *Trex1* -/- MEFs, I hypothesized that treatment with these compounds would reduce the immune signature in the *Trex1* -/- MEFs. To interrogate this, *Trex1* -/- MEFs were treated with increasing doses of ACM (OST inhibitor) or Swain (α-mannosidase inhibitor). Treatment with both reduced the ISG *Ifit1* in the *Trex1* -/- MEFs reiterating the immunogenicity of the Man(β1-4)GlcNAc disaccharide and its potential role in the development and progression of the RVCL pathology (**Figure 3.10 A**-**B**).

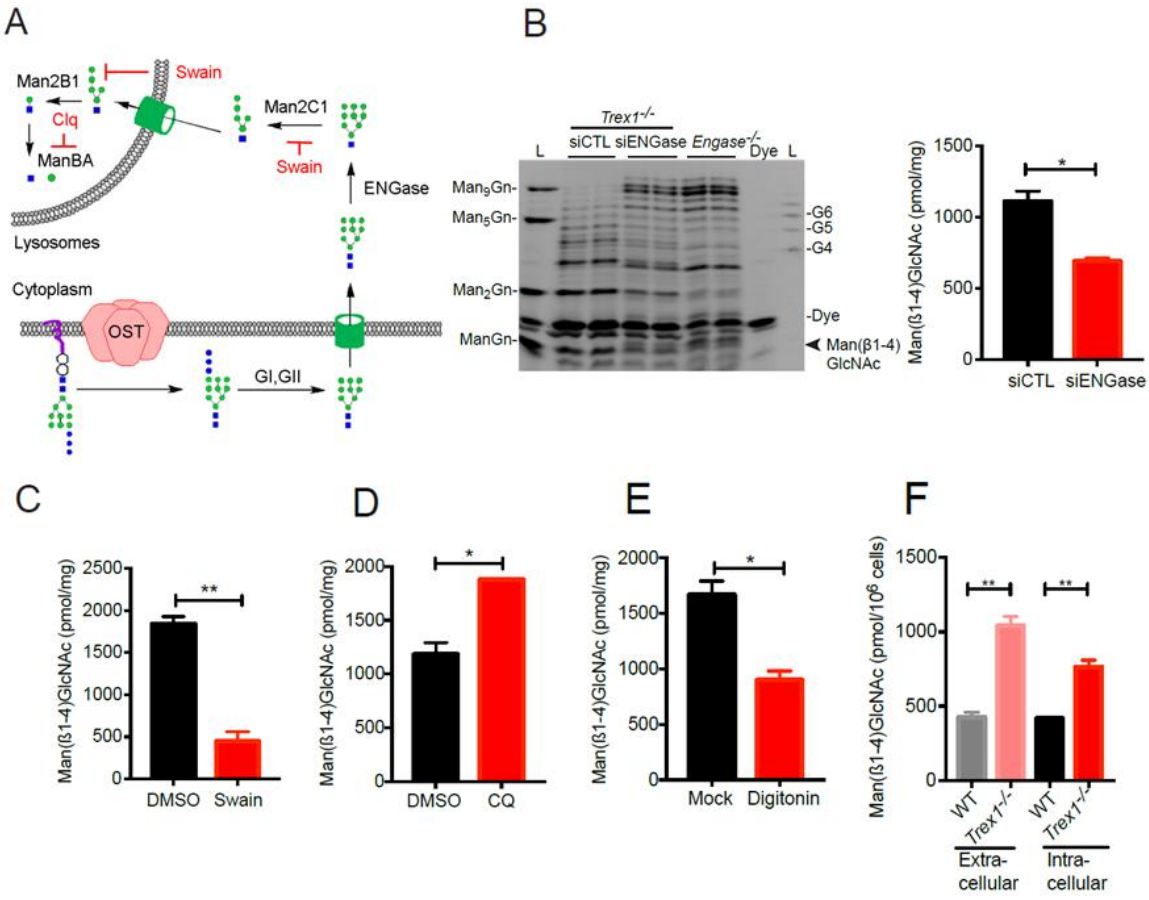

Figure 3.9: The Manβ1-4GlcNAc disaccharide is produced by the enzymatic process of ENGase and alpha mannosidases

(A) Summary of the catabolic processing of lumenal fOS and the pharmacological inhibitors (red) that blocks these steps.
(B) FACE analysis of *Trex1* -/- MEFs fOS after ENGase was knockdown with siRNA and the quantification of the Man(β1-4)GlcNAc disaccharide.
(C) Quantification of the Man(β1-4)GlcNAc disaccharide in *Trex1* -/- MEFs treated with Swain. Values obtained from FACE analysis.
(D) Quantification of the Man(β1-4)GlcNAc disaccharide in *Trex1* -/- MEFs treated with Clq. Values obtained from FACE analysis.
(E) Quantification of the Man(β1-4)GlcNAc disaccharide in *Trex1* -/- MEFs permeabilized with digitonin. Values obtained from FACE analysis.
(F) Quantification of the Man(β1-4)GlcNAc disaccharide levels in the extracellular (media) and intracellular space in wild type and *Trex1* -/- MEFs. Values obtained from FACE analysis.

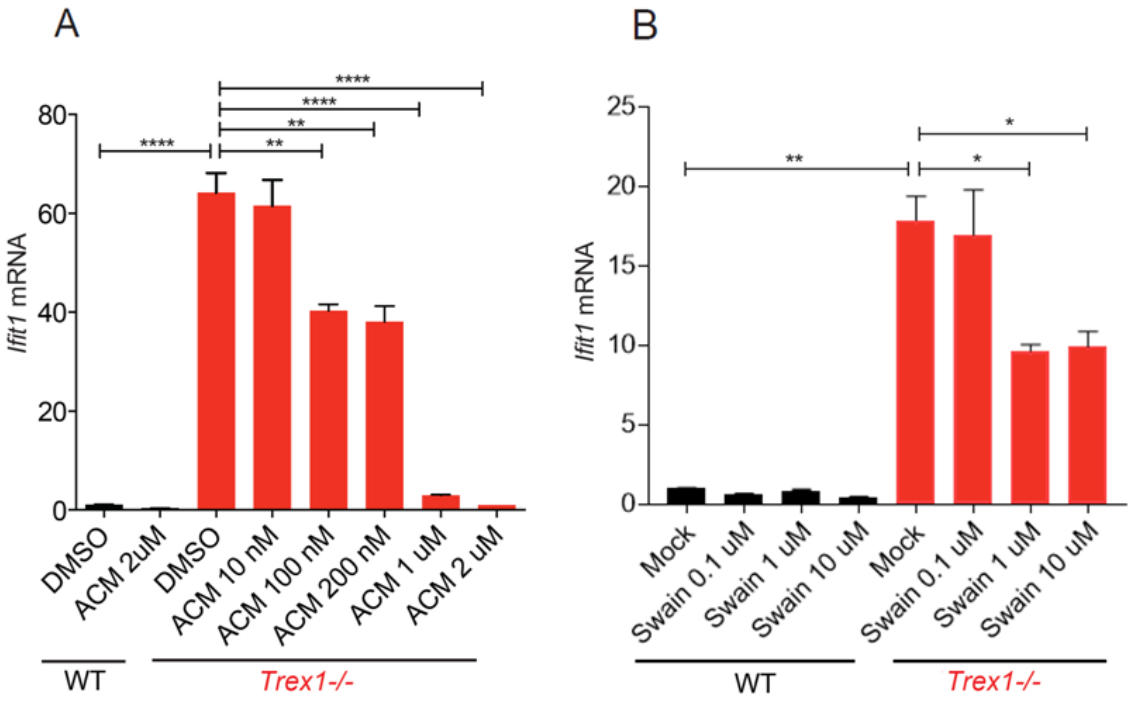

Figure 3.10: Reduction of the Manβ1-4GlcNAc disaccharide levels with ACM and Swain reduced the intrinsic immune activation in *Trex1 -/-* cells.

(A) qRT-PCR analysis of *Ifit1* in wild type and *Trex1 -/-* MEFs after treatment with increasing amounts of ACM.
(B) qRT-PCR analysis of *Ifit1* in wild type and *Trex1 -/-* MEFs after treatment with increasing amounts of Swain.

Discussion

TREX1 is a bi-functional protein where its N-terminus removes bioactive self DNA ligands and the C-terminus regulates the release of bioactive self-glycan ligands [110]. Dysregulation of either of these functions has been associated with autoimmune disorders (e.g. AGS, FCL, SLE and RVCL) (**Figure 1.3**). However, the clinical etiologies between diseases associated with the dysregulation of the N-terminus DNAse function (AGS and FCL) versus dysregulation of the C-terminus function (RVCL and SLE) are quite distinct [62, 65]. Although extensive characterization has been previously performed to understand the nature and the sensing of the self-DNA ligands, little is known in regard to the nature of the self-glycan ligand responsible for the immune activation in the presence of mutations that affect the TREX1 C-terminus function [11, 124]. By using *Trex1 -/-* cells I discovered that the bioactive self-glycan is an unexpected simple Man(β1-4)GlcNAc disaccharide. Moreover, I also found that the sensing of the Man(β1-4)GlcNAc disaccharide is dependent on TBK1. This finding places TBK1 as an attractive therapeutic target for all TREX1 related diseases since it sits at a node between self-DNA and self-glycan sensing. Previous work has already shown that treating *Trex1 -/-* mice with TBK1 inhibitors improves their overall survival and reduces their autoimmune phenotypes [125]. I anticipate TREX1 RVCL patients to benefit from a similar treatment.

Several questions that still remain to be addressed are how is the Man(β1-4)GlcNAc disaccharide recognized? Does the Manβ1-4GlcNAc disaccharide mimic pathogen glycans? Outside the TREX1 scenario, when are self-glycan ligands produced?

The obvious candidates for sensing self-glycans would be lectins, specifically the CLR family. In the case of the Man(β1-4)GlcNAc disaccharide, previous public glycan arrays from the Consortium of Functional Glycomics (CFG) have shown positive affinity from several myeloid CLRs. Among these, MCL, myeloid-DAP12-associating lectin (MDL-1), Langerin (CD207), Dectin-2, MINCLE, LSECtin and surfactant protein D (SFTPD) showed affinity towards the Man(β1-4)GlcNAc disaccharide but not Dectin-1 or MGL. Notably, ligands for Dectin-2, MCL, and MINCLE did not generate an immune profile comparable to the Man(β1-4)GlcNAc disaccharide suggesting that perhaps other CLRs or other immune receptors that require TBK1 could be responsible for the immune recognition. In addition, the accepted understanding is that classical CLR signaling (e.g. Ligand->CLR->Syk->Response) acts independently of TBK1. However, examples, where a cross-talk between Syk and TBK1 exist, has been reported for other immune receptors [126]. Another consideration is that the Man(β1-4)GlcNAc disaccharide could be binding non specifically to nucleic acid sensors or to Galectin-8 who requires TBK1 to signal [106]. Here I show that to some degree the Man(β1-4)GlcNAc disaccharide signals through the adaptor protein STING. But, whether this is through cGAS or simply direct binding to STING remains to be elucidated. Binding directly to cGAS, however, seems unlikely just because of the sheer magnitude of the response generated, since DNA or cGAMP stimulations usually results in hundreds of fold increase of *CXCL10* and other ISGs.

Although the Manβ1-4GlcNAc disaccharide has not been found on pathogens molecules it has been associated with microbial metabolic activity to paves the way for

colonization or infection [127, 128]. Bacterial pathogens will digest N-glycans on cells to facilitate the infection process. In doing so, many pathogenic bacteria will produce the Man(β1-4)GlcNAc disaccharide and other fOS as by-products [129]. It is feasible to think that perhaps large production of the Man(β1-4)GlcNAc disaccharide and fOS is associated with infection and the self-glycans could be functioning as danger signals. To support this notion, previous work has demonstrated that fOS concentrations increase when cells are infected with herpes simplex virus 1 (HSV-1) [73]. In addition, previous reports have also demonstrated that O-glycans on the HSV-1 viral surface can activate the expression of *CXCL10* and *CXCL9* in an IFN-independent manner again highlighting the importance of glycans as immune modulators whether they are fOS or glycoconjugates [130].

LLO-derived fOSs appears to be abundantly produced in many lower organisms but largely absent in mammalian cells that have evolved an elaborate innate immune sensing network [115]. I hereby propose that instead of being a simple by-product of OST catalysis, fOSs have signaling properties as modulators of the innate immune system. Therapeutic targeting of the biogenesis or immune sensing pathways of mammalian fOSs such as Man(β1-4)GlcNAc disaccharide should thus be considered for treating *TREX1-fs*RVCL, and potentially other chronic diseases.

Acknowledgment and contribution

I would like to thank Ichiro Matsuo (RIKEN) and his group for the synthetic glycans, Tadashi Suzuki (RIKEN) and his group for structural analysis and the *ENGase* -

/- MEFs. I would like to thank Jennifer Kohler for valuable discussion regarding the diazirine derivatives and disaccharide synthesis. I would like to thank Ricardo Irizarry-Caro (UTSW) for wild-type and *Myd88/Trif -/-* BMDM and members of the Nan Yan and Mark Lehrman lab for valuable discussions. The financial supports are AI098569, AR067135, GM038545 and NSF GRFP.

Kanae Sano synthesized the $Man_2GlcNAc$, ManGlcNAc (α and β) and the GlcGlcNAc

Junichi Seino, Ph.D. contributed to the structural analysis in table 3.1.

Nicole Dobbs, Ph.D. contributed to figure 3.5 C and 3.7 A-B.

Maroof Hasan, Ph.D. contributed to figure 3.10 A.

CHAPTER FOUR: PHOSPHORYLATION REGULATES THE INTERACTION BETWEEN TREX1 C-TERMINUS AND OLIGOSACCHARYLTRANSFERASE (OST).

This chapter is a modification of the published article - Mitotic phosphorylation of TREX1 C-terminus disrupts TREX1 regulation of the oligosaccharyltransferase complex. Cell Reports March 14, 2017

Introduction

TREX1, also known as DNase III, is a 3'->5' DNA exonuclease tail-anchored at the endoplasmic reticulum (ER). Mutations in *TREX1* are associated with a broad spectrum of autoimmune and inflammatory phenotypes, including Aicardi-Goutières syndrome (AGS), familial chilblain lupus (FCL), systemic lupus erythematosus (SLE) and retinal vasculopathy with cerebral leukodystrophy (RVCL) [26]. Missense mutations that disrupt TREX1 DNase activity cause self-DNA to accumulate in the cytosol, which triggers the cGAS-STING innate immune sensing pathway and type I interferon (IFN) response [10, 34]. Previous work has shown that frame-shift mutations that truncate the C-terminal ER localization region, without affecting DNase activity, cause dysregulation of the ER complex oligosaccharyltransferase (OST), leading to the rapid release of immunogenic fOS [110]. These two distinct functions of TREX1 are spatially separated into the N- and C-terminus of the protein. But how the interaction between the TREX1 C-terminus and OST is regulated has not been explored. The only post-translational modification of TREX that has been described to date is the ubiquitination of TREX1 C-terminus that regulates its ER localization but not the DNase activity [41]. No phosphorylation event has been described for TREX1.

Phosphorylation (addition of a phosphate group) is the cells most abundant post-translational modification (PTM) and it is of particular interest because of its transient regulatory function of proteins. The mitotic phase of the cell cycle is characterized by widespread protein phosphorylation. Many kinases become active during mitosis, three of which, CDK, PLK, and Aurora families have been most intensely studied. CDK1 is the master regulator of mitotic entry. It binds cyclin B before the entry into mitosis and the cyclin B/CDK1 complex is activated when inhibitory phosphorylation on CDK1 is removed by CDC25 phosphatase [131]. When mitotic chromosomes are aligned and attached to spindle, CDK1 activity is turned off by proteasomal degradation of its regulatory subunit, cyclin B. It is estimated that several thousand proteins are phosphorylated by CDK1 alone [132]. Only a fraction of this vast array of regulations has been studied. Here, I describe cell cycle-dependent regulatory phosphorylation event by mitotic cyclin B/CDK1 on TREX1 C-terminus that interferes with its interaction with OST.

Experimental procedure

Cells, plasmids, and antibodies

HeLa and 293T cells were maintained in Dulbecco's modified Eagle's medium (DMEM) with 10% (v/v) heat-inactivated fetal bovine serum (FBS), 2 mM L-glutamine, 10 mM HEPES and 1 mM sodium pyruvate (complete DMEM) with the addition of 100 U/ml penicillin, 100 mg/ml streptomycin and cultured at 37°C with 5% CO_2. Antibodies used in this study include anti-TREX1 (mouse, 1:200 dilution, sc-271870, Santa Cruz), anti-

Cyclin B1 (rabbit, 1:500 dilution, sc-752, Santa Cruz), anti-Tubulin (mouse, 1:20,000 dilution, B-5-1-2, Sigma), anti-V5 (mouse, 1:5,000, R-960-25, Life Technology) anti-Myc (mouse, 1:5000 dilution, sc-40, Santa Cruz), anti-calreticulin (rabbit, 1:1000 dilution, ab4-100, Abcam), anti-calnexin (Abcam, Ab4-100), anti-V5 agarose beads (goat, 2ug per IP, S190-119, Bethyl) and anti-Myc (rabbit, 2ug per IP, sc-789, Santa Cruz).

Fluorescence Microscopy

For microscopy, HeLa cells grown on coverslips were transfected with either wild-type or mutant variants TREX1-V5 plasmids. 24 hrs after transfection, cells were subsequently fixed in 4% paraformaldehyde and permeabilized in a 0.25% Triton X solution. Cells were later stained with anti-V5 and anti-calreticulin and Alexa Fluor 488 and 546 conjugated secondary antibodies (Invitrogen) respectively. Coverslips were mounted in Vectashield (Vector Laboratory) mounting solution with DAPI and imaged using a Zeiss Imager M2 fluorescence microscope with AxioVision software.

TREX1 *in vitro* phosphorylation and DNase Activity Assay

TREX1 exonuclease activity was assayed as described in [110]. Briefly, approximately $1x10^6$ 293T were transfected with either wild-type or mutant TREX1-V5 plasmids. Cells were lysed in IP buffer (20 mM Tris-HCl [pH 7.4], 150 mM NaCl, 0.5% NP-40, and 1x protease inhibitor) and the post-nuclear supernatant was isolated by centrifugation at 20,000g and mixed with anti-V5 agarose beads (Bethyl). Upon overnight incubation, at 4^oC the beads were subsequently washed twice with IP buffer and twice with low-salt IP

buffer (50 mM NaCl). Washed beads were resuspended in 50 µl of DNase buffer (20 mM Tris-HCl [pH 7.4], 5 mM $MgCl_2$, 2 mM DTT, 100 mg/ml BSA, and 0.5% NP-40). Beads bound TREX1 was subject to either *in vitro* phosphorylation or DNase assay. For TREX1 *in vitro* phosphorylation, beads bound TREX1 was incubated with 20U of recombinant CDK1 (NEB) following the manufacturer suggestion. Samples were later analyzed by Phos-tag immunoblotting. To assess TREX1 DNase function, samples were divided into 3 equal volumes and mixed with 90 ul of pre-warmed to 37^{o}C DNase reaction buffer (20 mM Tris-HCl [pH 7.4], 5 mM $MgCl_2$, 2 mM DTT, 100 mg/ml BSA, 1/1,200 SYBR Green, and 5 ng/µl or 10 ng/µl ssDNA) followed by real-time quantification of the DNA/SYBR complex using a SynergyHT microplate reader (Biotek).

Co-immunoprecipitation and proteomic analysis

Approximately 2x10^{6} 293T cells were transfected with wild-type, mutant variants or truncated variants TREX1-V5, Myc-RPN1 or Myc-DDOST plasmids. Cells were collected and lysed as described above. The supernatant was subsequently mixed with anti-Myc and Dynabeads Protein G (Life Technology) and incubated overnight at 4^{o}C. Next, samples were washed once with IP buffer, twice with high salt IP buffer (500 mM NaCl) and once with a low salt IP buffer (50 mM NaCl). Immunocomplexes were eluted with 3x Sample buffer and boiling. Samples were subsequently analyzed by immunoblotting. For mass spectrometry PTM analysis TREX1-V5 was overexpressed in mitosis synchronized HeLa cells and isolated as described above. Samples were submitted to the UTSW proteomic core facility for PTM identification.

Phos-Tag SDS-PAGE

Mitosis synchronized or non-synchronized cells were collected and lysed in RIPA buffer with 1x protease inhibitors and phosphatase inhibitors (25 mM NaF and 1 mM Na_3VO_4). The post-nuclear supernatant protein content was determined using Pierce BCA Protein Assay (Thermo). Samples were either treated with Lambda Protein Phosphatase (NEB) or loaded directly into a 10% Polyacrylamide phos-tag gel (50 μM Phos-Tag (Wako) and 100 uM $MnCl_2$). Prior to electroblotting, gels were soaked in transfer buffer with 1 mM EDTA for 10 min. Samples were subsequently analyzed by immunoblotting.

Cell cycle synchronizations

For G1/S synchronization (double-thymidine block), HeLa cells were plated at 25-30% confluency and treated with 2 nM thymidine for 18 hours. Then, cells were washed two times with warm PBS and grown in fresh medium for 9 hours. Then, cells were treated again with 2 mM thymidine for 15 hours to arrest at G1/S phase. In selective experiments, cells were released into S phase by washing two times with warm PBS and adding fresh conditioned medium. For M phase synchronization (thymidine-nocodazole block), cells were plated at 40% confluency and treated with 2 nM thymidine for 24 hours. Then, cells were washed two times with warm PBS and grown in fresh medium for 3 hours. Cells were then treated with 100 ng/mL Nocodazole for 12 hours. Dishes were knocked with knuckles to dislodge mitotic cells from the plate. These round cells are arrested in mitosis. To release these cells into G1, nocodazole was removed by washing two times with warm PBS and adding fresh medium.

Results

Cyclin B/CDK1 phosphorylates TREX1 in mitosis

A previous high-throughput phospho-proteomic study identified various phosphorylation sites on TREX1 that were occupied during mitosis [132]. To confirm these findings, the migration of TREX1 was analyzed by SDS-PAGE containing Phos-tag, which retards migration of phosphorylated proteins [133]. I used an antibody that specifically recognizes human TREX1, and yields a single band on immunoblots with regular SDS-PAGE (**Figure 4.1 A**). Addition of Phos-tag in the SDS-PAGE, causes TREX1 to migrated as a double-band with a third, weaker-intensity, super-shifted band and as the phospho-proteomic study implied this super-shifted band was more pronounced in cells that were arrested in M phase (Noc) but not in G1+S phase (Thy) (**Figure 4.1 B**). To characterize the kinetics of TREX1 phosphorylation in greater detail, HeLa cells were synchronized in G1+S phase with double-thymidine treatment and measured TREX1 phosphorylation after they were released into S+G2 phase. TREX1 phosphorylation coincided with cyclin A degradation, which is an event that occurs in early mitosis (**Figure 4.1 C**). To monitor de-phosphorylation kinetics, HeLa cells were arrested in mitosis with thymidine/nocodazole treatment, where the majority of TREX1 is phosphorylated, and released the cells into G1 phase by washing out nocodazole. TREX1 was gradually dephosphorylated within three hours after cells exited mitosis, coinciding with the disappearance of cyclin B (**Figure 4.1 D**). PP1/PP2 play an important role in dephosphorylating phosphorylated mitotic substrates at the culmination of cell division [134].

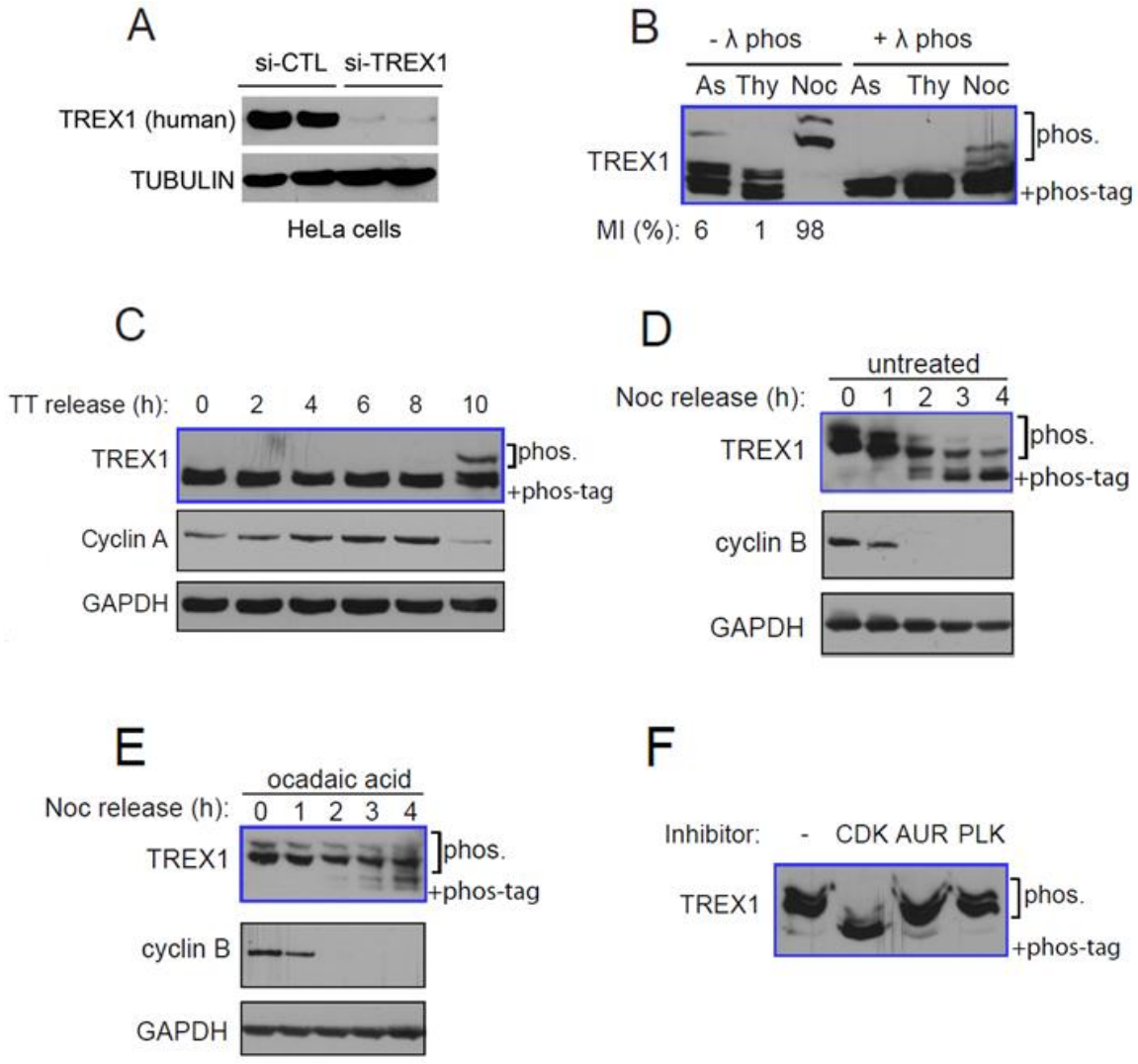

Figure 4.1: TREX1 is phosphorylated during mitosis by CDK1

(A) Immunoblot of siRNA knockdown of endogenous TREX1 in HeLa cells.
(B) Phos-tag immunoblot of asynchronously (As) grown, G1/S arrested with thymidine (Thy) or mitosis arrested with nocodozole (Noc) HeLa cells with or without Λ phosphatase treatment. Mitotic index (MI) was determine by counting phosphorylation of H3 serine 10 by fluorescent microscopy
(C) Phos-tag immunoblot of G1/S arrested HeLa cells and corresponding time points after removal thymidine treatment.
(D) Phos-tag immunoblot of mitosis arrested HeLa cells and corresponding time points after removal of nocodazole.
(E) Phos-tag immunoblot of mitosis arrested HeLa cells treated with ocadaic acid and corresponding time points after removal of nocodazole.
(F) Phos-tag immunoblot of mitosis arrested HeLa cells treated with RO3306 (CDKi), ZM447439 (AURi) or BI2536 (PLKi).

TREX1 dephosphorylation was inhibited by okadaic acid suggesting that PP1/PP2 phosphatase is responsible for removing the phosphate PTMs (**Figure 4.1 E**). There are three major types of mitotic kinases: cyclin-dependent kinases (CDK1), Aurora kinases and Polo-like kinases (PLK1) [134]. To determine which enzyme is responsible for the mitotic phosphorylation of TREX1, mitosis arrested cells were treated with inhibitors for each kinase. Only the CDK1 inhibitor caused phosphorylated TREX1 to shift to the unphosphorylated form, suggesting that TREX1 mitotic phosphorylation is dependent on CDK1 (**Figure 4.1 F**). In conclusion, TREX1 is robustly phosphorylated by cyclin B associated CDK1 in mitosis and quickly dephosphorylated after mitotic exit.

The major TREX1 mitotic phosphorylation site resides in the C-terminus

To identify the phosphorylated sites on TREX1, immunoprecipitated TREX1-V5 from mitotic HeLa cells was examined by mass spectrometry. About 47% of the protein (17 out of 26 serines) was covered by this analysis. This approach uncovered three phosphorylated serines, S261, S166 and S167 (**Figure 4.2 A**). These three serines and previously reported phosphorylated residue at S78 to alanine or in combination to examine which was modified in mitosis. Next, asynchronized (AS) or M phase-arrested HeLa cells were transfected with these serine to alanine mutants and examined the level of phosphorylation by Phos-tag containing SDS-PAGE (**Figure 4.2 B**). Wild-type TREX1-V5 was completely hyper-phosphorylated in mitotic cells. S78A mutant was largely phosphorylated in mitotic cells similar to WT TREX1, but there is a detectable residual amount of TREX1 remained unphosphorylated. S261A mutant was largely

unphosphorylated in mitotic cells, and S78A/S261A double mutant completely abolished TREX1 mitotic phosphorylation. In contrast, S166A/S167A double mutant retained its mitotic phosphorylation but lost the double band in both interphase and mitotic cells (**Figure 4.2 B**). All other mutants exhibited the double band in Phos-tag containing SDS-PAGE. Therefore, the phosphorylation of S166/S167 is solely responsible for the appearance of the double band and is cell cycle-independent. To further determine whether CDK1 directly phosphorylates TREX1 at S78 and S261, I performed *in vitro* kinase assay using recombinant CDK1 and isolated wild-type or mutant TREX1 (V5-tagged). Wild-type TREX1 and S166A/S167A mutant were successfully phosphorylated by CDK1 in vitro, whereas S78A/S261A mutant was not phosphorylated (**Figure 4.2 C**). Two additional triple and quadruple serine mutants (S78A/S166A/S261A and S78A/S166A/S167A/S261A) were also not phosphorylated (**Figure 4.2 C**). Collectively, this data concludes that mitotic phosphorylation of TREX1 occurs on S78 and S261 with S261 being the major phosphorylation site, and the mitotic phosphorylation is mediated by CDK1.

The S78, S167 and S261 residues are conserved in various mammalian TREX1 homologs (**Figure 4.3 A**). TREX1 DNase domain is highly conserved, but most of the linker region is not. Intriguingly, the CDK1 phosphorylation site at S261 falls in a motif with considerably higher conservation compared to the rest of the linker region (**Figure 4.3 B**). This suggests that TREX1 phosphorylation at S261 during mitosis highlights an evolutionarily conserved feature associated with the C-terminus.

A

Site	Peptide Spectrum Match	Score
S261	NTSPSLGESR	PTMScore: 135 ID Prob: 1
S167	ASSPSEHGPRK	PTMScore: 125 ID Prob: 1
S166	ASSPSEHGPR	PTMScore: 125 ID Prob: 0.8703

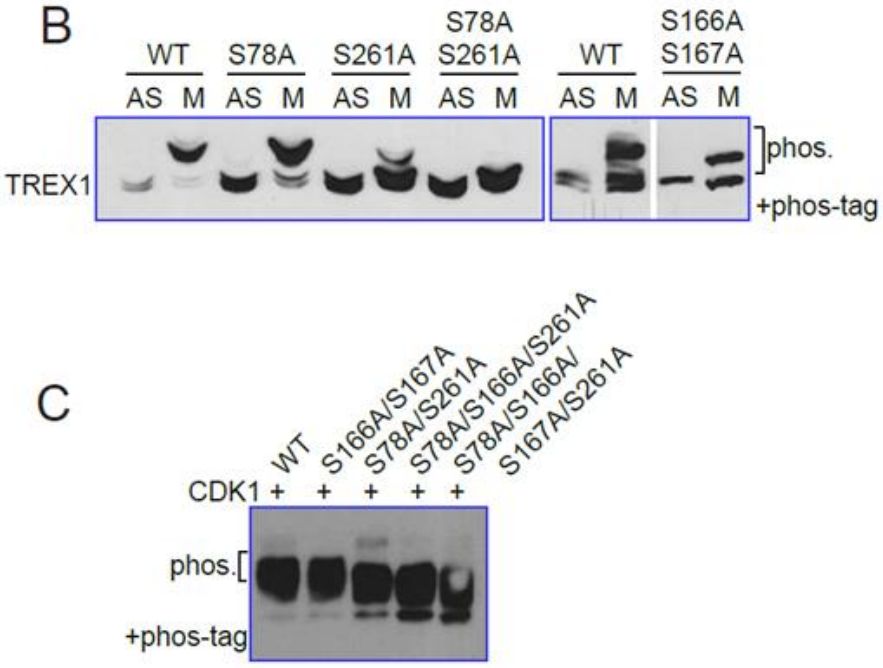

Figure 4.2: Mapping of TREX1 mitotic phosphorylation sites

(A) List of mass spectrometry identified phosphorylation sites on TREX1. TREX1-V5 was overexpressed in mitosis arrested HeLa cells and isolated by IP for proteomic analysis.
(B) Phos-tag immunoblot analysis of various phosphor-deficient TREX1 variants as indicated in mitosis arrested HeLa cells. S78 and S261 are the predominant mitotic phosphorylation sites.
(C) Phos-tag immunoblot analysis of *in-vitro* phosphorylation of various TREX1 constructs as indicated by recombinant CDK1. TREX1-V5 tagged constructs were isolated by IP and beads bound TREX1 were incubated with recombinant CDK1.

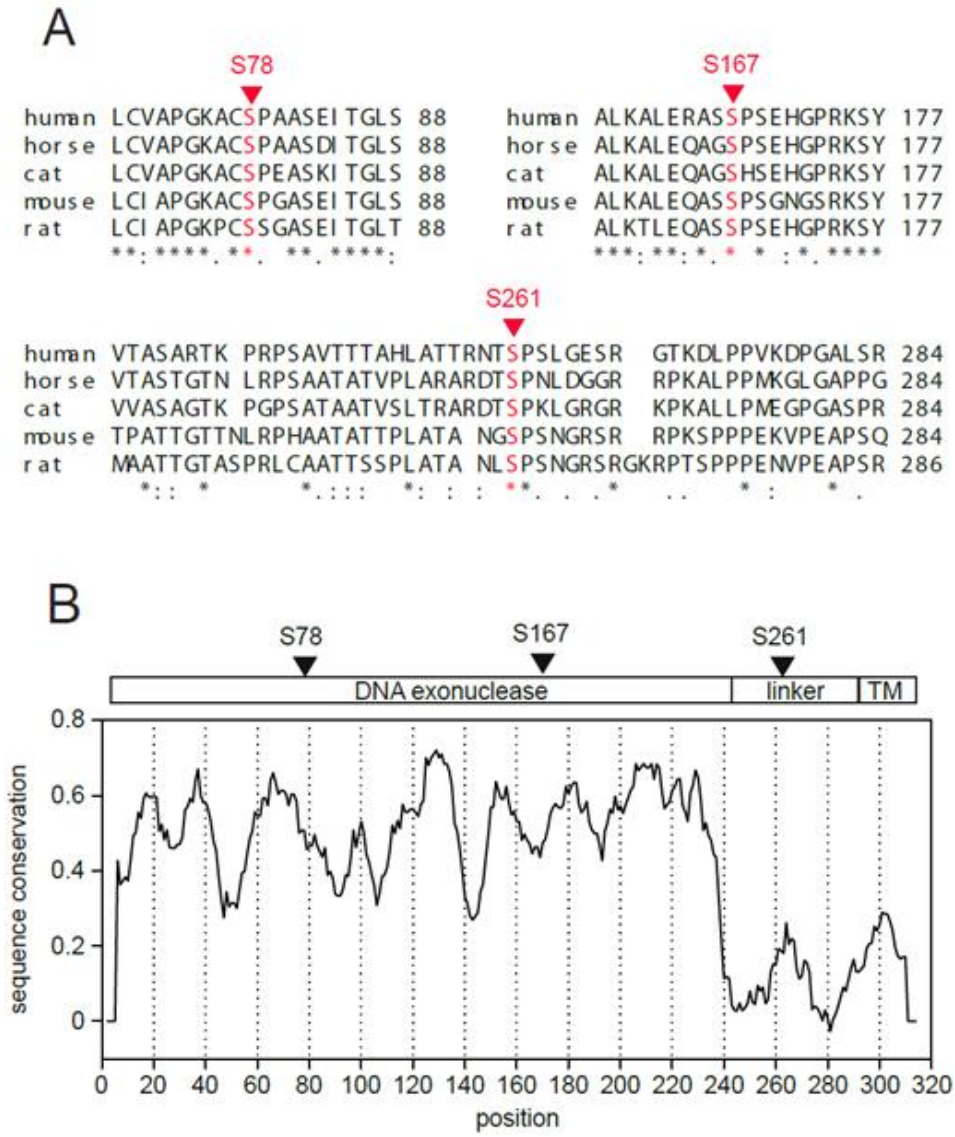

Figure 4.3: Mitotic phosphorylation sites on TREX1 are evolutionarily conserved

(A) Clusta alignment of five mammalian TREX1 homologs. The uniprot accession numbers are human (Q9NSU2), horse (F6PVF5), cat (M3X2S3), mouse (Q91XB0) and rat (Q5BK16).
(B) Plotcon analysis using EBLOSUM62 for sequence conservation among various TREX1 homologs. Mitotic phosphorylation sites are indicated at the top of the diagram.

Mitotic phosphorylation does not affect TREX1 DNase-activity or ER localization

I next sought to determine whether TREX1 phosphorylation plays a role in regulating TREX1 DNase activity or TREX1 ER localization. First, I compared the DNase activity between wild-type TREX1, phosphomimetic mutant S78D/S261D and phosphor-deficient S78A/S261A and S166A/S167A mutants. All TREX1 double and quadruple serine mutants exhibited DNase activity indistinguishable from wild type (**Figure 4.4 A**). I also found that all serine mutants localize properly to the ER as wild-type TREX1 (**Figure 4.4 B**). Collectively, these experiments suggest that TREX1 DNase activity or ER localization are not affected by phosphorylation.

Mitotic phosphorylation disrupts TREX1 interaction with the OST complex

I next tried to determine whether mitotic phosphorylation alters TREX1 interaction with the OST complex. Previous work has shown that TREX1 C-terminus harbors a DNase-independent function that regulates OST activity through the interaction of subunits RPN1 and DDOST [110]. To refine the interaction interface between TREX1 C-terminus (235-314) and OST, I generated several C-terminal truncations and examined their ability to interact with OST subunits RPN1 and DDOST (**Figure 4.5 A-C**). Wild-type TREX1 and 1-290 co-immunoprecipitated with RPN1 and DDOST to a similar level. Truncation 1-272 (mimics D272fs mutation associated with SLE) partially reduced TREX1:RPN1 interaction. Truncation 1-232 (mimics V232fs mutation associated with RVCL) nearly completely abolished TREX1:RPN1 interaction while 1-212 truncation

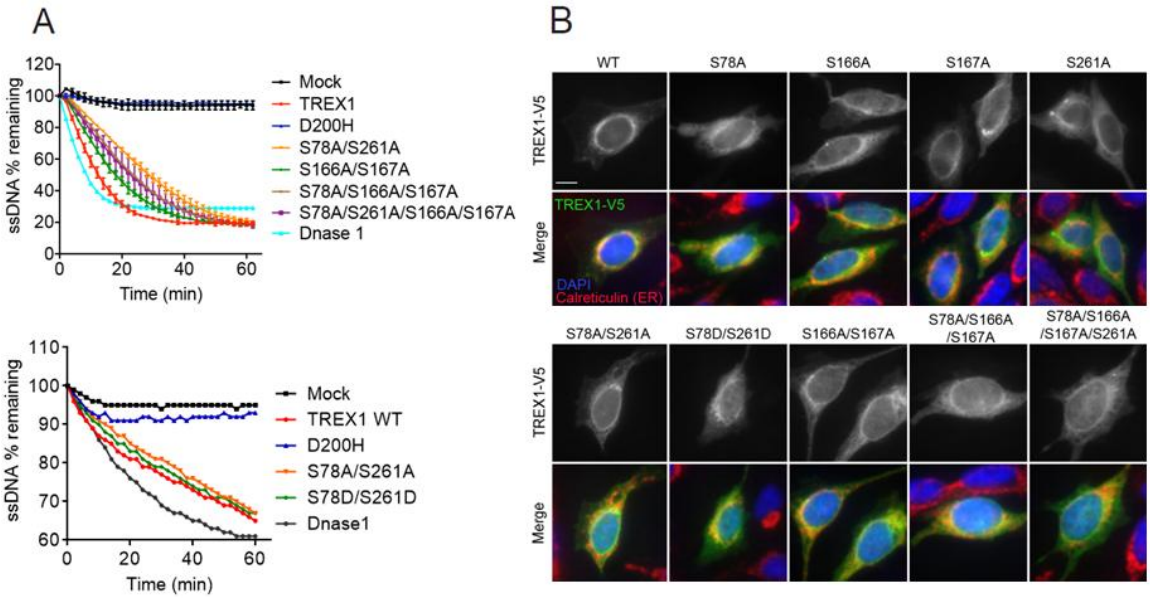

Figure 4.4: TREX1 mitotic phosphorylation do not affect the DNase activity of ER localization

(A) DNase assay on the phospho-deficient and phospho-mimetic TREX1. All variants are V5 tagged and were isolated by IP. Beads bound TREX1 was incubated with a 30-mer ssDNA ssubtrate. The D200H mutations impaired TREX1 DNase function and was used as a negative control. Recombinant DNase 1 was used as a positive control.

(B) Fluorescence microscopy analysis of the phospho deficient and phospho mimetic TREX1-V5 variants. Staining included anti-V5 (Green), and anti-Calreticulin (Red, ER marker).

(mimics P212fs mutation associated with SLE) lead to reduced detectable expression of this TREX1 variant (**Figure 4.5 A-C**). These interaction studies suggest that TREX1 interacts with RPN1 and DDOST through a region between V232 and D272. Interestingly, this is the most evolutionarily conserved motif within the linker region (**Figure 4.3 B**). Since the major mitotic phosphorylation site S261 falls exactly in this region, I next examined whether the two mitotic phosphorylation residues (S78 and S261) are required for TREX1:RPN1 and TREX1:DDOST interaction, or whether mitotic phosphorylation alters this interaction. S78A/S261A mutant did not affect TREX1:RPN1 interaction when compared to wild-type, suggesting these two residues are not required for interaction (**Figure 4.5 D**). In contrast, S78D/S261D mutant (phosphomimetic) reduced TREX1:RPN1 and TREX1:DDOST interaction, suggesting mitotic phosphorylation disrupts TREX1 interaction with the OST complex. These findings demonstrate that mitotic phosphorylation of TREX1 regulates the interaction between TREX1 and OST and possibly OST's function.

TREX1 C-terminus SLE mutations do not affect interaction with the OST complex

In addition to the RVCL fs mutations, many single mutations associated with SLE are found in the C-terminus of TREX1 (**Figure 1.3 and Table 1.1**) [31]. Like the V235fs mutation, most of the SLE associated mutations in the C-terminal region of TREX1 retain the DNase function (**Table 1.1**) [41]. This observation led to the hypothesis that C-terminus SLE associated mutations might interfere with the interaction of TREX1 and OST's subunits RPN1 and DDOST. First I examined the DNase activity of the

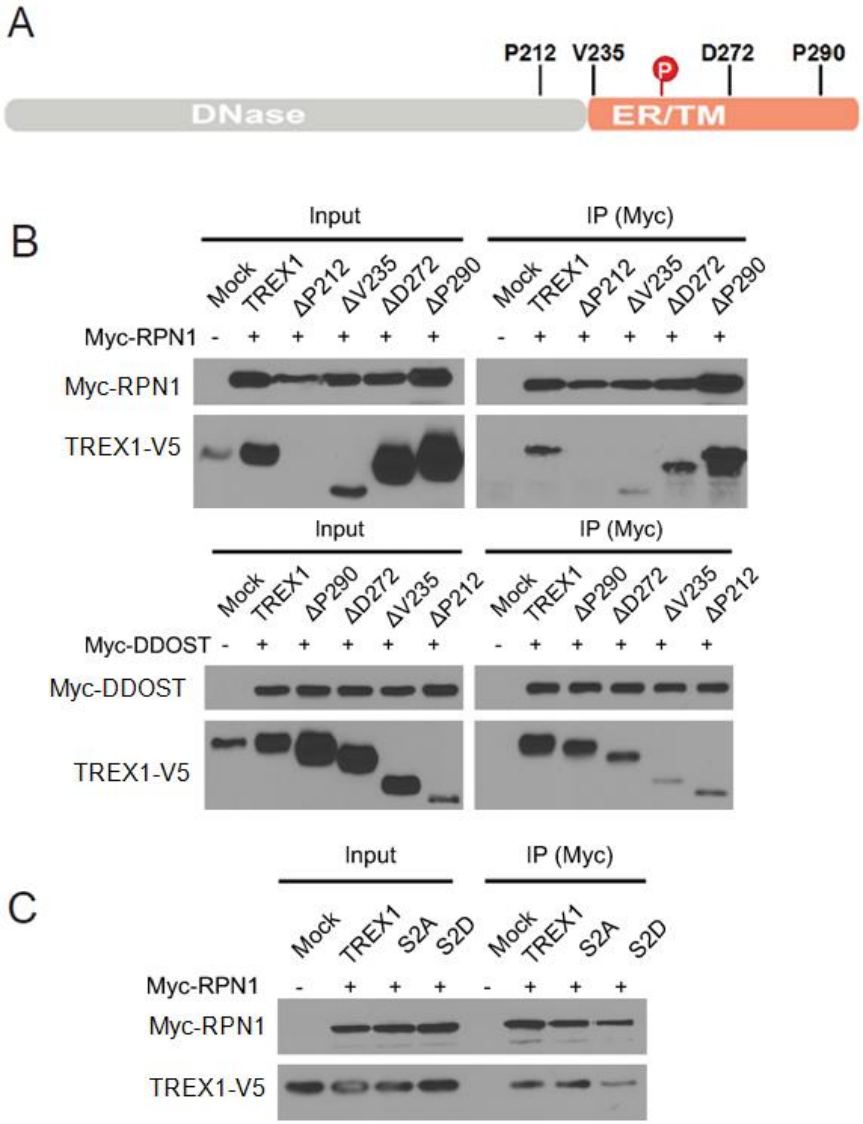

Figure 4.5: TREX1 mitotic phosphorylation disrupt the interaction with the OST complex

(A) A schematic diagram of TREX1 depicting the truncation points used for the co-IP analyses.
(B) Immunoblot analysis of co-IP between TREX1, the truncation variants and RPN1 or DDOST.
(C) Immunoblot analysis of co-IP between TREX1, the phosphor-deficient S2A (S78A/S261A), phosphor-mimetic S2D (S78D/S261D) variants and RPN1.

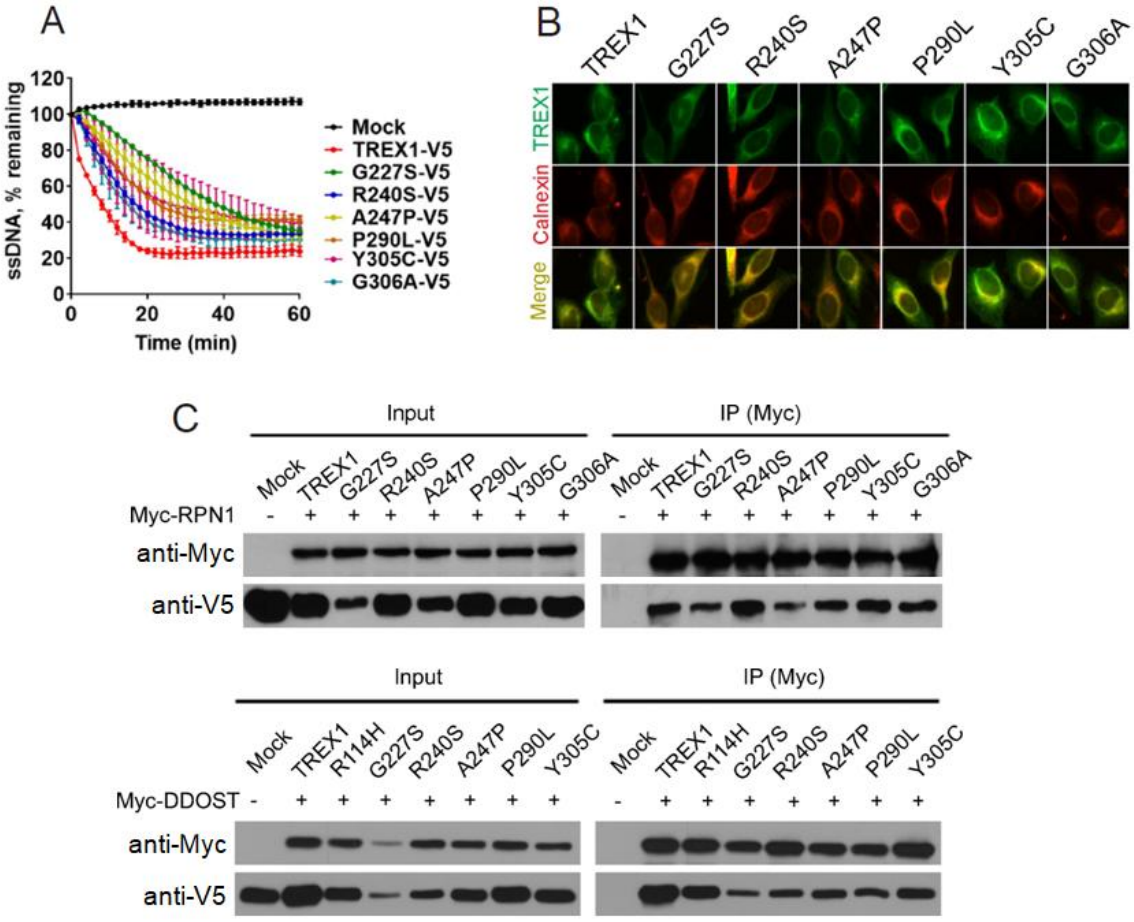

Figure 4.6: SLE associated point mutations on TREX1 do not affect the DNase activity, ER localization or interaction with OST.

(A) DNase assay on the SLE associated TREX1 point mutations as indicated. All variants are V5 tagged and were isolated by IP. Beads bound TREX1 was incubated with a 30-mer ssDNA substrate.
(B) Fluorescence microscopy analysis of the SLE associated TREX1 point mutations as indicated. Staining included anti-V5 (Green), and anti-Calnexin (Red, ER marker).
(C) Immunoblot analysis of co-IP between TREX1, the SLE associated TREX1 point mutations variants as indicated and RPN1 or DDOST.

C-terminus SLE associated mutations G227S, R240S, A247P, P290L, Y305C and G306A and compared it to wild-type TREX1. All TREX1 C-terminus SLE associated mutations exhibited DNase activity (**Figure 4.6 A**). Second, I checked if these mutations affected the proper translocation to the ER. All TREX1 C-terminus SLE associated mutations localized to the ER like wild-type TREX1 (**Figure 4.6 B**). Third, I investigated if TREX1 C-terminus SLE associated mutations could abolish the interaction between TREX1:RPN1 and TREX1:DDOST. None of the TREX1 C-terminus SLE associated mutations failed to interact with OST (**Figure 4.6 C**). Jointly, this data concludes that C-terminus SLE associated mutations do not affect TREX1 DNase activity, ER localization or interaction with OST.

Discussion

TREX1 mutations are associated with several autoimmune and inflammatory diseases. The different clinical etiologies of these diseases and their distribution into N- or C-terminus of the protein suggested at least two distinct functions of TREX1 [110]. The DNase domain located at the N-terminus is critical for clearance of cytosolic DNA, and mutations disrupting DNase activity lead to activation of the innate immune cGAS-STING signaling pathway and elevated IFN and ISG signatures [10, 34]. The C-terminus of TREX1 is critical for ER localization, and recent work showed that it also regulates the activity of the OST complex involved in N-glycosylation [110]. Clusters of frame-shift mutations truncating the C-terminus lead to the accumulation of bioactive fOS without affecting the DNase activity [110]. But how this interaction is regulated is poorly

understood.

Here, I report how a mitotic phosphorylation regulates TREX1 interaction with OST. I found that TREX1 is predominately phosphorylated at the S261 residue during mitosis by cyclin B/CDK1 and that the enzyme that dephosphorylates TREX1 is likely a PP1/PP2 type serine/threonine phosphatase. The S261 mitotic phosphorylation site is located in a conserved motif within the linker region that connects the DNase domain with the tail-anchored insertion motif. The linker region as a whole is less conserved compared to the DNase domain, but interestingly all mammalian homologs contain a CDK1 consensus site in this area, indicating an evolutionarily conserved function might be associated with this PTM. I mapped the RPN1 and DDOST interaction domain to this conserved motif within the linker region and demonstrated that phosphomimetic mutations of the mitotic phosphorylation sites S78 and S261 substantially reduced the affinity of TREX1 for RPN1. In addition, TREX1 C-terminus mutations associated with SLE do not affect TREX1 DNase activity, ER localization or the affinity for RPN1 or DDOST. This finding led to the hypothesis that perhaps another molecular phenotype could account for the TREX1 C-terminus mutations associated with SLE since within the assays performed they behaved indistinguishable from wild-type TREX1.

Together, these findings suggest a model where TREX1 C-terminus is phosphorylated (at S261) during mitosis, and this phosphorylation event disrupts the TREX1:OST interaction. Given the importance of TREX1 to stabilize OST on the ER, any disruption to this interaction could potentially lead to a tremendous accumulation of bioactive fOS by the constant hydrolysis of LLOs throughout the lifespan of the cell. The

only exception may be during mitosis, when the nuclear membrane, the Golgi and ER breaks down and protein translation is placed on hold, due to a reduction in mRNA transcription [135, 136]. By not allowing TREX1 to interact with the OST, the available LLO pool would be quickly and transiently depleted to produce new LLOs at the end of mitosis in each daughter cell. The fact that during mitosis the ER is partitioned and production of new glycoproteins is reduced support this idea [137]. However, previous work has measured the amounts of LLOs during the course of the cell cycle and although a difference was observed when the M phase LLO pool was compared to the S phase, the LLO pool in G1 was comparable to the amounts in M phase [138]. In contrast, no work has been done to examine if fOS are generated at comparable rates over the course of the cell cycle. A possibility still exists that idle LLOs in mitosis are rapidly hydrolyzed to produce larger quantities of fOS. Further investigation is needed to better define this temporal regulation of OST during mitosis, which may shed light on the biology of the OST complex as well as mechanisms of immune diseases associated with TREX1 C-terminus.

Acknowledgment and contribution

I thank Hongtao Yu (UT Southwestern) for the cyclin B plasmid and members of the Nan Yan lab for helpful discussions. This work is supported by the U.S. NIH grants AI098569 and AR067135, Alliance for Lupus Foundation, Welch Foundation I-1831, and NSF graduate student fellowship.

Martin Kucej, Ph.D. contributed to figures 4.1 C-F, 4.2 A-B and 4.3 A-B.

CHAPTER FIVE: CONCLUDING REMARKS

Mammalian self-nucleic acids are well known for their causal association with autoimmune disease. These self-nucleic acids can erroneously active CDS mediated innate immune responses designed for detecting invading pathogens, thus leading to autoimmunity. Mutations that affect TREX1 DNase function are the hallmark of such scenarios. But this model does not reconcile with mutations in TREX1 C-terminus that do not affect the DNase activity. This key observation inspired me to research the role of TREX1 C-terminus and its connection with autoimmune diseases.

TREX1 C-terminus is crucial for localizing the enzyme to the cytosolic surface of the ER. I found that this ER localization is important for preventing OST from hydrolyzing LLOs into fOS. Normally, OST hydrolyzes a small fraction of the LLO pool but in the absence of TREX1, this hydrolysis phenotype is drastically enhanced. Moreover, RVCL associated *TREX1-fs* mutations (e.g. V235fs) also display the same enrichment of fOS in mice and in patient cells. TREX1 C-terminus communicates with OST through the interaction of the subunits RPN1 and DDOST and a small conserved patch within residues 235-272 on TREX1 C-terminus. This OST LLO hydrolysis dysregulation led to two hypotheses: one, the rapid hydrolysis might deplete the available LLO pool and affect the overall N-glycosylation efficiency; or two, that the fOS themselves were immunogenic. Surprisingly, even though a profound amount of LLOs are hydrolyzed to produce fOS global N-glycosylation was not affected to a significant degree. However, the OST dysregulation in *Trex1* -/- cells did cause a ~40% reduction in

the total LLO pool. This reduction may have metabolic implications since more nutrients and resources would be required to produce the activated nucleotide sugar substrates used to assemble LLOs [139]. Indeed a hyperactive metabolic rate has been previously observed and characterized in *Trex1* -/- mice [140]. Unexpectedly, the products of OST dysregulation are immunogenic to macrophages and generate an immune signature comparable to the intrinsic signature observed in the *Trex1* -/- and RVCL patient cells. To my knowledge, this is the first example of an endogenous free glycan functioning as an immune modulator.

Microbial glycans are efficiently recognized by the host immune system, although it is unclear whether mammalian self-glycans can also activate immune responses in chronic disease. The bioactive fOS pool from *Trex1* -/- cells primarily consisted of atypical mannose containing glycans which resemble paucimannose like structures. From the bioactive pool, I identified a simple Man(β1-4)GlcNAc disaccharide that strongly induced the activation of ISG and chemokines. The Man(β1-4)GlcNAc disaccharide is produced from hydrolyzed LLOs by OST in the ER lumen, processed by ENGase in the cytosol, and sensed by a TBK1-dependent innate immune pathway. Suppressing OST activity with ACM reduced the Man(β1-4)GlcNAc disaccharide levels as well as the intrinsic immune activation in *Trex1* -/- cells. Patients carrying *TREX1-fs* mutations (e.g. RVCL) develop a systemic disease with high mortality. Thus, the biogenesis and immune sensing pathways uncovered here provides a mechanistic insight into immediate targets for therapeutic options. ACM, in particular, is a promising therapeutic option since previous work using an RVCL mouse model demonstrated that ACM treatment alleviates

their immune symptoms and increases survivability [65, 110]. Of note, a clinical trial using ACM to treat *TREX1-fs*RVCL patients is ongoing (NCT02723448).

Aside from RVCL, the accumulation of Man(β1-4)GlcNAc disaccharide has also been observed in *MANBA* deficiency or β-mannosidosis. The *MANBA* gene encodes for the only β-mannosidase in humans and acts at the last step of oligosaccharide catabolism in the lysosomes. Previous work has suggested that *MANBA* is the rate-liming step in the oligosaccharide catabolic pathway [79]. Naturally, a large load of substrate would create a back up in the catabolic pathway at the Man(β1-4)GlcNAc disaccharide intermediate. In addition to accumulation of the Man(β1-4)GlcNAc disaccharide, *MANBA* deficiency shares remarkable molecular and clinical similarity to *TREX1*-deficiency and *TREX1-fs*RVCL [141]. A previous study showed that *Trex1 -/-* cells have defective lysosome biogenesis and accumulate large vacuoles in the cell, a phenotype similar to that was observed in *MANBA -/-* mice with lysosome storage disease [142]. Two of the clinical features associated with RVCL such as the deterioration of the cerebral white matter and demyelination are also associated with β-mannosidosis [143]. Thus, therapeutic options developed to treat *TREX1-fs*RVCL may also benefit patients with β-mannosidosis.

Here, I also describe a mitotic phosphorylation that regulates the interaction between TREX1 and OST. The PTM is added by CDK1 at the entry of mitosis on residues S261 and quickly removed by PP1/PP2 phosphatases at the end of mitosis. The cellular LLO levels have been previously shown to vary dynamically throughout the cell cycle [138]. Although not examined here, this observation raises the possibility that fOS

could also have a dynamic nature. On this note, a previous study showed that ER stress induces the accumulation of fOS. The same study proposed that the regulator of this rapid release of fOS by OST is mannose 6 phosphate (M6P). One possibility is that the mechanism behind the influence of M6P involves the transient phosphorylation of TREX1 C-terminus; this would allow for a transient burst in the release of fOS that will be eventually transformed into the bioactive Man(β1-4)GlcNAc disaccharide. ER stress has been implicated in cancer, prion diseases and pathogen infections; settings that involve the immune system [144]. One attractive hypothesis is that perhaps M6P and phosphorylation of TREX1 C-terminus control the destruction of LLO by OST to produce self-glycan ligands that function as a danger signal.

Another interesting finding noted here is that TREX1 C-terminus SLE-associated mutations do not affect any of the TREX1 associated functions (DNase function, ER localization, and interaction with OST). This raises the question of how do these mutations cause autoimmune disease. One possibility is that these SLE-associated mutations affect the expression levels of the endogenous protein perhaps by reducing transcription or translation thus leading to reduced level of TREX1 protein. Since most of these C-terminus SLE associated mutations are dominant, a dosage effect or haploinsufficiency could be the underlying mechanism.

In summary, my graduate work describes a novel function associated with TREX1 C-terminus where it prevents the accumulation of a bioactive Man(β1-4)GlcNAc disaccharide associated with a TBK1 dependent immune activation (**Figure 5.1**).

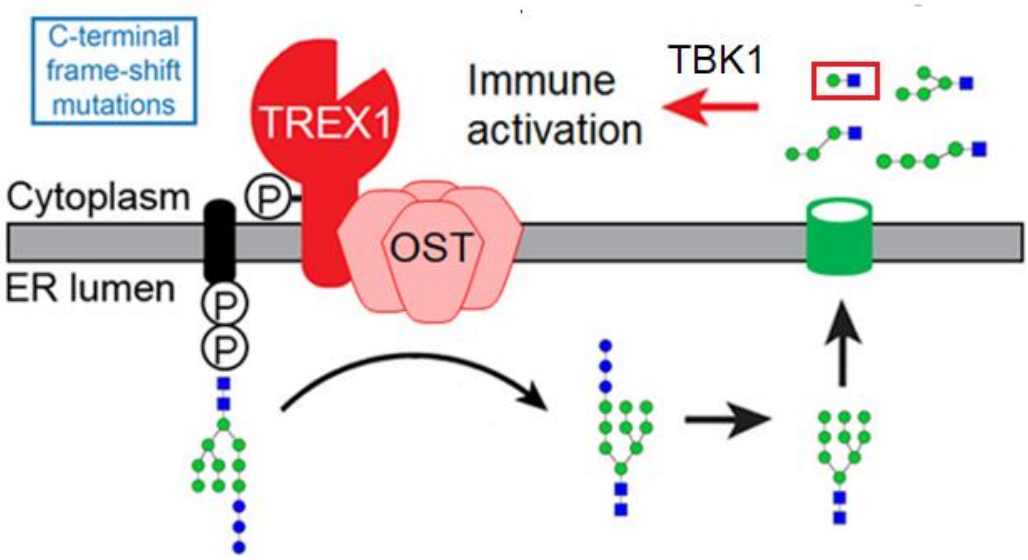

Figure 5.1: Proposed model of TREX1 C-terminus function. In the presence of fs mutations that truncate TREX1 C-terminus, accelerated release of fOS by OST lead to the accumulation of a bioactive disaccharide that activates a TBK1 dependent immune response.

BIBLIOGRAPHY

1. Mogensen, T.H., *Pathogen Recognition and Inflammatory Signaling in Innate Immune Defenses.* Clinical Microbiology Reviews, 2009. **22**(2): p. 240-273.
2. Akira, S., S. Uematsu, and O. Takeuchi, *Pathogen Recognition and Innate Immunity.* Cell, 2006. **124**(4): p. 783-801.
3. Marshak-Rothstein, A., *Toll-like receptors in systemic autoimmune disease.* Nature Reviews Immunology, 2006. **6**(11): p. 823-835.
4. Green, R.S., et al., *Mammalian N-Glycan Branching Protects against Innate Immune Self-Recognition and Inflammation in Autoimmune Disease Pathogenesis.* Immunity, 2007. **27**(2): p. 308-320.
5. Kobayashi, K.S. and R.A. Flavell, *Shielding the double‐edged sword: negative regulation of the innate immune system.* Journal of Leukocyte Biology, 2004. **75**(3): p. 428-433.
6. Rodero, M.P. and Y.J. Crow, *cGMP-AMP synthase paves the way to autoimmunity.* Proceedings of the National Academy of Sciences, 2015. **112**(42): p. 12903-12904.
7. Yasutomo, K., et al., *Mutation of DNASE1 in people with systemic lupus erythematosus.* Nature Genetics, 2001. **28**(4).
8. Yoshida, H., et al., *Lethal anemia caused by interferon-β produced in mouse embryos carrying undigested DNA.* Nature Immunology, 2004. **6**(1).
9. Zheng, L., et al., *Fen1 mutations result in autoimmunity, chronic inflammation and cancers.* Nature Medicine, 2007. **13**(7).
10. Stetson, D.B., et al., *Trex1 Prevents Cell-Intrinsic Initiation of Autoimmunity.* Cell, 2008. **134**(4): p. 587-598.
11. Volkman, H.E. and D.B. Stetson, *The enemy within: endogenous retroelements and autoimmune disease.* Nature Immunology, 2014. **15**(5): p. 415-422.
12. Chen, Q., L. Sun, and Z.J. Chen, *Regulation and function of the cGAS–STING pathway of cytosolic DNA sensing.* Nature Immunology, 2016. **17**(10).
13. Perrino, F.W., H. Miller, and K.A. Ealey, *Identification of a 3'-->5'-exonuclease that removes cytosine arabinoside monophosphate from 3' termini of DNA.* The Journal of biological chemistry, 1994. **269**(23): p. 16357-16363.
14. Lindahl, T., et al., *Biochemical properties of mammalian TREX1 and its association with DNA replication and inherited inflammatory disease.* Biochemical Society Transactions, 2009. **37**(3): p. 535-538.
15. Mazur, D.J. and F.W. Perrino, *Identification and Expression of the TREX1 and TREX2 cDNA Sequences Encoding Mammalian 3′→5′ Exonucleases.* Journal of Biological Chemistry, 1999. **274**(28): p. 19655-19660.
16. Mazur, D.J. and F.W. Perrino, *Excision of 3′ Termini by the Trex1 and TREX2 3′→5′ Exonucleases CHARACTERIZATION OF THE RECOMBINANT PROTEINS.* Journal of Biological Chemistry, 2001. **276**(20): p. 17022-17029.
17. Höss, M., et al., *A human DNA editing enzyme homologous to the Escherichia coli DnaQ/MutD protein.* The EMBO …, 1999.

18. Yang, Y.-G., T. Lindahl, and D.E. Barnes, *Trex1 Exonuclease Degrades ssDNA to Prevent Chronic Checkpoint Activation and Autoimmune Disease.* Cell, 2007. **131**(5): p. 873-886.
19. de Silva, U., et al., *The Crystal Structure of TREX1 Explains the 3′ Nucleotide Specificity and Reveals a Polyproline II Helix for Protein Partnering.* Journal of Biological Chemistry, 2007. **282**(14): p. 10537-10543.
20. Lehtinen, D.A., et al., *The TREX1 Double-stranded DNA Degradation Activity Is Defective in Dominant Mutations Associated with Autoimmune Disease.* Journal of Biological Chemistry, 2008. **283**(46): p. 31649-31656.
21. Bailey, S.L., et al., *Defects in DNA degradation revealed in crystal structures of TREX1 exonuclease mutations linked to autoimmune disease.* DNA Repair, 2012. **11**(1): p. 65-73.
22. Brucet, M., et al., *Structure of the Dimeric Exonuclease TREX1 in Complex with DNA Displays a Proline-rich Binding Site for WW Domains.* Journal of Biological Chemistry, 2007. **282**(19): p. 14547-14557.
23. Crow, Y.J. and N. Manel, *Aicardi-Goutieres syndrome and the type I interferonopathies.* Nature Reviews Immunology, 2015. **15**(7): p. 429-440.
24. Ramantani, G., et al., *Expanding the phenotypic spectrum of lupus erythematosus in Aicardi‐Goutières syndrome.* Arthritis & Rheumatism, 2010. **62**(5): p. 1469-1477.
25. Barizzone, N., et al., *Rare Variants in the TREX1 Gene and Susceptibility to Autoimmune Diseases.* BioMed Research International, 2013. **2013**: p. 1-6.
26. Crow, Y.J. and J. Rehwinkel, *Aicardi-Goutieres syndrome and related phenotypes: linking nucleic acid metabolism with autoimmunity.* Human molecular genetics, 2009.
27. Crow, Y.J., et al., *Mutations in the gene encoding the 3′-5′ DNA exonuclease TREX1 cause Aicardi-Goutières syndrome at the AGS1 locus.* Nature Genetics, 2006. **38**(8): p. 917-920.
28. Fye, J.M., et al., *Dominant Mutations of the TREX1 Exonuclease Gene in Lupus and Aicardi-Goutières Syndrome.* Journal of Biological Chemistry, 2011. **286**(37): p. 32373-32382.
29. Lee-Kirsch, M., et al., *A mutation in TREX1 that impairs susceptibility to granzyme A-mediated cell death underlies familial chilblain lupus.* Journal of Molecular Medicine, 2007. **85**(5): p. 531-537.
30. Orebaugh, C.D., et al., *The TREX1 Exonuclease R114H Mutation in Aicardi-Goutières Syndrome and Lupus Reveals Dimeric Structure Requirements for DNA Degradation Activity.* Journal of Biological Chemistry, 2011. **286**(46): p. 40246-40254.
31. Lee-Kirsch, M., et al., *Mutations in the gene encoding the 3′-5′ DNA exonuclease TREX1 are associated with systemic lupus erythematosus.* Nature Genetics, 2007. **39**(9): p. 1065-1067.

32. Richards, A., et al., *C-terminal truncations in human 3′ -5′ DNA exonuclease TREX1 cause autosomal dominant retinal vasculopathy with cerebral leukodystrophy.* Nature Genetics, 2007. **39**(9): p. 1068-1070.
33. Crow, Y.J., *Aicardi-goutieres syndrome.* Aicardi-goutieres syndrome, 2014.
34. Gao, D., et al., *Activation of cyclic GMP-AMP synthase by self-DNA causes autoimmune diseases.* Proceedings of the National Academy of Sciences, 2015. **112**(42).
35. Vance, R.E., *Cytosolic DNA Sensing: The Field Narrows.* Immunity, 2016. **45**(2): p. 227-228.
36. Yan, N. and Z.J. Chen, *Intrinsic antiviral immunity.* Nature Immunology, 2012. **13**(3).
37. Patrick, K.L., S.L. Bell, and R.O. Watson, *For Better or Worse: Cytosolic DNA Sensing during Intracellular Bacterial Infection Induces Potent Innate Immune Responses.* Journal of Molecular Biology, 2016. **428**(17): p. 3372-3386.
38. Barrat, F.J., K.B. Elkon, and K.A. Fitzgerald, *Importance of Nucleic Acid Recognition in Inflammation and Autoimmunity.* Annual review of medicine, 2016. **67**: p. 323-336.
39. Rice, G., et al., *Heterozygous Mutations in TREX1 Cause Familial Chilblain Lupus and Dominant Aicardi-Goutières Syndrome.* The American Journal of Human Genetics, 2007. **80**(4): p. 811-815.
40. Rice, G., et al., *Clinical and Molecular Phenotype of Aicardi-Goutières Syndrome.* The American Journal of Human Genetics, 2007. **81**(4): p. 713-725.
41. Orebaugh, C.D., et al., *The TREX1 C-terminal Region Controls Cellular Localization through Ubiquitination.* Journal of Biological Chemistry, 2013. **288**(40): p. 28881-28892.
42. Haaxma, C.A., et al., *A de novo p.Asp18Asn mutation in TREX1 in a patient with Aicardi–Goutières syndrome.* American Journal of Medical Genetics Part A, 2010. **152A**(10): p. 2612-2617.
43. Günther, C., et al., *Familial Chilblain Lupus Due to a Novel Mutation in the Exonuclease III Domain of 3′ Repair Exonuclease 1 (TREX1).* JAMA Dermatology, 2015. **151**(4): p. 426-431.
44. Schuh, E., et al., *Multiple sclerosis–like lesions and type I interferon signature in a patient with RVCL.* Neurology - Neuroimmunology Neuroinflammation, 2015. **2**(1).
45. Tüngler, V., R.M. Silver, and H. Walkenhorst, *Inherited or de novo mutation affecting aspartate 18 of TREX1 results in either familial chilblain lupus or Aicardi–Goutières syndrome.* British journal of …, 2012.
46. Namjou, B., et al., *Evaluation of the TREX1 gene in a large multi-ancestral lupus cohort.* Genes and Immunity, 2011. **12**(4): p. 270-279.
47. de Vries, B., et al., *TREX1 gene variant in neuropsychiatric systemic lupus erythematosus.* Annals of the Rheumatic Diseases, 2010. **69**(10): p. 1886-1887.
48. Pelzer, N., et al., *Heterozygous TREX1 mutations in early-onset cerebrovascular disease.* Journal of Neurology, 2013. **260**(8): p. 2188-2190.

49. Sugiura, K., et al., *Severe Chilblain Lupus Is Associated with Heterozygous Missense Mutations of Catalytic Amino Acids or their Adjacent Mutations in the Exonuclease Domains of 3′ -Repair Exonuclease 1.* Journal of Investigative Dermatology, 2012. **132**(12): p. 2855-2857.
50. Abe, J., et al., *A nationwide survey of Aicardi–Goutières syndrome patients identifies a strong association between dominant TREX1 mutations and chilblain lesions: Japanese cohort study.* Rheumatology, 2014. **53**(3): p. 448-458.
51. Dhamija, R., et al., *Evolution of brain lesions in a patient with TREX1 cerebroretinal vasculopathy.* Neurology, 2015.
52. Olivieri, I., et al., *Dysregulation of the immune system in Aicardi-Goutières syndrome: another example in a TREX1-mutated patient.* Lupus, 2013. **22**(10): p. 1064-1069.
53. Ellyard, J.I., et al., *Brief Report: Identification of a Pathogenic Variant in TREX1 in Early‐Onset Cerebral Systemic Lupus Erythematosus by Whole‐Exome Sequencing.* Arthritis & Rheumatology, 2014. **66**(12): p. 3382-3386.
54. Soong, B.-W., et al., *A homozygous NOTCH3 mutation p.R544C and a heterozygous TREX1 variant p.C99MfsX3 in a family with hereditary small vessel disease of the brain.* Journal of the Chinese Medical Association, 2013. **76**(6): p. 319-324.
55. Rice, G.I., et al., *Assessment of interferon-related biomarkers in Aicardi-Goutières syndrome associated with mutations in TREX1, RNASEH2A, RNASEH2B, RNASEH2C, SAMHD1, and ADAR: a case-control study.* The Lancet Neurology, 2013. **12**(12): p. 1159-1169.
56. Wu, J., et al., *Cyclic GMP-AMP Is an Endogenous Second Messenger in Innate Immune Signaling by Cytosolic DNA.* Science, 2013. **339**(6121): p. 826-830.
57. Dobbs, N., et al., *STING Activation by Translocation from the ER Is Associated with Infection and Autoinflammatory Disease.* Cell Host & Microbe, 2015. **18**(2): p. 157-168.
58. Wang, H., et al., *cGAS is essential for the antitumor effect of immune checkpoint blockade.* Proceedings of the National Academy of Sciences, 2017. **114**(7): p. 1637-1642.
59. Gao, D., et al., *Cyclic GMP-AMP Synthase Is an Innate Immune Sensor of HIV and Other Retroviruses.* Science, 2013. **341**(6148): p. 903-906.
60. Morita, M., et al., *Gene-Targeted Mice Lacking the Trex1 (DNase III) 3′ →5′ DNA Exonuclease Develop Inflammatory Myocarditis.* Molecular and Cellular Biology, 2004. **24**(15): p. 6719-6727.
61. Ahn, J., P. Ruiz, and G.N. Barber, *Intrinsic Self-DNA Triggers Inflammatory Disease Dependent on STING.* The Journal of Immunology, 2014. **193**(9): p. 4634-4642.
62. Grieves, J.L., et al., *Exonuclease TREX1 degrades double-stranded DNA to prevent spontaneous lupus-like inflammatory disease.* Proceedings of the National Academy of Sciences, 2015. **112**(16): p. 5117-5122.

63. Stam, A.H., et al., *Retinal vasculopathy with cerebral leukoencephalopathy and systemic manifestations.* Brain : a journal of neurology, 2016.
64. Tsukizawa, Y., et al., *Efficacy of immunotherapy in retinal vasculopathy with cerebral leukodystrophy.* Journal of the Neurological Sciences, 2017. **381**: p. 968-969.
65. Sakai, T., et al., *DNase-active TREX1 frame-shift mutants induce serologic autoimmunity in mice.* Journal of Autoimmunity, 2017. **81**: p. 13-23.
66. Kavanagh, D., et al., *New roles for the major human 3′-5′ exonuclease TREX1 in human disease.* Cell Cycle, 2008.
67. Mohorko, E., R. Glockshuber, and M. Aebi, *Oligosaccharyltransferase: the central enzyme of N-linked protein glycosylation.* Journal of Inherited Metabolic Disease, 2011. **34**(4): p. 869-878.
68. Dempski, R.E. and B. Imperiali, *Oligosaccharyl transferase: gatekeeper to the secretory pathway.* Current Opinion in Chemical Biology, 2002. **6**(6): p. 844-850.
69. Mohorko, E., et al., *Structural Basis of Substrate Specificity of Human Oligosaccharyl Transferase Subunit N33/Tusc3 and Its Role in Regulating Protein N-Glycosylation.* Structure, 2014. **22**(4): p. 590-601.
70. Ruiz-Canada, C., D.J. Kelleher, and R. Gilmore, *Cotranslational and Posttranslational N-Glycosylation of Polypeptides by Distinct Mammalian OST Isoforms.* Cell, 2009. **136**(2): p. 272-283.
71. Shrimal, S., N.A. Cherepanova, and R. Gilmore, *DC2 and KCP2 mediate the interaction between the oligosaccharyltransferase and the ER translocon.* J Cell Biol, 2017.
72. Cherepanova, N.A. and R. Gilmore, *Mammalian cells lacking either the cotranslational or posttranslocational oligosaccharyltransferase complex display substrate-dependent defects in asparagine linked glycosylation.* Scientific reports, 2016. **6**: p. 20946.
73. Gao, N., et al., *Mannose-6-phosphate regulates destruction of lipid-linked oligosaccharides.* Molecular biology of …, 2011.
74. Harada, Y., et al., *Eukaryotic Oligosaccharyltransferase Generates Free Oligosaccharides during N-Glycosylation.* Journal of Biological Chemistry, 2013. **288**(45): p. 32673-32684.
75. Moore, S., *Transport of free polymannose-type oligosaccharides from the endoplasmic reticulum into the cytosol is inhibited by mannosides and requires a thapsigargin-sensitive calcium store.* Glycobiology, 1998. **8**(4): p. 373-381.
76. Harada, Y., Y. Masahara-Negishi, and T. Suzuki, *Cytosolic-free oligosaccharides are predominantly generated by the degradation of dolichol-linked oligosaccharides in mammalian cells.* Glycobiology. **25**(11): p. 1196-1205.
77. Suzuki, T., et al., *Man2C1, an α-mannosidase, is involved in the trimming of free oligosaccharides in the cytosol.* Biochemical Journal, 2006. **400**(1): p. 33-41.
78. Moore, S., *Oligosaccharide transport: pumping waste from the ER into lysosomes.* Trends in Cell Biology, 1999. **9**(11): p. 441-446.
79. Winchester, B., *Lysosomal metabolism of glycoproteins.* Glycobiology, 2005. **15**(6).

80. Spiro, M.J. and R.G. Spiro, *Potential regulation of N-glycosylation precursor through oligosaccharide-lipid hydrolase action and glucosyltransferase-glucosidase shuttle.* The Journal of biological chemistry, 1991. **266**(8): p. 5311-5317.
81. Ma, Y. and B. He, *Recognition of Herpes Simplex Viruses: Toll-Like Receptors and Beyond.* Journal of Molecular Biology, 2014. **426**(6): p. 1133-1147.
82. Grootjans, J., et al., *The unfolded protein response in immunity and inflammation.* Nature Reviews Immunology, 2016. **16**(8): p. 469-484.
83. Barreto-Bergter, E. and R.T. Figueiredo, *Fungal glycans and the innate immune recognition.* Frontiers in cellular and infection microbiology, 2014. **4**: p. 145.
84. Comstock, L.E. and D.L. Kasper, *Bacterial glycans: key mediators of diverse host immune responses.* Cell, 2006. **126**(5): p. 847-850.
85. Marakalala, M.J. and H. Ndlovu, *Signaling C-type lectin receptors in antimycobacterial immunity.* PLOS Pathogens, 2017. **13**(6).
86. Goodridge, H.S., A.J. Wolf, and D.M. Underhill, *β-glucan recognition by the innate immune system.* Immunological Reviews, 2009. **230**(1): p. 38-50.
87. Bueter, C.L., C.A. Specht, and S.M. Levitz, *Innate Sensing of Chitin and Chitosan.* PLoS Pathogens, 2013. **9**(1).
88. Saijo, S., et al., *Dectin-2 Recognition of α-Mannans and Induction of Th17 Cell Differentiation Is Essential for Host Defense against Candida albicans.* Immunity, 2010. **32**(5): p. 681-691.
89. Carroll, E.C., et al., *The Vaccine Adjuvant Chitosan Promotes Cellular Immunity via DNA Sensor cGAS-STING-Dependent Induction of Type I Interferons.* Immunity, 2016. **44**(3): p. 597-608.
90. Wolf, A.J., et al., *Hexokinase Is an Innate Immune Receptor for the Detection of Bacterial Peptidoglycan.* Cell, 2016. **166**(3): p. 624-636.
91. Holm, C.K., S.R. Paludan, and K.A. Fitzgerald, *DNA recognition in immunity and disease.* Current opinion in immunology, 2013.
92. Kawasaki, T., et al., *The second messenger phosphatidylinositol-5-phosphate facilitates antiviral innate immune signaling.* Cell host & microbe, 2013. **14**(2): p. 148-158.
93. Yan, N., et al., *The cytosolic exonuclease TREX1 inhibits the innate immune response to human immunodeficiency virus type 1.* Nat Immunol, 2010. **11**(11): p. 1005-13.
94. Hasan, M., et al., *Trex1 regulates lysosomal biogenesis and interferon-independent activation of antiviral genes.* Nat Immunol, 2013. **14**(1): p. 61-71.
95. Saitoh, T., et al., *Atg9a controls dsDNA-driven dynamic translocation of STING and the innate immune response.* Proc Natl Acad Sci USA, 2009. **106**(49): p. 20842-6.
96. Gao, N. and M.A. Lehrman, *Non-radioactive analysis of lipid-linked oligosaccharide compositions by fluorophore-assisted carbohydrate electrophoresis.* Methods in enzymology, 2006. **415**: p. 3-20.

97. Gehrke, N., et al., *Oxidative Damage of DNA Confers Resistance to Cytosolic Nuclease TREX1 Degradation and Potentiates STING-Dependent Immune Sensing.* Immunity, 2013. **39**(3): p. 482-495.
98. Barber, G.N., *STING (Stimulator of interferon genes), a regulator of innate immune resppnse*, in *Google Patent*. 2012, University Of Miami: USA. p. 409.
99. Kelleher, D.J. and R. Gilmore, *An evolving view of the eukaryotic oligosaccharyltransferase.* Glycobiology, 2006. **16**(4): p. 47R-62R.
100. Gao, N., et al., *Mannose-6-phosphate regulates destruction of lipid-linked oligosaccharides.* Mol Biol Cell, 2011. **22**(17): p. 2994-3009.
101. Cline, A., et al., *A Zebrafish Model Of PMM2-CDG Reveals Altered Neurogenesis And A Substrate-Accumulation Mechanism For N-Linked Glycosylation Deficiency.* Mol Biol Cell, 2012. **23**(21): p. 4175-4187.
102. Richards, A., et al., *C-terminal truncations in human 3'-5' DNA exonuclease TREX1 cause autosomal dominant retinal vasculopathy with cerebral leukodystrophy.* Nat Genet, 2007. **39**(9): p. 1068-70.
103. Taylor, K.L., et al., *Identification of interferon-beta-stimulated genes that inhibit angiogenesis in vitro.* Journal of interferon & cytokine research : the official journal of the International Society for Interferon and Cytokine Research, 2008. **28**(12): p. 733-740.
104. Bodnar, R.J., et al., *IP-10 induces dissociation of newly formed blood vessels.* J Cell Sci, 2009. **122**(Pt 12): p. 2064-77.
105. Sancho, D. and C. e Sousa, *Signaling by Myeloid C-Type Lectin Receptors in Immunity and Homeostasis.* Annual review of immunology, 2012. **30**(1): p. 491-529.
106. Rabinovich, G.A., Y. van Kooyk, and B.A. Cobb, *Glycobiology of immune responses.* Annals of the New York Academy of Sciences, 2012. **1253**(1): p. 1-15.
107. Paciotti, S., et al., *Accumulation of Free Oligosaccharides and Tissue Damage in Cytosolic α-Mannosidase (Man2c1)-deficient Mice.* Journal of Biological Chemistry, 2014. **289**(14): p. 9611-9622.
108. Cox, T.M. and B.M. Cachón‐González, *The cellular pathology of lysosomal diseases.* The Journal of Pathology, 2012. **226**(2): p. 241-254.
109. Yan, N., *Immune Diseases Associated with TREX1 and STING Dysfunction.* Journal of Interferon & Cytokine Research, 2017. **37**(5): p. 198-206.
110. Hasan, M., et al., *Cytosolic Nuclease TREX1 Regulates Oligosaccharyltransferase Activity Independent of Nuclease Activity to Suppress Immune Activation.* Immunity, 2015. **43**(3): p. 463-474.
111. Orzalli, M.H., et al., *cGAS-mediated stabilization of IFI16 promotes innate signaling during herpes simplex virus infection.* Proceedings of the National Academy of Sciences, 2015. **112**(14).
112. Thaiss, C.A., et al., *Chemokines: A New Dendritic Cell Signal for T Cell Activation.* Frontiers in Immunology, 2011. **2**: p. 31.
113. Griffith, J.W., C.L. Sokol, and A.D. Luster, *Chemokines and Chemokine Receptors: Positioning Cells for Host Defense and Immunity.* Immunology, 2014. **32**(1): p. 659-702.

114. Thurston, T.L.M., et al., *Recruitment of TBK1 to cytosol‐invading Salmonella induces WIPI2‐dependent antibacterial autophagy.* The EMBO Journal, 2016. **35**(16): p. 1779-1792.
115. Harada, Y., H. Hirayama, and T. Suzuki, *Generation and degradation of free asparagine-linked glycans.* Cellular and molecular life sciences, 2015.
116. Bennett, D.C., et al., *High-throughput Screening Identifies Aclacinomycin as a Radiosensitizer of EGFR-Mutant Non-Small Cell Lung Cancer.* Translational Oncology, 2013. **6**(3): p. 382-391.
117. Kessler, B., et al., *z-VAD-fmk inhibits peptide:N-glycanase and may result in ER stress.* Cell Death and Differentiation, 2005. **13**(1): p. 163.
118. Haga, Y., et al., *Establishment of a real-time analytical method for free oligosaccharide transport from the ER to the cytosol.* Glycobiology, 2009. **19**(9): p. 987-994.
119. Hebert, D.N., et al., *The intrinsic and extrinsic effects of N-linked glycans on glycoproteostasis.* Nature Chemical Biology, 2014. **10**(11): p. 902-910.
120. Iannotti, M.J., et al., *A Golgi-localized Mannosidase (MAN1B1) Plays a Non-enzymatic Gatekeeper Role in Protein Biosynthetic Quality Control.* Journal of Biological Chemistry, 2014. **289**(17): p. 11844-11858.
121. Tulsiani, D.R. and O. Touster, *Substrate specificities of rat kidney lysosomal and cytosolic alpha-D-mannosidases and effects of swainsonine suggest a role of the cytosolic enzyme in glycoprotein catabolism.* The Journal of biological chemistry, 1987. **262**(14): p. 6506-6514.
122. Olden, K., et al., *The potential importance of swainsonine in therapy for cancers and immunology.* Pharmacology & Therapeutics, 1991. **50**(3): p. 285-290.
123. Majima, H., and Ohta, K., *Clinical studies of aclacinomycin A (ACM).* Biomedicine & Pharmacotherapy, 1987. **41**(5): p. 233-237.
124. Gray, E.E., et al., *Cutting Edge: cGAS Is Required for Lethal Autoimmune Disease in the Trex1-Deficient Mouse Model of Aicardi–Goutières Syndrome.* The Journal of Immunology, 2015. **195**(5): p. 1939-1943.
125. Hasan, M., et al., *Cutting Edge: Inhibiting TBK1 by compound II ameliorates autoimmune disease in mice.* The Journal of …, 2015.
126. Lin, Y.-C., et al., *The Tyrosine Kinase Syk Differentially Regulates Toll-like Receptor Signaling Downstream of the Adaptor Molecules TRAF6 and TRAF3.* Sci. Signal., 2013. **6**(289).
127. Curtis, M.M., et al., *The Gut Commensal Bacteroides thetaiotaomicron Exacerbates Enteric Infection through Modification of the Metabolic Landscape.* Cell Host & Microbe, 2014. **16**(6): p. 759-769.
128. Cuskin, F., et al., *Human gut Bacteroidetes can utilize yeast mannan through a selfish mechanism.* Nature, 2015. **517**(7533): p. 165-169.
129. Robb, M., et al., *Molecular Characterization of N-glycan Degradation and Transport in Streptococcus pneumoniae and Its Contribution to Virulence.* PLoS pathogens, 2017. **13**(1).
130. Iversen, M.B., et al., *An innate antiviral pathway acting before interferons at epithelial surfaces.* Nature Immunology, 2016. **17**(2): p. 150-158.

131. Lindqvist, A., V. Rodríguez-Bravo, and R.H. Medema, *The decision to enter mitosis: feedback and redundancy in the mitotic entry network.* The Journal of Cell Biology, 2009. **185**(2): p. 193-202.
132. Dephoure, N., et al., *A quantitative atlas of mitotic phosphorylation.* Proceedings of the National Academy of Sciences, 2008. **105**(31): p. 10762-10767.
133. Kinoshita, E., E. Kinoshita-Kikuta, and T. Koike, *Separation and detection of large phosphoproteins using Phos-tag SDS-PAGE.* Nature Protocols, 2009. **4**(10): p. 1513-1521.
134. Mochida, S. and T. Hunt, *Protein phosphatases and their regulation in the control of mitosis.* EMBO reports, 2012. **13**(3): p. 197-203.
135. Tanenbaum, M.E., N. Stern-Ginossar, and W.-J.S. Elife, *Regulation of mRNA translation during mitosis.* Elife, 2015.
136. Seemann, J., et al., *Partitioning of the Matrix Fraction of the Golgi Apparatus During Mitosis in Animal Cells.* Science, 2002. **295**(5556): p. 848-851.
137. Kano, F., et al., *NSF/SNAPs and p97/p47/VCIP135 are sequentially required for cell cycle‐dependent reformation of the ER network.* Genes to Cells, 2005. **10**(10): p. 989-999.
138. Fukushima, K., T. Ohkura, and K. Yamashita, *Synthesis of lipid-linked oligosaccharides is dependent on the cell cycle in rat 3Y1 cells.* Journal of biochemistry, 1997. **121**(3): p. 415-418.
139. Harada, Y., et al., *Metabolically programmed quality control system for dolichol-linked oligosaccharides.* Proceedings of the National Academy of Sciences, 2013. **110**(48): p. 19366-19371.
140. Hasan, M., et al., *Chronic innate immune activation of TBK1 suppresses mTORC1 activity and dysregulates cellular metabolism.* Proceedings of the National Academy of Sciences, 2017. **114**(4): p. 746-751.
141. Stensland, H., et al., *Identification of two novel β-mannosidosis-associated sequence variants: Biochemical analysis of β-mannosidase (MANBA) missense mutations.* Molecular Genetics and Metabolism, 2008. **94**(4): p. 476-480.
142. Zhu, M., et al., *β-Mannosidosis mice: a model for the human lysosomal storage disease.* Human Molecular Genetics, 2006. **15**(3): p. 493-500.
143. J, L.-P.M.S., *Magnetic resonance findings in leucodystrophies and MS.* Int MS J, 2009.
144. Garg, A.D., et al., *ER stress-induced inflammation: does it aid or impede disease progression?* Trends in Molecular Medicine, 2012. **18**(10): p. 589-598.